THE ELECTRONIC STRUCTURE OF NITROGEN DIOXIDE I. MULTI-CONFIGURATION SELF-CONSISTENT-FIELD CALCULATION OF THE LOW-LYING ELECTRONIC STATES: II. SPECTRAL INTERPRETATION

Dissertation for the Degree of Ph. D.
MICHIGAN STATE UNIVERSITY
GREGORY DAVID GILLISPIE
1975

This is to certify that the

thesis entitled

THE ELECTRONIC STRUCTURE OF NITROGEN DIOXIDE
I. MULTI-CONFIGURATION SELF-CONSISTENT-FIELD
CALCULATION OF THE LOW-LYING ELECTRONIC STATES:
II. SPECTRAL INTERPRETATION

presented by

Gregory David Gillispie

has been accepted towards fulfillment
of the requirements for

Ph.D. degree in Chemistry

Major professor

Date 2/14/1975

O-7639

ABSTRACT

THE ELECTRONIC STRUCTURE OF NITROGEN DIOXIDE
I. MULTI-CONFIGURATION SELF-CONSISTENT-FIELD
CALCULATION OF THE LOW-LYING ELECTRONIC STATES;
II. SPECTRAL INTERPRETATION

By

Gregory David Gillispie

Multi-configuration self-consistent-field (MC-SCF) wave-functions have been computed for the low-lying $\tilde{X}^2A_1$, $\tilde{A}^2B_2$, $\tilde{B}^2B_1$, $\tilde{C}^2A_2$, $^4B_2$, $^4A_2$, and $^2\Sigma_g^+$ electronic states of NO_2. The minima of the $\tilde{A}^2B_2$, $\tilde{B}^2B_1$, and $\tilde{C}^2A_2$ states have all been found to be within 2 eV of the minimum of the $\tilde{X}^2A_1$ ground state; for these states, C_{2v} potential surfaces have been constructed for purposes of a spectral interpretation. The $^4B_2$, $^4A_2$, and $^2\Sigma_g^+$ states are all more than 4 eV above the minimum of the ground state and have been examined in less detail.

The study described here is an improvement on previous NO_2 ab initio calculations in three important areas: (1) The double-zeta-plus-polarization quality basis set is larger and more flexible; (2) The treatment of molecular correlation is more extensive; and (3) The

electronic energies have been calculated for several different bond lengths and bond angles in each state.

For the four lowest doublet states the following spectral data have been obtained:

	T_e (eV)	R_e(Å)	θ_e(degrees)	ω_1(cm^{-1})	ω_2(cm^{-1})	μ(debyes)
$\tilde{C}^2A_2$	1.84	1.27	110	1360	798	0.05
$\tilde{B}^2B_1$	1.66	1.20	180	1192	960	0.00
$\tilde{A}^2B_2$	1.18	1.26	102	1461	739	0.46
$\tilde{X}^2A_1$	0.00 (0.00)	1.20 (1.1934)	134 (134.1)	1351 (1358)	758 (757)	0.37 (0.32)

The ground state experimental constants are included in parentheses. The estimated accuracy of the various parameters is ± 0.02 Å for bond length, ± 2° for bond angle, ± 10% for the vibrational frequencies, ± 0.10 debye for dipole moments, and ± 0.3 eV for the adiabatic excitation energies.

Contrary to previous theoretical studies, but consistent with recent experimental evidence, the lowest excited state is of $^2B_2$ electronic symmetry. Franck-Condon factors were calculated between the $\tilde{X}^2A_1$ and $\tilde{A}^2B_2$ states; from these a theoretical $\tilde{A}^2B_2 \leftarrow \tilde{X}^2A_1$ absorption spectrum was generated. This spectrum, based solely on the ab initio data, is successful in accounting for many of the features in the low resolution NO_2 absorption between 8500 and 6000 Å. On the basis of experimental hot and cold band

intensity ratios, along with the ratios predicted from the Franck-Condon factors, a suggestion is made that the $\tilde{A}^2B_2 \leftarrow \tilde{X}^2A_1$ origin is lower than the present experimental assignment of 1.48 eV. The $\tilde{A}^2B_2$ rotational constants as inferred from the accurate ab initio equilibrium geometry are vastly different from the results of experimental rotational analyses; this dissonance has been attributed to vibronic coupling of the $\tilde{A}^2B_2$ state with high vibrational levels of the ground electronic state.

It is also proposed that the origin of the $\tilde{B}^2B_1 \leftarrow \tilde{X}^2A_1$ absorption is about 925 cm^{-1} lower than the present assignment of 14 743 cm^{-1} (1.83 eV); the analysis is based upon a consideration of isotopic band shifts and the implication of these for the $\tilde{B}^2B_1$ asymmetrical stretching frequency. The $\tilde{B}^2B_1$ state has a linear equilibrium geometry and its bond length is less than 0.01 Å longer than in the $\tilde{X}^2A_1$ ground electronic state.

Among the topics which are discussed in view of the computed potential energy surfaces are: predissociation for $\lambda<3979$ Å and in the 2491 Å band system, the $NO(^2\Pi) + O(^3P)$ chemiluminescence, the photodissociation of NO_2 by the 6943 Å line of the ruby laser for which a single photon has an energy equal to only 57% of the NO_2 dissociation energy, a photodetachment experiment in NO_2^- which may involve the $^2B_1$ "ring state" of NO_2, the ability of level dilution to explain the anomalous fluorescence lifetime

in NO_2, and the evidence supporting strong vibronic coupling of the $\tilde{A}^2B_2$ and $\tilde{X}^2A_1$ states.

The overlapping of the $\tilde{A}^2B_2 \leftarrow \tilde{X}^2A_1$ and $\tilde{B}^2B_1 \leftarrow \tilde{X}^2A_1$ absorptions in the 5200 to 3700 Å region and the observation of Douglas and Huber that all bands become diffuse for $\lambda<3979$ Å require that predissociation mechanisms be found for both the $\tilde{A}^2B_2$ and $\tilde{B}^2B_1$ states. In the latter state, predissociation by vibration is the most likely possibility, while the $\tilde{A}^2B_2$ state could also undergo predissociation by vibration or be heterogeneously predissociated by high vibrational levels of the ground state. Possible mechanisms are suggested for predissociation of the upper state of the $2^2B_2 \leftarrow \tilde{X}^2A_1$ 2491 Å band system into either $N(^4S) + O_2(^3\Sigma_g^-)$ or into $NO(^2\Pi) + O(^3P)$.

The visible and near-infrared $NO(^2\Pi) + O(^3P)$ chemiluminescence must primarily be due to the electric-dipole allowed transitions $\tilde{A}^2B_2 \rightarrow \tilde{X}^2A_1$ and $\tilde{B}^2B_1 \rightarrow \tilde{X}^2A_1$, especially the former. The 3.7 μm feature in the recombination has been tentatively assigned to a $\tilde{C}^2A_2 \rightarrow \tilde{A}^2B_2$ electronic transition, rather than an $\tilde{X}^2A_1$ vibrational transition as has been suggested in the literature.

The ruby laser photodissociation experiment has been interpreted by Gerstmayr, Harteck, and Reeves in terms of two consecutive single photon absorptions. If this be so, the likely sequence is $\tilde{A}^2B_2 \leftarrow \tilde{X}^2A_1$ followed by $\tilde{C}^2A_2 \leftarrow \tilde{A}^2B_2$.

Herbst, Patterson, and Lineberger have found an NO_2^- photodetachment process which is different from $NO_2^-(\tilde{X}^1A_1) + h\nu \rightarrow NO_2(\tilde{X}^2A_1) + e$. Although they have attributed their data to $NO_2^{-*} + h\nu \rightarrow NO + O + e$ where NO_2^{-*} is a $[N_{O}{}^{O}]^-$ peroxy isomer, we suggest that the process

$$NO_2^-(\text{Ring state}) + h\nu \rightarrow NO_2(\text{Ring state}) + e$$

be also considered. The "ring states" are the nearly equilateral triangle conformation states which have been found in <u>ab initio</u> calculations on both NO_2 and O_3, which is isoelectronic with NO_2^-.

It has been suggested several times in the literature that the anomalously long fluorescence lifetime observed in NO_2 could be understood in terms of level dilution of the emitting state by a high density of $\tilde{X}^2A_1$ vibrational levels. However, the level density ratio of $\tilde{X}^2A_1$ to $\tilde{A}^2B_2$ is much smaller than was inferred from the data of earlier, less accurate <u>ab initio</u> calculations. Consequently, this mechanism can only account for a small part of the anomalous fluorescence lifetime effect.

An unusual feature has been found for the $^2\Sigma_g^+$ state. The equilibrium geometry of this linear state has two unequal bond lengths of 1.20 Å and 1.42 Å and the inversion barrier is approximately 800 cm^{-1}.

THE ELECTRONIC STRUCTURE OF NITROGEN DIOXIDE

I. MULTI-CONFIGURATION SELF-CONSISTENT-FIELD CALCULATION OF THE LOW-LYING ELECTRONIC STATES: II. SPECTRAL INTERPRETATION

By

Gregory David Gillispie

A DISSERTATION

Submitted to
Michigan State University
in partial fulfillment of the requirements
for the degree

DOCTOR OF PHILOSOPHY

Department of Chemistry

1975

ACKNOWLEDGMENTS

I wish to thank Professor R. N. Hammer who first showed me the excitement of chemistry and who guided me through my undergraduate years. A debt of gratitude is also owed my teachers in physical chemistry and quantum mechanics: Professors J. L. Dye, G. E. Leroi, R. H. Schwendeman, J. F. Harrison, F. H. Horne, R. I. Cukier, W. Repko, and A. U. Khan.

The financial support of the National Science Foundation, the Chemistry Department of Michigan State University, and the Argonne National Laboratory Center for Educational Affairs is also gratefully acknowledged. Special thanks are due Dr. A. C. Wahl for extending the opportunity for me to work in his group at Argonne National Laboratory, Dr. M. Krauss of the National Bureau of Standards for numerous insightful discussions and suggestions, and Mr. Al Hinds for helpful comments concerning the computer codes used in the calculations.

Most of all, I would like to express my sincerest appreciation of the role that my advisor, Professor A. U. Khan, has played in my development. Not only has he been a

friend as well as advisor, but has also always taught me to grow both as a person and a scientist. His encouragement and enthusiasm has inspired me throughout the five years of our association; without it, this study would not have been possible.

TABLE OF CONTENTS

LIST OF TABLES

LIST OF FIGURES

CHAPTER I

INTRODUCTION

The nitrogen dioxide (NO_2) molecule has long been of chemical interest because, although highly reactive, it is a stable free radical of non-zero spin with a high propensity for dimerization. More recently, heightened ecological consciousness has focused attention on the role of NO_2 in the photochemical smog cycle common to polluted urban atmospheres. In a similar vein, aeronomists have been attracted to the chemiluminescence known as the "air afterglow" or the "night afterglow" arising from emission from excited electronic states of NO_2, which are generated in the recombination of ground state nitric oxide molecules and oxygen atoms.

Drawn to the molecule in many cases by the features mentioned above, the molecular spectroscopists have found additional challenges to be met. In absorption NO_2 exhibits a discrete, nearly continuous spectrum from 8500 Å to 3000 Å. However, the spectrum is so complex and irregular that traditional methods of spectroscopic analysis have been less successful in elucidating the nature of the

excited states involved than for many other molecules of comparable size. The diffuseness observed in the rotational structure at the first dissociation limit but the continuing vibronic structure is indicative of a predissociative process. Additionally, fluorescence lifetimes obtained from broadband excitation range from 40 to 90 μsec, some two orders of magnitude longer than the value of 0.26 μsec deduced from the integrated absorption coefficient. Related issues include whether or not the decay is exponential and its dependence on the wavelength of excitation.

The common thread of these characteristics is that each involves the electronic structure of NO_2, especially that of the excited states. In 1965 Douglas and Huber [1] succeeded in analyzing the unperturbed K'=0 sub-bands in a bending progression of a $^2B_1 \leftarrow \tilde{X}^2A_1$ transition. However, the observed bands in the 4600-3800 Å spectral region are far from the extrapolated system origin between 8500 Å and 6500 Å predicted from a consideration of band isotopic shifts. No K'>O or upper state stretching features were found so the $^2B_1$ geometry could not be inferred, although the state is expected to be linear, or nearly so, from the qualitative arguments of Walsh [2]. More recently, laser-induced fluorescence [3-7] and microwave-optical double resonance [8, 9] (MODR) experiments have identified a $^2B_2$ excited state in the visible and near-infrared regions. The vibrational assignments of this state [5] are tentative, though, and the rotational analyses are for energetically

isolated regions in which widely differing rotational constants have been reported. Consequently, although it is now firmly established that at least two electric-dipole allowed transitions, $^2B_2 \leftarrow \tilde{X}^2A_1$ and $^2B_1 \leftarrow \tilde{X}^2A_1$, contribute to the visible and near-infrared absorption of NO_2, the excited state spectroscopic parameters and excitation energies are still subjects of intense research.

The complexity of the spectra and the difficulty in analysis have been ascribed to various perturbations among the levels in this region. Attempts to identify the existence, nature, and mechanism of these perturbations have been greatly frustrated by the availability of several candidates. Non-empirical theoretical calculations [10-15] have predicted low-lying $^2A_2$, $^4A_2$, $^4B_2$, and $2^2A_1(^2\Sigma_g^+)$ states in addition to the experimentally observed $\tilde{X}^2A_1$, $^2B_2$, and $^2B_1$ states. However, the quantitative accuracy of these calculations is insufficient to justify using the theoretical results as the basis of a critical examination of the experimental data. An <u>ab initio</u> calculation which gives reliable values for bond lengths, angles, and excitation energies would provide the necessary framework for such an interpretation. In fact, in view of the complexity, accurate theoretical potential energy surfaces and descriptions of the electronic structure of the various electronic states involved are probably crucial in order to choose from competing perturbing mechanisms which disrupt the spectrum.

In this study calculations are described which are significant improvements over the published literature. The basis set used for the trial variational wavefunction is larger and more flexible and the treatment of molecular correlation more extensive. In addition, the geometry has been varied for all the low-lying electronic states to cover a region sufficient to analyze the visible and near-infrared spectrum. The emphasis of this study is primarily on the description of the electronic states necessary for such an analysis; therefore, the reaction surfaces for dissociation and O + NO recombination and the region of very small bond angle have been given only a cursory examination.

The electronic structure of such a variety of states can be described quantitatively by a multi-configuration variational trial wavefunction. In order to provide the most compact description, it is necessary that both the molecular orbitals and the configuration weights be simultaneously varied and optimized. This has been accomplished through the multi-configuration self-consistent-field (MC-SCF) formalism of Das and Wahl [16]. The experience of application of the MC-SCF technique to diatomic molecules has shown that the dominant correlation effects are included in a set of Optimized Valence Configurations (OVC) which primarily determine the molecular extra correlation energy (MECE), that is, the additional correlational energy due to bond formation. The present study

will discuss in detail the extension of the OVC method to triatomic systems.

After an analysis of the OVC approach to triatomic molecules is presented, the relative merits of MC-SCF calculations and the more traditional SCF and configuration interaction (CI) treatments are contrasted in Chapter II. The method of selection of configurations and the quality of the basis set are discussed and the present results are compared with those of previous theoretical studies. The details of fitting the ab initio energies at various geometries to potential surfaces are described; the resulting $\tilde{X}^2A_1$ equilibrium geometry, vibrational frequencies, and dipole moment are compared with the experimentally determined values in an effort to gauge the accuracy and predictive capabilities of this study.

Chapter III commences with a qualitative discussion of the electronic spectroscopy of NO_2 in which a synthesis of relevant experimental data into the theoretical framework is attempted. Among the features which are treated are a characterization of the spectral regions in which the various electronic states manifest themselves, the observed predissociative processes, the visible and infrared $NO(^2\Pi) + O(^3P)$ chemiluminescence, and the source of the anomalous fluorescence lifetime. Attention is then focused on some of the finer details of the two absorption systems which carry most, if not all, of the absorption oscillator strength in the visible and near-infrared. Toward this

end, a technique is developed for evaluation of Franck-Condon overlap integrals from the ab initio potential surfaces. The $^2B_1 \leftarrow \tilde{X}^2A_1$ absorption is analyzed first with special consideration devoted to a prediction of the origin of this system, based on band isotope shifts. The apparently stronger $^2B_2 \leftarrow \tilde{X}^2A_1$ absorption is examined next; a primary aid is an absorption spectrum constructed from the computed Franck-Condon factors. Many of the long wavelength experimental absorption features can be correlated with those of this spectrum which is generated almost entirely by non-empirical means. A reassignment of the $^2B_2$ origin is proposed which is supported by the relative intensities of hot and cold bands. Finally, it is suggested that vibronic interaction of the $^2B_2$ state with high vibrational levels of the $\tilde{X}^2A_1$ ground state provides the only consistent explanation for the incompatibility of the experimentally determined $^2B_2$ rotational constants and those inferred from the ab initio Born-Oppenheimer geometry of this state. Chapter IV summarizes the most important conclusions of this study.

CHAPTER II

MC-SCF CALCULATION OF THE LOW-LYING ELECTRONIC STATES

The OVC Approach to Triatomic MC-SCF Calculations and the Partitioning of the Orbital Basis

The MC-SCF calculations reported in this work were performed with the BISON-MC program developed by Das and Wahl [17]. The details of the MC-SCF method and the computational procedures employed in this program have been discussed elsewhere [16] and only a brief review of the MC-SCF theory will be given here.

The total electronic wavefunction is represented by a linear combination of configurations, Φ_k,

$$\psi(\vec{r}_1, \ldots\ldots, \vec{r}_m) = \sum_k A_k \Phi_k(\vec{r}_1, \ldots\ldots, \vec{r}_m) \qquad (1)$$

where the $\vec{r}_i$ represent the spin and space coordinates of the i^{th} electron. The configurations are appropriately projected linear combinations of antisymmetrized determinants over a set of molecular spin orbitals, $\{\phi_i\}$,

$$\Phi_k(\vec{r}_1, \ldots\ldots, \vec{r}_m) = \hat{\mathcal{O}}_{\alpha,s} |\phi_1(\vec{r}_1) \ldots\ldots \phi_m(\vec{r}_m)| \qquad (2)$$

where the symbol $\hat{\mathcal{S}}_{\alpha,s}$ indicates that the determinant has been projected to be an eigenfunction of the total spin and to possess the overall orbital symmetry of the electronic state in question. For a C_{2v} geometry, the BISON-MC system of codes only recognizes the symmetry operations of the identity and reflection through the molecular plane. This constraint, forced by programmatic considerations, can have serious implications for the orbital optimization of excited states. For example, if one is attempting to treat the $^2B_2$ state of NO_2, "variational collapse" to the $^2A_1$ ground state may occur since both of these transform as $^2A'$ in the C_s point group recognized by the program. This difficulty was circumvented by choosing the initial guesses of the molecular orbitals to transform as the irreducible representations of the C_{2v} point group; in all cases the orbitals maintained the desired symmetry throughout the orbital optimization and "variational collapse" was averted. The spatial portion of each molecular spin orbital is expanded in terms of a set of atom-centered basis functions, $\{\chi_j\}$,

$$\phi_i = \sum_j c_{ij}\chi_j \qquad (3)$$

For NO_2 and other polyatomic molecules, it is convenient to use Gaussian-type functions (GTF) for which fast molecular integral programs are available. In this study, the necessary integrals were evaluated with the integral generating code of the POLYATOM [18] system, suitably

modified to provide an input into the BISON-MC system of codes.

The MC-SCF procedure variationally determines the CI mixing coefficients, A_k, and simultaneously, the basis function expansion coefficients, c_{ij}. This added flexibility over an SCF + CI treatment permits a significant truncation of the length of the CI expansion while still providing a satisfactory description of the electronic structure. However, the adequacy of the description will depend somewhat on the electronic property under consideration and the absolute lowering of the total energy is <u>not</u> necessarily the most desirable way to choose a configuration. The OVC method, in fact, attempts to distinguish between intra-atomic and inter-atomic types of correlation, specifically those portions of the correlation energy which vary significantly with geometry. In the case of diatomic molecules, quite compact MC-SCF wavefunctions have been found to quantitatively describe the binding in such molecules as F_2 [19], CO [20], and OH [21]. Here the analysis used for the diatomics is extended to the triatomic systems and modified as required.

The OVC model concentrates on the changes in the electronic structure which occur as the molecule forms. In the diatomic molecule case, these changes are referenced to an asymptote of Restricted Hartree-Fock (RHF) atoms. The base set of configurations is chosen to insure that the molecule formally dissociates into RHF atoms. Added to the

base set is a set which contributes to the molecular extra correlation energy (MECE) and whose correlation contribution vanishes at the dissociation limit. These two classes of configurations yield compact, physically meaningful wavefunctions. Only for very high accuracy has it been found that the smaller variation in the intra-atomic correlation energy with the internuclear separation must be considered [19].

The localization of electronic charge in the molecule is determined by one or a few dominant configurations. Since we are concerned primarily with the lowest state of a given spatial symmetry and multiplicity, the state is usually valence in character, i.e., no principal quantum number promotion, relative to the constituent atomic orbitals, occurs in the molecular orbitals from which the dominant configurations are constructed. It is then desirable to define a non-virtual space composed of both core and valence orbitals. This space contains those orbitals which are linear combinations of the orbitals occupied in the constituent atoms of the molecule and those additional orbitals with the same principal quantum numbers as the occupied orbitals. For an AB_2 triatomic composed of first row atoms, each atom has five accessible orbitals, the 1s, 2s, $2p_x$, $2p_y$, and $2p_z$. The non-virtual space therefore contains fifteen orbitals which are linear combinations of the fifteen accessible atomic orbitals. Of these, the core orbitals are those which are practically

the same in both the atoms and the molecule; the remaining non-virtual orbitals are the valence (i.e., bonding, non-bonding, and anti-bonding) orbitals. The virtual space contains all other orbitals. The experience from diatomic molecules would indicate that a relatively small part of the MECE contribution arises from excitations into virtual orbitals. Rather, such excitations mainly serve to describe atomic-like correlations, which are fairly constant over the entire range of inter-nuclear separations.

The identification of the valence space for an MC-SCF calculation is desirable because the majority of critical molecular correlation effects reside within it. We further define valence configurations as those with all core orbitals fully occupied and all virtual orbitals unoccupied. The base configurations are usually those whose contribution varies most rapidly with internuclear geometry and are always valence configurations. Since the MC-SCF approach optimizes the molecular orbitals and configuration mixing coefficients simultaneously, a calculation based only on a careful selection of valence configurations still yields the important portion of the correlation energy. The remainder of the correlation energy is assumed not to vary with valence state or with the geometry of a given state in the neighborhood of its equilibrium geometry and away from near degeneracies with states of the same symmetry and multiplicity.

In all of the states of NO_2 which we have considered, there are five orbitals which are invariably of core character. In terms of symmetry orbitals, they are $1\sigma_g$, $2\sigma_g$, $3\sigma_g$, $1\sigma_u$, and $2\sigma_u$ for linear geometries; they become $1a_1$, $2a_1$, $3a_1$, $1b_2$, and $2b_2$ for bent geometries. These correspond in a localized description to 1s atomic orbitals on each atom and 2s atomic orbitals on the oxygen atoms.

The role of the sixth lowest energy orbital, the $4a_1$ ($4\sigma_g$), merits further comment. Experience from MC-SCF calculations on first-row diatomics indicates that the core orbitals are the first four σ orbitals, accounting for most of the 1s and 2s character of the atoms. Correlation of these orbitals for purposes of consideration of differential atomic correlation affects the computed potential curves almost negligibly. If a similar situation prevails in NO_2, there will be six core orbitals.

However, a preliminary calculation clearly demonstrated that such is not the case. Initially the $4a_1$ orbital was held doubly occupied in all configurations used in the orbital optimization of the $\tilde{X}^2A_1$ and $^2B_2$ states. When excitations from this orbital were included, the adiabatic separation of the two states increased by 0.4 eV. Examination of basis set expansion coefficients of the $4a_1$ orbital in the two states reveals that in the $^2B_2$ state it is a nitrogen 2s core-like orbital; however, in the $^2A_1$

state, the nitrogen atom is strongly s-and-p hybridized and the $4a_1$ orbital is primarily describing N-O σ-bonding.

It might seem that this behavior could be rationalized in terms of the very different bond angles in the $^2A_1$ (134°) and $^2B_2$ (102°) states and subsequent changes in hybridization with bond angle. However, the $4a_1$ orbital retains its σ-bonding character in the $^2A_1$ state even as the bond angle is reduced to 105°; similarly, in the $^2B_2$ state, the $4a_1$ orbital is still mostly a nitrogen 2s atomic-like orbital for bond angles of 130° and greater. This behavior and the bonding in the various electronic states of NO_2 will be more critically examined in the future. At the present, though, suffice it to say that it is speculative in AB_2 (and ABC) triatomics to designate the first six (or more) molecular orbitals as core, and hence leave them uncorrelated in an MC-SCF calculation.

For a CI calculation based on SCF orbitals it is even less advisable to make such assumptions. In an MC-SCF calculation, the core orbitals are quite free of p_σ contamination because it is energetically favorable for the p_σ character to be rotated from the core orbitals into the valence orbitals during the orbital optimization. In the single configuration SCF method, however, the core orbitals often contain a substantial amount of p_σ character because the total electronic energy is invariant to a unitary transformation of the doubly occupied orbitals. Consequently, unless a suitable unitary transformation is made

before the CI is performed, it is likely that substantial amounts of valence correlation will be missed if any but the lowest orbitals are designated as core.

The previously described orbital partitioning has reduced the treatment of valence correlation in NO_2 to a 13 electron, 10 orbital problem. In principle, one would form all possible configurations of the desired orbital symmetry and multiplicity for this number of electrons and orbitals; the molecular orbitals and mixing coefficients would then be optimized in a single computation. In practice, the large number of configurations makes such an approach unfeasible. The OVC method effects a substantial reduction in the number of configurations by focusing only on the MECE contributions and ignoring for the most part differential atomic correlation. Usually, a maximum of 10 configurations is sufficient for first row diatomic applications. If the extension of the OVC method to triatomics were straightforward, the only modification necessary would be an increase in the maximum number of configurations to allow for the additional bond. However, there are conceptual complexities in the treatment of polyatomic, as opposed to diatomic, molecules and these are detailed in the next several paragraphs.

The principal difficulty is the existence of four distinct asymptotes (AB+C, BC+A, CA+B, A+B+C) for a general ABC triatomic, in contrast to the single A+B asymptote for an AB diatomic. No longer is the designation of the base

set of configurations (i.e., those configurations which allow dissociation into RHF fragments) unique; rather, it is dependent on the dissociation process of interest. For example, consider the RHF configuration of the $^2A_1$ state of NO_2

$$....(4a_1)^2(3b_2)^2(5a_1)^2(1b_1)^2(4b_2)^2(1a_2)^2(6a_1)^1$$

which cannot dissociate to RHF fragments for either the $NO(^2\Pi)$ + $O(^3P)$ or the $N(^4S)$ + $O_2(^3\Sigma_g^-)$ asymptotes. In order for dissociation into $NO(^2\Pi)$ + $O(^3P)$, configurations with three open shell orbitals, one of a' and two of a" symmetry, must be included in the base set of configurations. On the other hand, the $N(^4S)$ + $O_2(^3\Sigma_g^-)$ asymptote requires five open shell orbitals, and hence a different set of base configurations for dissociation in C_s symmetry. (Dissociation of the $^2A_1$ state to this asymptote is symmetry forbidden in C_{2v}.)

Similar problems arise when one attempts to identify the MECE configurations. Consider the various roles of a double excitation $\phi^2 \rightarrow \phi'^2$ within the valence space as an AB_2 triatomic dissociates into AB + B. At infinite separation of the two fragments, the possibilities are:

a. ϕ ends up with the AB fragment and ϕ' belongs to the B fragment, or vice-versa. Then this excitation is a triatomic MECE contributor since its effect vanishes for infinite separation of the atom and diatom.

b. Both ϕ and ϕ' belong to the atomic B fragment. The excitation in this case is a differential atomic (intra-atomic) correlation term.

c. Both ϕ and ϕ' belong to the AB fragment. Then the excitation is a differential diatomic correlation term, which has no counterpart for diatomic dissociation. The geometry dependence of the contribution of such terms to the correlation energy is quite large and its neglect does not appear to be justified.

Moreover, if the excitation belongs to case (a), for example, for AB + B dissociation, it may belong to case (b) or (c) for A + B_2 dissociation. Excitations from the valence space into the virtual space will also exhibit ambiguities in regard to classification into different types of correlation contributions.

Although some of the advantages of the OVC approach are lost for polyatomic molecules, the consequences are not great for this study. Our interest is in the potential energy hypersurfaces relatively near their minima, since we are attempting to treat the electronic spectroscopy and structure of NO_2. Thus, our configuration selection is concerned with insuring that the dominant correlation contributions are included near the equilibrium geometry of each state. It is not necessary to a priori identify the base configurations or distinguish MECE from intra-atomic or differential diatomic correlation contributions. We

shall continue to characterize the approach we have taken here as the OVC method, although it is not being applied in strictly the same manner as for diatomic molecules.

Details of Configuration Selection

At the time of this study, the program constraints at Argonne National Laboratory for a basis set of the size we employed were a maximum of 20 configurations for MC-SCF orbital optimization and a maximum of 99 configurations in a CI calculation. The procedure we have followed for each electronic state of NO_2 is to generate an OVC configuration list and an OVC-CI configuration list, of which the OVC list is a subset. The OVC list contains what we shall refer to as the dominant configurations, i.e., those configurations which are most important in describing electron distribution and correlation in the molecule. The molecular orbitals are optimized in an MC-SCF calculation using the OVC configuration list, yielding what we term the OVC wavefunction. When higher accuracy is desired, a CI calculation is performed using the OVC-CI configuration list and the OVC orbitals. The resulting wavefunction is referred to as the OVC-CI wavefunction.

The Restricted Hartree-Fock (RHF) configuration is by definition the most important configuration in the neighborhood of the equilibrium geometry; its normalized mixing coefficient is greater than 0.93 for all the states of NO_2 which have been examined. Identification of

additional dominant configurations is first made in terms of valence charge transfer excitations, which are best demonstrated in a linear molecule. Such excitations are by far the largest MECE contributors in diatomics, and are similarly important in NO_2, although they have not been specifically classed as MECE terms. The $^2\Pi_u$ state of NO_2 is used as an example to illustrate the origin of the term "charge transfer." Exclusive of the five core orbitals, the valence orbital occupation of the $^2\Pi_u$ RHF configuration is

$$(4\sigma_g)^2(3\sigma_u)^2(5\sigma_g)^0(4\sigma_u)^0(1\pi_u)^4(1\pi_g)^4(2\pi_u)^1.$$

The $4\sigma_g$ and $3\sigma_u$ orbitals account for the two N-O σ bonds and $5\sigma_g$ and $4\sigma_u$ are the corresponding anti-bonding σ orbitals. The $1\pi_u$ orbital is a delocalized bonding π orbital and $2\pi_u$ is the corresponding antibonding π orbital; $1\pi_g$ is non-bonding, having density only on the oxygen atoms in the absence of polarization functions in the basis set. The nodal characteristics of the orbitals are schematically illustrated in Figure 1.

Better than 80% of the valence correlation energy of this state is obtained within the following MC-SCF orbital occupancies:

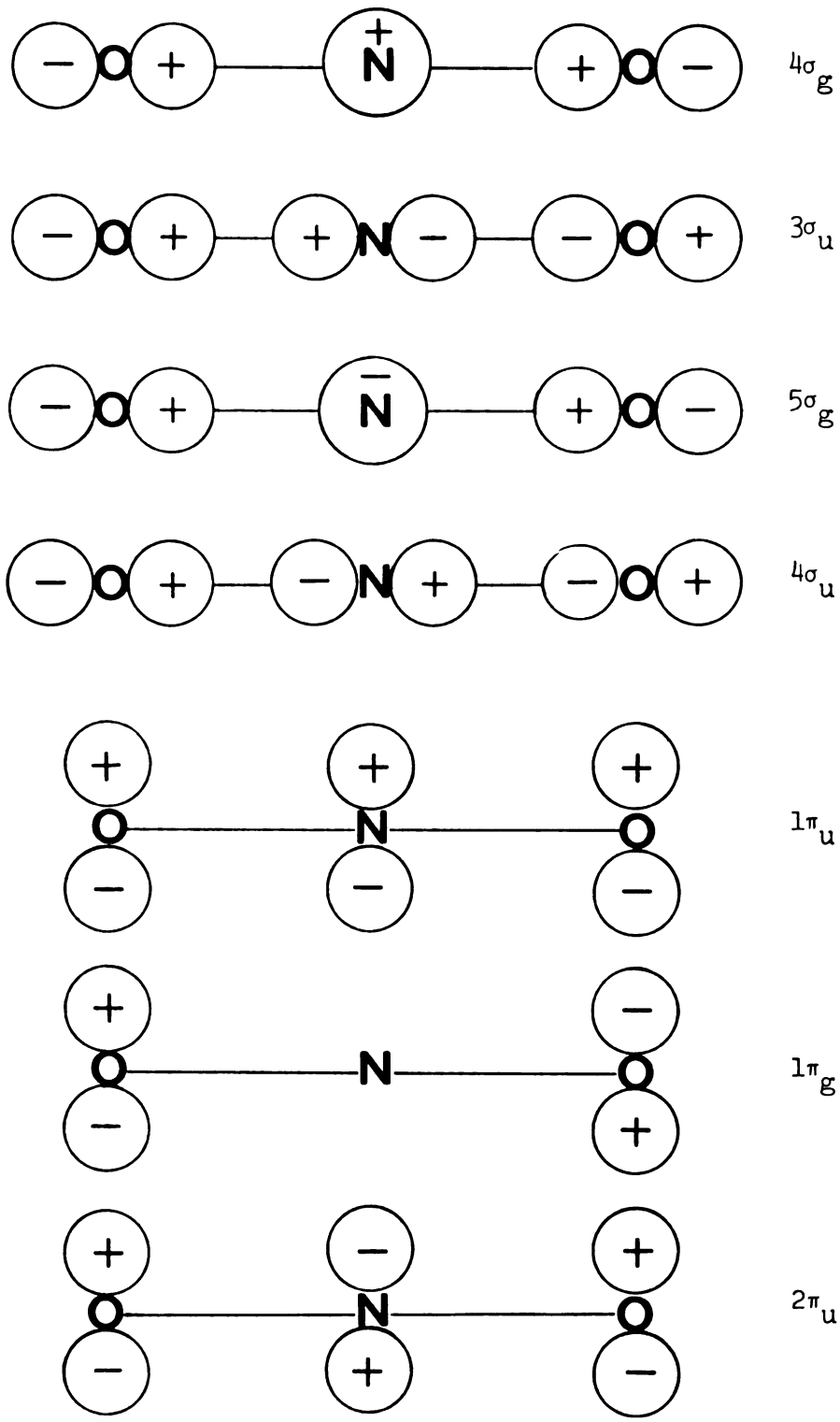

Fig. 1. The nodal structure of the valence molecular orbitals in linear NO_2.

	$4\sigma_g$	$3\sigma_u$	$5\sigma_g$	$4\sigma_u$	$1\pi_u$	$1\pi_g$	$2\pi_u$
(1)	2	2	0	0	4	4	1
(2)	2	0	2	0	4	4	1
(3)	2	0	0	2	4	4	1
(4)	0	2	2	0	4	4	1
(5)	2	2	0	0	2	4	3
(6)	2	1	0	1	3	4	2
(7)	1	2	1	0	3	4	2
(8)	2	2	0	0	4	2	3
(9)	2	1	1	0	4	3	2

The first is the RHF configuration. The next three correlate the σ bonds, the fifth correlates the π bond. The sixth and seventh simultaneously correlate a σ and a π bond and the final two allow for redistribution on charge within the valence orbitals. In each case, electron density (charge) is transferred <u>across</u> the bonds in the molecule in contrast to excitations which are primarily localized on a single center.

However, since the calculations were performed using (real) Gaussian basis functions, the π orbitals are two-fold degenerate rather than four-fold. Therefore, orbital occupancy 5, which is related to the RHF configuration by the double excitation $1\pi_u^2 \rightarrow 2\pi_u^2$, actually is spanned by four configurations: $1\pi_u^2(x) \rightarrow 2\pi_u^2(x)$, $1\pi_u^2(y) \rightarrow 2\pi_u^2(y)$, and $1\pi_u(x)1\pi_u(y) \rightarrow 2\pi_u(x)2\pi_u(y)$, which has two spin couplings. Also, any orbital occupancy with

more than one open shell can have the open shells coupled in various ways to give eigenfunctions of $\hat{S}^2$ and $\hat{S}_z$. The coupling is specified in vector addition fashion as the orbital occupancies are scanned from left to right. Orbital occupancy 7, for example, could give rise to as many as five open shells:

$$(4\sigma_g)^1\ (5\sigma_g)^1\ (1\pi_u(y))^1\ (2\pi_u(x))^1\ (2\pi_u(y))^1$$

and there are five possible ways to couple five open shells to give a doublet state.

The MC-SCF wavefunction, computed for the valence charge transfer excitations, gives a quite satisfactory qualitative description of electronic structure. As discussed in Appendix D, selection of the valence charge transfer configurations is well-defined for the ground states of polyatomic molecules such as HO_2, HONO, and CH_3NO, for which valence bond structures can be written. An exhaustive search of configuration lists is not necessary for an accurate description of electronic structure in these cases and this is a strong point in favor of the OVC approach, especially for large polyatomic molecules. Unfortunately, NO_2 does not have a satisfactory valence bond description and a more rigorous approach to configuration selection must be taken if the accuracy necessary for a spectral interpretation of NO_2 is to be achieved. We detail below the selection of the OVC and OVC-CI lists which are vital for this improved representation.

For reasons of economy, the OVC and OVC-CI configuration lists were optimized at a single geometry in each electronic state and then these lists were utilized for all the geometries considered in that state. Preliminary studies in a double-zeta quality basis set gave reasonable estimates of the equilibrium geometries in the states of interest and it was at these geometries that the configuration lists were determined. We further note that the configuration lists were optimized in this double-zeta basis set, rather than the extended basis set used for the actual construction of the potential energy surfaces.

Figure 2 displays a flow chart of the complete configuration selection and orbital optimization procedure. Although several individual steps are involved as depicted in the figure, many of them could be combined, eliminating intermediate operator intervention. The basic philosophy of the approach is to successively expand the configuration lists by examining various classes of configurations and retaining the most important configurations, as gauged by the magnitude of their mixing coefficients.

We identify four classes of configurations to be examined:

1. <u>The valence charge transfer (VCT) configurations</u>. These are specified in <u>a priori</u> fashion; the experience from studies as described in Appendix D is used as a guide to their selection.

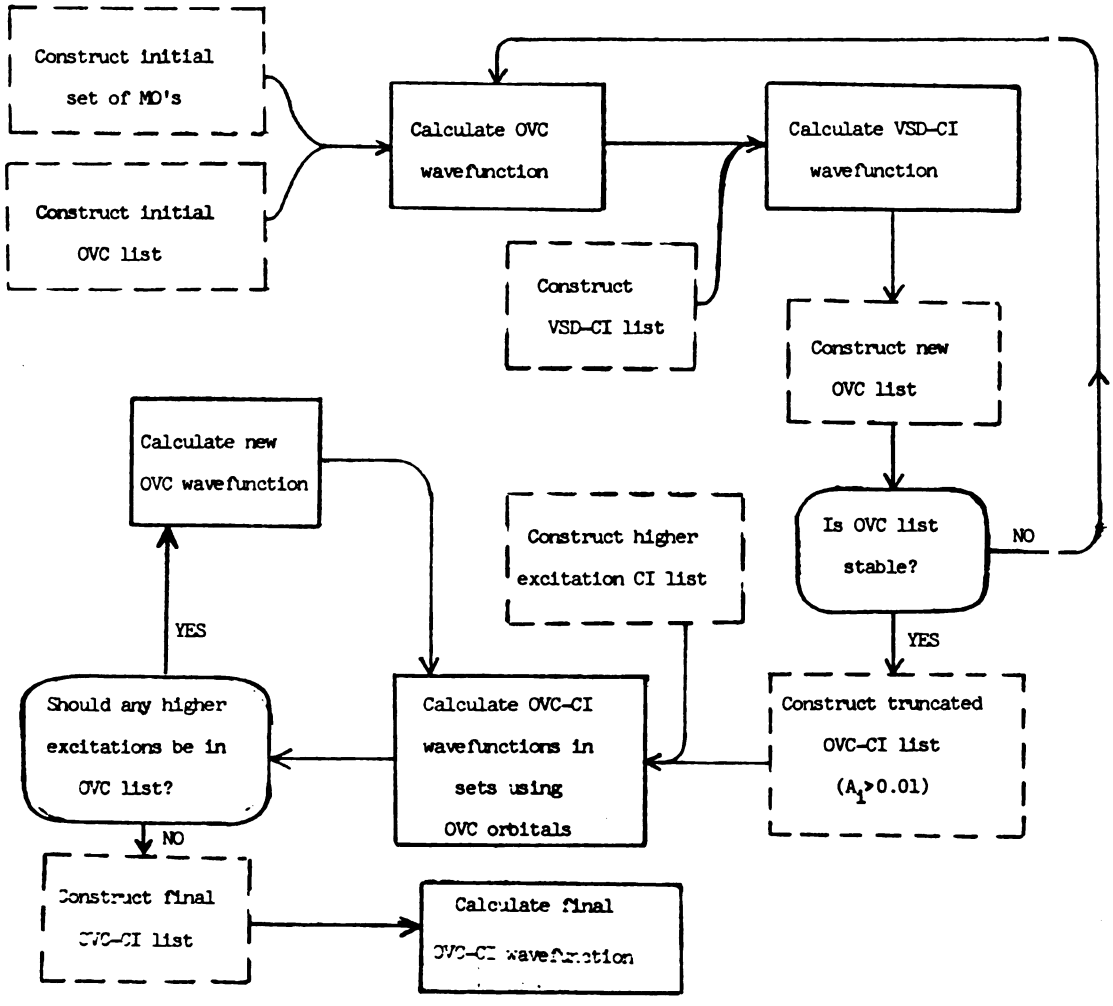

Fig. 2. Flow chart of the OVC and OVC-CI configuration selection and orbital optimization precedures.

2. Single and double excitations from the RHF configuration within the valence space. These comprise the "valence-singles-and-doubles" configuration interaction (VSD-CI) list and include the VCT configurations.
3. Triple and higher excitations within the valence space.
4. Single and double excitations from the valence space into the virtual space.

The initial step is to compute a CI wavefunction with the VSD-CI list using the orbitals from the original VCT MC-SCF calculation. On the basis of this wavefunction, the configurations with the largest mixing coefficients (usually A_k greater than 0.04) are collected into an initial OVC configuration list. A new MC-SCF wavefunction is computed for this list, followed by a VSD-CI on the new set of orbitals. In every case the OVC list was stable, i.e., those configurations with the largest mixing coefficients in the VSD-CI wavefunction are identical to the configurations which constitute the OVC list.

The next class of configurations to be examined is that of triple and higher excitations from the RHF configuration within the valence space. Rather than consider all possible excitations of this type (~3000 for a doublet state in C_{2v} symmetry), we have taken a modified approach. From the OVC configuration list of the $^2\Pi_u$ state of NO_2, given in Table I, we identify nine dominant σ orbital

TABLE I

$^2\Pi_u$ OVC CONFIGURATIONS AND MIXING COEFFICIENTS AT R=2.25 BOHRS, θ=180°

$4\sigma_g$	$3\sigma_u$	$5\sigma_g$	$4\sigma_u$	$1\pi_u^x$	$1\pi_g^x$	$2\pi_u^x$	$1\pi_u^y$	$1\pi_g^y$	$2\pi_u^y$	Spin-coupling	Mixing Coefficients
2	2	0	0	2	2	0	2	2	1		0.96285
2	2	0	0	2	1	1	2	1	2	0 0.5	0.11618
2	2	0	0	2	0	2	2	2	1		-0.11446
2	1	1	0	2	1	1	2	2	1	0 0.5 0 0.5	0.08986
2	2	0	0	0	2	2	2	2	1		-0.07091
2	2	0	0	1	2	1	1	2	2	0 0.5	0.06519
2	1	0	1	1	2	1	2	2	1	0 0.5 0 0.5	0.06496
1	2	1	0	1	2	1	2	2	1	0 0.5 0 0.5	-0.05830
2	1	1	0	2	2	0	2	1	2	0 0.5	-0.05794
1	1	1	1	2	2	0	2	2	1	0 0.5 0 0.5	-0.05655
2	1	0	1	2	2	0	1	2	2	0 0.5	-0.04915
2	2	0	0	1	1	2	2	1	2	0 0.5	0.04631
2	0	2	0	2	2	0	2	2	1		-0.04494
1	2	1	0	2	2	0	1	2	2	0 0.5	0.04251
0	2	2	0	2	2	0	2	2	1		-0.04014
2	0	0	2	2	2	0	2	2	1		-0.03927
1	2	1	0	1	2	1	2	2	1	1 0.5 0 0.5	-0.03611
1	2	0	1	2	1	1	2	2	1	0 0.5 0 0.5	-0.03174

occupancies: $(4\sigma_g)^2(3\sigma_u)^2$, $(4\sigma_g)^2(3\sigma_u)^1(5\sigma_g)^1$, $(4\sigma_g)^2(3\sigma_u)^1(4\sigma_u)^1$, etc. All possible electron rearrangements within the π orbitals for each of the dominant σ orbital occupancies are formed; all which are single or double excitations from the RHF configuration are removed, since they have already been treated.in class 2. The rationalization of the restriction of class 3 configurations is that since the occupied σ orbitals are much lower in energy than the π orbitals, any configuration involving extreme disruption of the σ orbitals (e.g., $(4\sigma_g)^1(5\sigma_g)^1(4\sigma_u)^2$ is going to be so highly excited that its effect in a CI will be negligible. Effectively what is achieved is a full π electron CI for a well correlated σ core.

Slight modifications are necessary for the nonlinear electronic states, as the distinction of σ and π orbitals is no longer rigorous. These modifications are minimal for quasilinear cases, such as the $^2A_1$ ground state of NO_2, where the genealogy of the orbitals for the bent geometries is easily traced to the linear precursors. For strongly bent states, such as the $^2B_2$ and $^2A_2$ states, the individual orbital structures must be more carefully examined in order to distinguish those responsible for σ-bonding, but the task is not difficult.

Despite the reduction in number of class 3 configurations to be considered, there are still too many (~150) to be examined in a single calculation with our existing codes. We therefore truncate the VSD-CI list to

those configurations with normalized mixing coefficients of 0.01 or greater (~40 configurations). To these are added various sets of the triple and higher excitations in a series of CI calculations based on the OVC orbitals. The final OVC-CI list is selected by scanning the various CI runs, including the VSD-CI calculation, and choosing those configurations predicted to have the largest mixing coefficients up to the limit of 99 configurations. In a few instances triple excitations were found to be important enough to warrant their inclusion in the OVC orbital optimization. The best example is in the $^2B_2$ state where a triple excitation has a very substantial mixing coefficient of 0.07718.

Finally, class 4 of configurations, single and double excitations from the valence space into the virtual space, must be addressed. The types of excitations which were examined are: (1) single excitations, $\phi \rightarrow \chi$; (2) diagonal double excitations, $\phi^2 \rightarrow \chi^2$; and (3) double excitations, $\phi\phi' \rightarrow \phi''\chi$, in which one electron is excited into the virtual space, while another is rearranged within the valence space. Our investigation was limited to the lowest energy virtual orbitals, namely $5\sigma_u$ and $3\pi_u$ for linear geometries; the former becomes $6b_2$ for bent geometries, while the latter splits into $8a_1$ and $3b_1$. For this particular investigation, an orbital basis was calculated in MC-SCF fashion for the most important 15 OVC configurations, plus the excitations $3\sigma_u^2 \rightarrow 5\sigma_u^2$, $4\sigma_g^2 \rightarrow 5\sigma_u^2$,

$1\pi_u^2 \rightarrow 3\pi_u^2$, and $1\pi_g^2 \rightarrow 3\pi_u^2$, which optimize the virtual orbitals. This was followed by a CI calculation using this orbital basis, including the most important valence configurations (again those with mixing coefficients greater than 0.01) and the class 4 excitations under investigation. For the $^2\Pi_u$ state, no configurations involving the $5\sigma_u$ orbital were significant contributors to the wavefunction. This is undoubtedly due to the high energy character of this orbital, which results from a complicated nodal structure along the internuclear axis. Consequently, the $5\sigma_u$ orbital was deleted from further consideration.

The magnitude of the energy lowering of the remaining virtual configurations was nearly 0.02 hartrees, but constant to 5×10^{-4} hartrees over the range of bond lengths 2.25 to 2.45 bohrs. A similar study for the $^2A_1$ ground state gave an equally constant energy lowering for bond length variation, and the magnitude of the virtual correlation energy was within 0.002 hartrees (0.05 eV) of that found for the $^2\Pi_u$ state.

In the final calculations used to construct the potential surfaces, class 4 configurations were neglected. As support for this simplification we note that:

1. The magnitude of virtual correlation appears nearly constant with geometry variation near the equilibrium geometry. Thus the characteristics of the potential surface of a given state are essentially independent of virtual correlation.

2. The magnitude of virtual correlation does not appear to vary substantially from state to state. Thus the electronic spectroscopy of the molecule, which reflects the energy separation of the various electronic states, is nearly independent of virtual correlation.

In order to present a more quantitative illustration of the configuration selection process, we cite some details for the $\tilde{X}^2A_1$ ground state. For this state only, the OVC-CI configuration list was actually determined in the extended double-zeta-plus-polarization quality basis set used for the generation of the potential surfaces. The optimization was performed for a bond length of 2.2552 bohrs and an angle of 134°, the experimental equilibrium geometrical parameters; the OVC wavefunction at this geometry is given in Table II.

The energy of the $^2A_1$ RHF configuration is -204.0607 hartrees for the OVC orbitals. We note that this is <u>not</u> the $^2A_1$ SCF energy in this basis since the orbitals were determined for a set of configurations rather than the single RHF configuration; in the double-zeta basis, the SCF energy is 0.01 hartrees lower than the energy of the RHF configuration calculated for the OVC orbitals. The OVC energy is -204.2080 hartrees; the energy for the 99 most important VSD-CI configurations, based on the OVC orbitals, is lowered to -204.2309 hartrees. For the OVC-CI wavefunction, triple and higher excitation configurations were also

TABLE II

$^2A_1$ OVC CONFIGURATIONS AND MIXING COEFFICIENTS AT R=2.2552 BOHRS, θ=134°

$4a_1$	$3b_2$	$7a_1$	$5b_2$	$5a_1$	$4b_2$	$6a_1$	$1b_1$	$1a_2$	$2b_1$	Spin-coupling	Mixing Coefficients
2	2	0	0	2	2	1	2	2	0		0.96242
2	2	0	0	2	2	1	2	0	2		-0.11981
2	2	0	0	2	1	2	2	1	1	1 0.5	0.10787
2	2	0	0	2	1	2	2	1	1	0 0.5	-0.08134
2	2	0	0	2	2	1	0	2	2		-0.07492
2	1	1	0	2	2	1	2	1	1	0 0.5 1 0.5	0.06963
2	1	0	1	2	2	1	1	2	1	0 0.5 1 0.5	-0.05926
2	1	1	0	2	1	2	2	2	0	0 0.5	-0.05901
1	1	1	1	2	2	1	2	2	0	0 0.5 0 0.5	-0.05811
2	2	0	0	1	2	2	1	2	1	0 0.5	-0.05527
2	2	0	0	2	1	2	1	1	2	1 0.5	-0.05525
2	1	0	1	1	2	2	2	2	0	0 0.5	0.05144
1	2	1	0	2	2	1	1	2	1	0 0.5 1 0.5	0.05031
0	2	2	0	2	2	1	2	2	0		-0.05017
2	2	0	0	1	2	2	1	2	1	1 0.5	0.04785
2	0	0	2	2	2	1	2	2	0		-0.04095
2	1	1	0	2	2	1	2	1	1	0 0.5 0 0.5	-0.03816
2	0	2	0	2	2	1	2	2	0		-0.03756

included; the 99 most important lower the energy to -204.2422 hartrees. The total number of class 2 and class 3 valence configurations is 282, of which only 99 were included in the OVC-CI wavefunction. The effect of the truncation was examined in the following manner: the OVC-CI list was temporarily reduced to the 49 most important configurations (E=-204.2330 hartrees) and this list was combined with sets of the 183 omitted valence configurations in a series of CI calculations. Under the assumption of pairwise additivity of the neglected sets, the final energy would have been improved by only 0.004 hartrees for the entire 282 valence configurations rather than the more restricted set of 99 configurations. All of the information of this paragraph is summarized in Table III.

On the basis of these numbers, we estimate for the $\tilde{X}^2A_1$ state of NO_2 that: (1) the 18 configuration OVC wavefunction accounts for about 80% of the valence correlation energy; (2) the 99 configuration OVC-CI wavefunction accounts for greater than 95% of the valence correlation energy; and (3) triple and higher excitations from the RHF configuration contribute 6 to 8% of the valence correlation energy. It is important to note our definition of valence correlation energy as that portion of the correlation energy obtained <u>within</u> the set of orbitals designated as valence. Although only a fraction of the <u>total</u> correlation is accounted for, it is that portion of the correlation energy

TABLE III

ENERGIES OF VARIOUS $\tilde{X}^2A_1$ WAVEFUNCTIONS IN THE [4s3pld] BASIS

Wavefunction Description	Energy (In Hartrees)
RHF Configuration from OVC Orbitals	-204.0607
SCF (estimated)	-204.07
OVC (18 Configurations)	-204.2080
VSD-CI (99 Configurations)	-204.2309
OVC-CI (49 Configurations)	-204.2330
OVC-CI (99 Configurations)	-204.2422
Full Valence OVC-CI (282 Configurations, estimated)	-204.246

we have obtained which is crucial for a proper description of the electronic states.

The OVC configuration lists and mixing coefficients are given for the $^2B_2$, $^2A_2$, $^4B_2$, $^4A_2$, and $^2\Sigma_g^+$ states in Tables IV through VIII.

The Choice of the Basis Set and the Accuracy of the Computed Excitation Energies

The double-zeta basis set used in the preliminary calculations was the Dunning [4s3p] contraction [22] of the (9s5p) primitive Gaussian basis set of Huzinaga [23]. In this basis the SCF energy of the ground state at its experimental geometry is -203.9560 hartrees. A comparison

TABLE IV

$^2B_2$ OVC CONFIGURATIONS AND MIXING COEFFICIENTS AT R=2.40 BOHRS, θ=100°

$4a_1$	$3b_2$	$7a_1$	$5b_2$	$5a_1$	$4b_2$	$6a_1$	$1b_1$	$1a_2$	$2b_1$	Spin-coupling	Mixing Coefficients
2	2	0	0	2	1	2	2	2	0		0.93732
2	2	0	0	1	2	2	2	1	1	1 0.5	-0.19274
2	2	0	0	1	2	2	2	1	1	0 0.5	0.16026
2	2	0	0	2	1	2	0	2	2		-0.09914
2	2	0	0	2	1	2	2	0	2		-0.09048
2	2	0	0	1	2	2	1	1	2	1 0.5	0.07718
2	1	0	1	2	1	2	1	2	1	0 0.5 1 0.5	-0.06895
2	1	1	0	1	2	2	2	2	0	0 0.5	0.06826
2	1	1	1	2	1	1	2	2	0	1 0.5 1 0.5	0.06163
2	2	2	0	2	1	0	2	2	0		-0.05862
2	2	1	0	2	1	1	1	2	1	1 0.5 1 0.5	-0.05635
2	0	0	2	2	1	2	2	2	0		-0.05504
2	1	1	0	2	1	2	2	1	1	0 0.5 1 0.5	0.05381
2	2	0	1	1	2	1	2	2	0	1 0.5	0.05306
2	2	0	0	1	2	2	1	1	2	0 0.5	-0.04603
2	1	0	1	2	1	2	1	2	1	0 0.5 0 0.5	0.04142
2	2	0	1	2	1	1	2	1	1	1 0.5 1 0.5	0.03754
2	1	1	0	1	2	2	2	0	2	0 0.5	-0.02848

TABLE V

$^2A_2$ OVC CONFIGURATIONS AND MIXING COEFFICIENTS AT R=2.40 BOHRS, θ=110°

$4a_1$	$3b_2$	$7a_1$	$5b_2$	$5a_1$	$4b_2$	$6a_1$	$1b_1$	$1a_2$	$2b_1$	Spin-coupling	Mixing Coefficients
2	2	0	0	2	2	2	2	1	0		0.94771
2	2	0	0	2	2	2	1	1	1	0 0.5	-0.18062
2	2	0	0	2	2	2	1	1	1	1 0.5	0.14193
2	2	0	0	2	2	2	0	1	2		-0.13609
2	1	1	1	2	2	1	2	1	0	1 0.5 0 0.5	-0.07332
2	1	0	1	2	2	2	1	1	1	0 0.5 1 0.5	0.06337
2	2	1	0	2	2	1	1	1	1	0 0.5 1 0.5	-0.06239
2	2	2	0	2	2	0	2	1	0		-0.05798
2	1	1	0	2	2	2	1	2	0	0 0.5	-0.05091
2	0	0	2	2	2	2	2	1	0		-0.05090
2	1	1	0	2	2	2	2	0	1	0 0.5	0.04887
2	2	0	1	2	2	1	2	0	1	0 0.5	-0.03772
2	2	0	1	2	2	1	1	2	0	0 0.5	0.03762
2	0	2	0	2	2	2	2	1	0		-0.03705
2	1	0	1	2	2	2	1	1	1	0 0.5 0 0.5	0.03476
2	2	1	0	2	2	1	1	1	1	0 0.5 0 0.5	-0.03050

TABLE VI

$^4B_2$ OVC CONFIGURATIONS AND MIXING COEFFICIENTS AT R=2.45 BOHRS, θ=125°

$4a_1$	$3b_2$	$7a_1$	$5b_2$	$5a_1$	$4b_2$	$6a_1$	$1b_1$	$1a_2$	$2b_1$	Spin-coupling	Mixing Coefficients
2	2	0	0	2	2	1	2	1	1	1 1.5	0.96061
2	2	0	0	2	1	2	1	2	1	1 1.5	-0.18625
2	2	0	0	1	2	2	1	1	2	1 1.5	0.09478
2	1	1	0	2	2	1	1	2	1	0 0.5 1 1.5	-0.07884
2	1	1	0	2	1	2	2	1	1	0 0.5 1 1.5	-0.07134
2	1	0	1	1	2	2	2	1	1	0 0.5 1 1.5	0.06967
1	2	1	0	2	2	1	1	1	2	0 0.5 1 1.5	0.06381
2	1	0	1	2	2	1	1	1	2	0 0.5 1 1.5	-0.05907
2	2	0	1	2	2	0	1	2	1	1 1.5	-0.05500
0	2	2	0	2	2	1	2	1	1	1 1.5	-0.05497
2	0	0	2	2	2	1	2	1	1	1 1.5	-0.04642
2	0	2	0	2	2	1	2	1	1	1 1.5	-0.04043

TABLE VII

$^4A_2$ OVC CONFIGURATIONS AND MIXING COEFFICIENTS AT R=2.45 BOHRS, θ =115°

$4a_1$	$3b_2$	$7a_1$	$5b_2$	$5a_1$	$4b_2$	$6a_1$	$1b_1$	$1a_2$	$2b_1$	Spin-coupling	Mixing Coefficients
2	2	0	0	2	1	1	2	2	1	1 1.5	0.98598
2	1	0	1	1	1	2	2	2	1	0 0.5 1 1.5	-0.06620
2	1	0	1	2	1	1	1	2	2	0 0.5 1 1.5	0.06517
0	2	2	0	2	1	1	2	2	1	1 1.5	-0.06205
2	1	1	0	2	1	1	2	1	2	0 0.5 1 1.5	-0.06168
2	0	0	2	2	1	1	2	2	1	1 1.5	-0.05644
2	2	0	0	1	1	2	1	2	2	1 1.5	0.05139
1	2	1	0	2	1	1	1	2	2	0 0.5 1 1.5	-0.05091
2	1	1	0	1	2	1	2	2	1	0 0.5 1 1.5	-0.04286
2	0	2	0	2	1	1	2	2	1	1 1.5	-0.03618

TABLE VIII

$^2\Sigma_g^+$ OVC CONFIGURATIONS AND MIXING COEFFICIENTS AT R=2.45 BOHRS, θ=180°

$4\sigma_g$	$3\sigma_u$	$5\sigma_g$	$4\sigma_u$	$1\pi_u^x$	$1\pi_g^x$	$2\pi_u^x$	$1\pi_u^y$	$1\pi_g^y$	$2\pi_u^y$	Spin-coupling	Mixing Coefficients
2	2	1	0	2	2	0	2	2	0		0.95110
2	2	1	0	2	0	2	2	2	0		-0.11080
2	2	1	0	2	2	0	2	0	2		-0.10670
2	2	1	0	0	2	2	2	2	0		-0.09145
2	2	1	0	2	1	1	2	1	1	1 0.5 1 0.5	-0.08590
2	2	1	0	2	2	0	0	2	2		-0.08521
2	2	1	0	1	2	1	1	2	1	1 0.5 1 0.5	-0.07689
2	1	1	1	2	2	0	2	2	0	0 0.5	-0.07611
2	2	0	1	2	2	0	2	1	1	1 0.5	0.07600
2	2	1	0	2	1	1	2	1	1	1 0.5 0 0.5	0.07319
2	2	0	1	2	1	1	2	2	0	1 0.5	0.07283
2	1	2	0	2	2	0	2	1	1	1 0.5	-0.06010
2	1	1	1	2	2	0	1	2	1	1 0.5 1 0.5	-0.05858
2	0	1	2	2	2	0	2	2	0		-0.05194
2	1	2	0	2	1	1	2	2	0	0 0.5	0.05071
1	2	2	0	2	2	0	1	2	1	0 0.5	-0.04833
1	2	2	0	1	2	1	2	2	0	0 0.5	-0.04774
2	1	2	0	2	1	1	2	2	0	1 0.5	-0.04405
2	1	2	0	2	2	0	2	1	1	0 0.5	0.04153

with the results of Burnelle and Dressler [12] amply demonstrates the efficacy of the optimized Dunning contraction. These authors also contracted the Huzinaga basis to [4s3p] but in an ad hoc fashion; the energy of -203.8857 hartrees which they obtained is more than 0.07 hartrees above that for the optimized contraction and is indicative of the sensitivity of the energy to the contraction scheme.

The SCF energy obtained in the [4s3p] basis is some 0.164 hartrees from the Hartree-Fock limit of -204.12 hartrees as estimated by Schaefer and Rothenberg [24]. However, these authors demonstrated that allocation of a full set of single component Cartesian d-functions to each nuclear center lowers the SCF energy more than 0.12 hartrees over that obtained for the [4s2p] Dunning contraction [22]. Since the [4s2p] contraction is about 0.01 hartrees inferior to the [4s3p] contraction for NO_2, it is expected that the [4s3p] basis augmented with d-functions should be no further than 0.05 hartrees from the estimated Hartree-Fock limit. Such a basis, hereafter referred to as [4s3p1d] or simply 431, is the one used here for all reported calculations.

Due to the relative insensitivity of the energy to the choice of orbital exponent, no attempt was made to optimize the exponents of the d-functions; rather the exponent was chosen as 1.0 for the nitrogen atom and 1.35 for the oxygen atoms. The former is close to the optimum value found by Dunning in SCF calculations on the nitrogen

molecule [25] and the latter represents a reasonable scaling of the nitrogen exponent.

A comparison of the OVC results in the [4s3p] and [4s3pld] basis sets in Table IX reveals that the computed transition energies between the ground state and the various excited states are increased in every case in going to the larger basis. The magnitude of this effect ranges from about 0.2 eV for the $^2B_2 - \tilde{X}^2A_1$ separation to nearly 0.8 eV in the case of $^4B_2 - \tilde{X}^2A_1$.

The energies that were obtained using the [4s3pld] basis set at all geometries for the states considered here are given in Tables X through XVI for the $\tilde{X}^2A_1$, $^2B_1(^2\Pi_u)$, $^2B_2$, $^2A_2$, $^4B_2$, $^4A_2$, and $^2\Sigma_g^+$ states, respectively. In all cases the iterative OVC process was continued until the energy had converged to 1×10^{-5} hartrees. Much of this information is summarized in Figure 3 where the energy variation with bond angle is depicted for the optimal bond length of each state.

Computed bond angles are little different in the [4s3p] and [4s3pld] basis sets, generally agreeing to within 3°. However, the bond lengths are considerably shortened when the d-functions are added to the basis. For each state, the [4s3pld] basis gives a computed equilibrium bond length 0.10 ± 0.02 bohrs shorter than for the [4s3p] basis. The same trend was noted for the ground state of O_3 [26] in a calculation similar in approach to this one.

TABLE IX

BASIS SET DEPENDENCE OF NO_2 STATE ENERGIES

STATE	BASIS SET*	E(SC)**	E(OVC)**	GEOMETRY***
$^2A_1$	43	-203.9486	-204.1078	R=2.25, θ=134°
	431	-204.0607	-204.2080	
$^2B_2$	43	-203.8808	-204.0729	R=2.40, θ=105°
	431	-203.9841	-204.1640	
$^2A_2$	43	-203.9053	-204.0693	R=2.40, θ=110°
	431	-203.9988	-204.1550	
$^2B_1$	43	-203.9029	-204.0753	R=2.25, θ=180°
	431	-204.0042	-204.1639	
$^4B_2$	43	-203.8961	-203.9924	R=2.40, θ=125°
	431	-203.9701	-204.0634	
$^4A_2$	43	-203.9226	-203.9832	R=2.40, θ=110°
	431	-204.0078	-204.0638	
$^2\Sigma_g^+$	43	-203.7326	-203.9370	R=2.40, θ=180°
	431	-203.8169	-204.0101	

*The [4s3p] basis set contraction of Dunning [22] is designated 43, while 431 denotes the 43 basis augmented with d-functions.

**E(SC) is the energy of the RHF configuration in hartrees for the OVC wavefunction and is generally about 0.01 hartrees above the SCF energy of that configuration for the same geometry. E(OVC) is the energy of the OVC wavefunction.

***The geometries were chosen to be near the equilibrium geometry for each state. The bond lengths are expressed in bohrs.

TABLE X

THE $^2A_1$ ELECTRONIC ENERGY SURFACE AND DIPOLE MOMENT*

R	θ	E(SC)	E(OVC)	E(OVC-CI)	μ(OVC)	μ(OVC-CI)
2.35	105	-203.97698	-204.14524		0.2775	
2.40	110	-203.98714	-204.16501		0.2344	
2.30	115	-204.02482	-204.18193		0.2543	
2.35	115	-204.01486	-204.17918		0.2322	
2.35	120	-204.02601	-204.18900		0.2107	
2.3052	124	-204.04326	-204.19897		0.2024	
2.25	125	-204.05424	-204.20196		0.2142	
2.2552	129	-204.05816	-204.20597	-204.24033	0.1869	0.1852
2.3052	129	-204.04846	-204.20331	-204.23959	0.1732	0.1722
2.20	130	-204.06434	-204.20434	-204.23663	0.1931	0.1907
2.35	130	-204.03701	-204.19805	-204.23604	0.1554	0.1551
2.2052	134	-204.06649	-204.20674	-204.23907	0.1647	0.1617
2.2552	134	-204.06069	-204.20795	-204.24220	0.1519	
2.3052	134	-204.05043	-204.20462	-204.24075	0.1433	0.1416
2.3552	134	-204.03636	-204.19756	-204.23560	0.1318	0.1309
2.2552	139	-204.06031	-204.20704	-204.24107	0.1206	0.1175
2.3052	139	-204.04962	-204.20329	-204.23918	0.1119	0.1094
2.3552	139	-204.03530	-204.19585	-204.23370	0.1039	0.1018
2.20	140	-204.06638	-204.20550	-204.23737	0.1202	0.1168
2.2552	144	-204.05716	-204.20359	-204.23734	0.0863	0.0826
2.3052	144	-204.04640	-204.19964	-204.23529	0.0803	0.0770
2.25	155	-204.04346	-204.18884		0.0143	
2.25	165	-204.02440	-204.16961		-0.0351	

*The dipole moment is expressed in atomic units; one atomic unit of dipole moment is equal to 2.54 debye.

TABLE XI

THE $^2B_1(^2\Pi_u)$ ELECTRONIC ENERGY SURFACE AND DIPOLE MOMENT

R	θ	E(SC)	E(OVC)	E(OVC-CI)	μ(OVC)	μ(OVC-CI)
2.2552	134	-203.95197	-204.11862		0.1742	
2.3052	134	-203.94883	-204.12183		0.1573	
2.3552	134	-203.94177	-204.12089		0.1402	
2.2552	144	-203.97412	-204.13785		0.1464	
2.25	155	-203.99066	-204.15170		0.1097	
2.25	165	-203.99955	-204.15961		0.0703	
2.25	170	-204.00210	-204.16201		0.0459	
2.30	170	-203.99453	-204.16078		0.0433	
2.25	175	-204.00637	-204.16343		0.0231	
2.30	175	-203.99592	-204.16204		0.0217	
2.25	179	-204.00414	-204.16389		0.0050	
2.20	180	-204.00745	-204.16071	-204.17685	0.0	0.0
2.25	180	-204.00415	-204.16390	-204.18115	0.0	0.0
2.30	180	-203.99637	-204.16246	-204.18083	0.0	0.0
2.35	180	-203.98500	-204.15722	-204.17676	0.0	0.0
R_1	R_2^*					
2.21	2.33	-203.99994	-204.16123	-204.17878	0.1048	0.1039
2.15	2.39	-203.99508	-204.15331	-204.17047	0.2129	0.2109

*The bond angle is 180° for the final two entries of this table.

TABLE XII

THE $^2B_2$ ELECTRONIC ENERGY SURFACE AND DIPOLE MOMENT

R	θ	E(SC)	E(OVC)	E(OVC-CI)	μ(OVC)	μ(OVC-CI)
2.35	95	-203.99417	-204.16177		0.2302	
2.40	95	-203.98715	-204.16245	-204.19456	0.2360	0.2271
2.45	95	-203.97661	-204.15971	-204.19326	0.2406	0.2299
2.30	100	-204.00032	-204.16273		0.1801	
2.35	100	-203.99612	-204.16614	-204.19741	0.1861	0.1797
2.40	100	-203.98789	-204.16562	-204.19830	0.1905	
2.45	100	-203.97635	-204.16186	-204.19593	0.1966	0.1865
2.30	105	-203.99807	-204.16271	-204.19310	0.1319	0.1272
2.35	105	-203.99302	-204.16526	-204.19706	0.1373	0.1314
2.40	105	-203.98391	-204.16402	-204.19721	0.1435	0.1356
2.45	105	-203.97184	-204.15968	-204.19424	0.1483	0.1388
2.50	105	-203.95689	-204.15278		0.1503	
2.35	110	-203.98574	-204.16014	-204.19239	0.0849	0.0800
2.40	110	-203.97634	-204.15858		0.0897	
2.45	110	-203.96386	-204.15400	-204.18895	0.0936	0.0867
2.30	115	-203.98036	-204.14948		0.0248	
2.35	115	-203.97480	-204.15149		0.0299	
2.40	115	-203.96539	-204.14991		0.0342	
2.35	120	-203.96070	-204.13983		-0.0269	
2.3052	124	-203.95222	-204.12654		-0.0759	
2.3052	129	-203.93264	-204.10987		-0.1336	
2.35	130	-203.92442	-204.10889		-0.1394	
2.2552	134	-203.91085	-204.08347		-0.1899	
2.3052	134	-203.91074	-204.09094		-0.1874	
2.3552	134	-203.90638	-204.09425		-0.1842	

TABLE XIII

THE $^2A_2$ ELECTRONIC ENERGY SURFACE AND DIPOLE MOMENT

R	θ	E(SC)	E(OVC)	E(OVC-CI)	μ(OVC)	μ(OVC-CI)
2.40	100	-203.98961	-204.14520		0.1166	
2.35	105	-204.00088	-204.15010		0.0593	
2.40	105	-203.99710	-204.15297		0.0682	
2.45	105	-203.98944	-204.15239	-204.17267	0.0780	0.0835
2.35	110	-204.00356	-204.15312		0.0081	
2.40	110	-203.99882	-204.15500	-204.17446	0.0164	0.0219
2.45	110	-203.99027	-204.15358	-204.17437	0.0269	0.0324
2.50	110	-203.97892	-204.14941	-204.17159	0.0372	0.0426
2.35	115	-204.00075	-204.15100		-0.0443	
2.40	115	-203.99531	-204.15231		-0.0349	
2.45	115	-203.98631	-204.15042		-0.0245	
2.40	125	-203.97688	-204.13546		-0.1408	
2.35	130	-203.96829	-204.12090		-0.2022	
2.3052	134	-203.95615	-204.10340		-0.2501	

TABLE XIV

THE $^4B_2$ ELECTRONIC ENERGY SURFACE AND DIPOLE MOMENT

R	θ	E(SC)	E(OVC)	E(OVC-CI)	μ(OVC)	μ(OVC-CI)
2.45	120	-203.96357	-204.06275		0.0622	
2.40	125	-203.97006	-204.06340		0.0451	
2.45	125	-203.96538	-204.06368		0.0380	
2.50	125	-203.95775	-204.06110		0.0307	
2.40	130	-203.96961	-204.06236		0.0225	
2.45	130	-203.96473	-204.06236		0.0173	
2.40	180	-203.88316	-203.98088	-203.99874	0.0	0.0
2.45	180	-203.88090	-203.98275	-204.00134	0.0	0.0
2.50	180	-203.87593	-203.98181	-204.00112	0.0	0.0

TABLE XV

THE $^4A_2$ ELECTRONIC ENERGY SURFACE AND DIPOLE MOMENT

R	θ	E(SC)	E(OVC)	E(OVC-CI)	μ(OVC)	μ(OVC-CI)
2.45	105	-204.00754	-204.06388		0.0278	
2.40	110	-204.00780	-204.06378		0.0171	
2.45	110	-204.00829	-204.06556		-0.0017	
2.50	110	-204.00696	-204.06485		-0.0262	
2.45	115	-204.00695	-204.06479		-0.0358	

TABLE XVI

THE $^2\Sigma_g^+$ ELECTRONIC ENERGY SURFACE AND DIPOLE MOMENT

R_1	R_2^*	E(SC)	E(OVC)	E(OVC-CI)	μ(OVC)	μ(OVC-CI)
2.40	2.40	-203.81693	-204.01006	-204.07646	0.0	0.0
2.45	2.45	-203.81271	-204.00953	-204.07942	0.0	0.0
2.50	2.50	-203.80041	-204.00621	-204.07815	0.0	0.0
2.40	2.52	-204.81304	-204.01040	-204.07987	0.1631	0.1594
2.34	2.58	-203.82215	-204.01385	-204.08127	0.3089	0.2990
2.28	2.64	-203.83535	-204.01896	-204.08267	0.4661	0.4481
2.22	2.70	-203.85030	-204.02471	-204.08315	0.6072	0.5828
2.16	2.76	-203.86488	-204.02984	-204.08203	0.7449	0.7184

*The bond angle is 180° for all entries in this table.

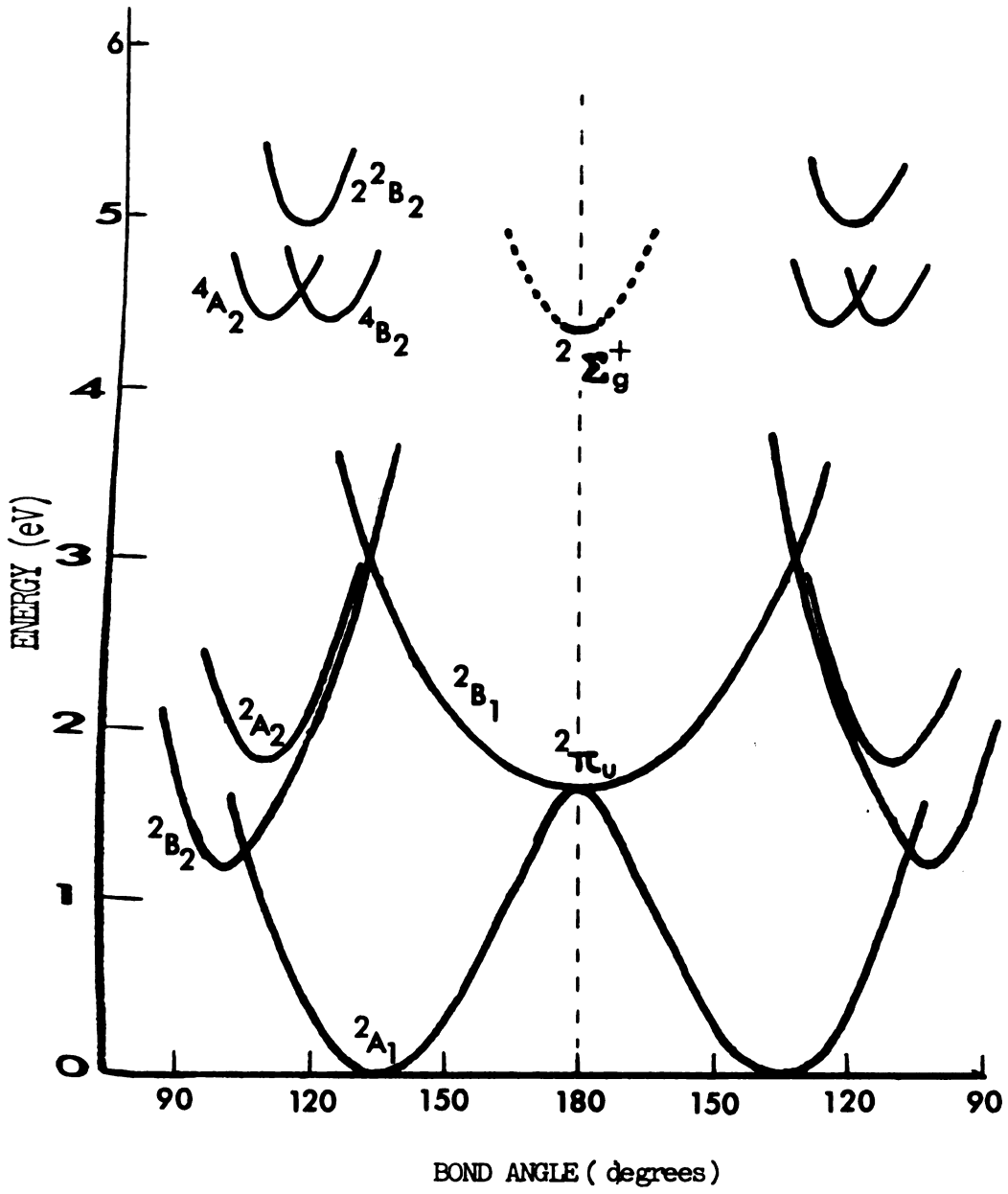

Fig. 3. Electronic energy as a function of bond angle for the low-lying electronic states of NO_2.

For the four lowest doublet states, the equilibrium bond length of each state has been used in the construction of the curves. The 2^2B_2 state was not included in this study; its position is known experimentally. The sharp rise in energy as the $^2\Sigma_g^+$ state is bent is based on SCF studies in a double-zeta quality basis set.

The results we present here represent one of the first attempts to produce well-correlated wavelengths in a double-zeta-plus-polarization quality basis set for several electronic states of a non-hydrogen containing polyatomic molecule. Unfortunately, excitation energies are not well characterized experimentally in NO_2 due to the spectroscopic complications. Consequently, not enough data is available for a rigorous assessment of the accuracy of the computed excitation energies. On the basis of the following analysis, however, we do not expect that the computed adiabatic transition energies for the 4 low-lying doublet states are more than 0.3 eV in error.

We first assume that the magnitude of the correlation energy contributed by the configurations we have considered would remain constant as the basis set is expanded from its present quality to a Hartree-Fock limit quality basis set; this approximation must be very good once the polarization functions have been included in the basis. Under this assumption, the error in the computed excitation energies is partitioned into a differential basis set error and a differential correlation error. The basis set error (the difference in the SCF energy of the RHF configuration computed in the [4s3pld] basis and for a Hartree-Fock limit basis) must be nearly the same for the $\tilde{X}^2A_1$, $^2B_1$, $^2B_2$, and $^2A_2$ states. We base this statement on the fact that the same orbitals are involved in forming the RHF configuration for each state. (Actually, a different orbital is involved

in the $^2B_1$ RHF configuration, which is related to the $^2A_1$ RHF configuration by the single excitation $6a_1 \rightarrow 2b_1$. However, the $6a_1$ and $2b_1$ orbitals are the degenerate components of the $1\pi_u$ orbital for linear geometries.)

The single configuration (SC) energies are very good approximations to the true SCF energies; from Table IX we see that the lowering of the SC energies for these excited states when the d-functions are added to the basis is equal to the $\tilde{X}^2A_1$ SC lowering to within 8% for the $^2B_2$ state, 10% for the $^2B_1$ state, and 17% for the $^2A_2$ state. The estimate of Schaefer and Rothenberg places the [4s3pld] basis within 0.05 hartrees of the Hartree-Fock limit. If in the approach to the HF limit from [4s3pld] there is the same percent variation as in adding the d-functions to the [4s3p] basis, the maximum differential basis set error will be 0.17 x 0.05 = 0.0085 hartrees = 0.22 eV for the low-lying doublet states. The d-functions have a profound effect on the basis because they make possible the accumulation of electron density on the central nitrogen atom in certain orbitals ($1\pi_g$, $1a_2$) which is symmetry forbidden in an sp-basis. The symmetry of the d-functions on the nitrogen atom is such that the $1a_2$ orbital will acquire some binding character as opposed to its essentially nonbonding character in the absence of polarization functions in the basis. Therefore, the prediction is for the SC energy of the $^2A_2$ state to be improved less than for the other three doublet states since the $1a_2$ orbital is only singly occupied

in its RHF configuration rather than doubly occupied as in the other states; the data of Table IX confirm this behavior. It is our anticipation that changes in the relative quality of the basis set for the low-lying doublet states will be significantly smaller once the d-functions have been included in the basis. Consequently, we have reduced our estimate of the differential basis set error to 0.15 eV.

The core orbitals are almost identical in each of the low-lying doublet states and we shall assume that differential core correlation is negligible. Still to be considered are the differential valence and virtual correlation effects. We have only treated the virtual correlation in a cursory fashion, but the 0.05 eV differential virtual correlation found for the $^2A_1$ and $^2B_1$ states seems to be a reasonable estimate and is the one we have chosen to use. Regarding the valence correlation, we previously argued that we have considered all the important configurations by virtue of what is essentially a full π CI for well-correlated σ core. Further, we showed that our restriction to 99 configurations rather than the full set of 282 missed at most 0.002 hartrees (0.11 eV) for the ground state. The effect of the truncation did not seem any more serious for the other states, as measured by the mixing coefficients of the configurations which were deleted. Since we are again considering a differential effect, the valence correlation error is likely to be much smaller than the $^2A_1$ truncation

error of 0.11 eV. However, we have omitted some "highly σ-excited" configurations. Although these are certainly very small contributors individually, there are a sizeable number so we retain 0.10 eV as the estimate of the differential valence correlation error.

Should all these errors act in the same direction, the total uncertainty in the computed (0-0) transition energies would be 0.3 eV for transitions between the four lowest doublet states of NO_2. These error bars should be extended by 0.1 or 0.2 eV for the vertical excitation energies because the configuration lists were optimized at the equilibrium geometry of each state. The OVC configurations for the excited states are still the most important at the equilibrium geometry of the ground state, for which the vertical excitation energies are computed; however, the OVC-CI lists could be slightly improved for this geometry by reoptimization. Consequently, the computed vertical excitation energies will tend to be a bit too high. The OVC-CI energy is at most 1 eV lower than the OVC energy; furthermore, we are considering the differential change of this 1 eV contribution due to the reoptimization of the OVC-CI list. To this we assign a maximum of 0.2 eV.

An Analysis of Previous Theoretical Calculations and a Comparison With the Present Results

Since the first ab initio calculations on NO_2 appeared in the literature in 1968, many of the succeeding

experimental studies have relied on the theoretical work for guidance in the interpretation of the data. The results of our investigation, however, are in enough cases sufficiently different to warrant a reassessment of those interpretations. We therefore feel that a critical analysis of the previous theoretical treatments is necessary in order to justify our results.

Tables XVII through XIX summarize details of *ab initio* studies of NO_2 from the published literature and from this work. Table XVII provides a quick comparison of three important aspects of the calculations, Table XVIII displays the computed equilibrium geometries of the low-lying doublet states, and Table XIX contains the calculated excitation energies.

Both the work of Schaefer and Rothenberg [24] and that of Brundle *et al.* [27] are SCF studies of the ground state at its experimental geometry. Since this does not reveal anything directly applicable to the spectroscopy of the molecule, no further comment will be made except to compare the energy reported by Schaefer and Rothenberg and that reported in this work. Though the basis set we have used is actually slightly superior to theirs, our reported energy is higher. The energy we give is not an SCF energy; rather it is the energy of the RHF configuration, calculated for the OVC orbitals. Optimization of the orbitals for this single configuration alone rather than as a member of a set

TABLE XVII

COMPARISON OF IMPORTANT ASPECTS OF NO_2 *AB INITIO* CALCULATIONS

	$^2A_1$ SCF ENERGY	$^2A_1$ CI ENERGY LOWERING	VARIATION OF GEOMETRY	REFERENCE
Fink	-203.907	0.042	θ	10
Gangi and Burnelle	-203.8857	0.0575	θ	13
Brundle *et al.*	-203.9318	-----	-----	27
Del Bene*		-----	R, θ	14
Schaefer and Rothenberg	-204.0679	-----	-----	24
Hay	-201.2676	0.1931	θ	15
This work	-204.0607	0.1815	R, θ	

*Del Bene did not report any absolute energies. However the basis set is the same as that used by Hay and the energy will be very nearly the same.

TABLE XVIII

AB INITIO PREDICTIONS OF THE EQUILIBRIUM GEOMETRIES OF THE DOUBLET ELECTRONIC STATES OF NO_2

	$^2A_1$		$^2B_1$		$^2B_2$		$^2A_2$	
	R_e*	θ_e*	R_e	θ_e	R_e	θ_e	R_e	θ_e
Gangi and Burnelle (Reference 13)	——	134	——	180	——	101	——	112
Fink (Reference 10)	——	137	——	177	——	105	——	——
Del Bene (Reference 14)	1.24	132	1.25	180	1.30	95	1.30	116
This study**	1.19	135	1.20	180	1.25	101	1.27	110

*Bond lengths are expressed in Å and bond angles in degrees.

**The reported parameters were computed at the OVC level.

TABLE XIX

AB INITIO PREDICTIONS OF EXCITATION ENERGIES IN NO_2

	VERTICAL*					(0-0)*		
	Gangi and Burnelle	Fink**	Del Bene**	Hay	This work	Gangi and Burnelle	Del Bene**	This work
$^2A_1$	0.0	0.0	0.0	0.0	0.0	0.0	0.0	0.0
$^2B_1$	1.75	2.58	---	2.45	2.8	1.2	1.1	1.66
$^2B_2$	3.33	3.73	3.15	3.03	3.4	2.1	0.86	1.18
$^2A_2$	4.13	2.47	1.68	3.09	3.4	---	0.37	1.84
$^4B_2$	3.38	---	---	3.80	4.6	---	---	4.4
$^4A_2$	3.43	---	---	3.81	4.7	---	---	4.4
Reference	13	10	14	15		13	14	

*The excitation energies are given in eV and are not corrected for differential zero point energy.

**No configuration interaction was included in these studies.

of configurations would result in a further lowering of about 0.01 hartrees.

For a somewhat less than double-zeta quality basis set, Fink [10] calculated SCF energies of several states at 4 different bond angles and a fixed bond length of 1.19 Å. In a later study, he extended his basis to roughly double-zeta quality and recomputed the vertical excitation energies. Configuration interaction was also applied, but was limited to states of $^2A_1$ symmetry and only a total of 29 configurations were included.

The study of Del Bene [14] is noteworthy in that both the bond length and bond angle were varied to find the equilibrium geometry for the four lowest doublet states of NO_2. However, her basis set was the Pople et al. STO-3G minimal basis [28] and no configuration interaction was included. Nonetheless, such a treatment has been shown in the past to adequately reproduce geometrical trends even though calculated excitation energies must be viewed with caution. Del Bene's results are consistent with ours in that she predicts a low-lying $^2B_1$ excited state which is linear and has a bond length only slightly longer than in the ground state. The prediction of $^2B_2$ and $^2A_2$ excited states with longer bond lengths and smaller bond angles than for the ground state are also in agreement with our findings. Even though her calculated excitation energies are not too reliable, they do indicate large differences between the vertical and (0-0) transition energies,

especially for the $^2B_2$ state. As will be discussed at the beginning of Chapter III, we feel that lack of recognition of this fact has greatly contributed to misunderstandings regarding the visible absorption of NO_2.

The work of Gangi and Burnelle [13] is that most often cited by experimentalists in attempts to explain their data. There are numerous disagreements between their results and spectral interpretation and those which we present. Furthermore, these discrepancies are significant and we suggest that any analyses based on the data of Gangi and Burnelle should be carefully reexamined.

Undoubtedly the most important factor affecting the accuracy of their results is the limited nature of their CI. We discussed previously the probable error of any SCF-CI approach which treats as core any orbitals other than those which correspond to 1s orbitals in the atoms. Gangi and Burnelle, however, have arbitrarily designated the eight lowest molecular orbitals as core. Among these are the $5a_1$ and $1b_1$ orbitals which should undoubtedly be treated as valence since they correlate with the $1\pi_u$ orbital for linear geometries.

A preliminary calculation supports our reasoning. A minimal basis (STO-3G) SCF-CI calculation performed using the orbitals suggested by Gangi and Burnelle gave the same ordering of states and good agreement with their computed vertical excitation energies. The CI lists were then increased by including excitations from the $1b_1$ orbital in

forming configurations. The energy of the $^2B_2$ state relative to the ground state scarcely changed; however, the $^2B_1$ state was found more than 0.5 eV higher than before, while the $^2A_2$ state dropped nearly 1.5 eV relative to the ground state. The magnitude of these shifts clearly demonstrates the inadequate convergence of the CI expansions of Gangi and Burnelle.

The recent study of Hay [15] includes the most extensive treatment of correlation up to the time of the work which we report here. For the STO-3G basis, he performed SCF-CI calculations for the low-lying electronic states; the CI wavefunctions included all single and double excitations from the RHF configuration in each state and only the 1s-like molecular orbitals were designated as core. Although only vertical transitions were treated in this portion of his work, it is gratifying to us that he obtains the same ordering of states and rather close agreement with our calculated vertical transition energies.

Because the basis set is minimal, the configuration treatment of Hay is necessarily valence (as we have defined the term) in nature and similar in size to the one which we have employed, although our basis set is much better. His CI is lower in energy by 0.1931 hartrees over his ground state SCF result, compared to a lowering of 0.1815 hartrees for our final wavefunction over the energy of the $^2A_1$ RHF configuration computed with the OVC orbitals. As discussed previously, the actual SCF energy in our basis would be

about 0.01 hartrees lower if the orbitals were optimized only for the RHF configuration and our energy lowering due to introduction of correlation should be reduced by this amount. Nevertheless, it is likely that our treatment of correlation is more extensive since the CI of Hay is undoubtedly compensating for his limited basis as well as introducing correlation. Furthermore, there is a substantial oxygen 2s core correlation contribution in Hay's study which is not treated in the OVC-CI approach. As a check we also computed an OVC-CI energy for the ground state at its experimental geometry in the STO-3G basis and found an energy lowering over the SCF result of 0.1986 hartrees, slightly better than what Hay achieved. It is expected that the superiority of the OVC-CI procedure over SCF-CI will become more dominant as the flexibility of the basis set is increased.

Despite the great range in the quality of the various ab initio treatments and our doubts about the validity of certain aspects of previous calculations, a consensus does emerge on several points:

1. The ground state bond angle is well reproduced, the $^2B_1$ state is linear (the bond angle of 177° found by Fink undoubtedly results from his use of a quartic fit to 4 widely spaced points), and the $^2B_2$ and $^2A_2$ states are significantly more bent than is the $\tilde{X}^2A_1$ state.

2. The $^2B_1$ state is the first excited state <u>for vertical excitation</u>.
3. The vertical excitation energy of the $^2B_2$ state is substantially lowered by the introduction of electron correlation.
4. The $^4B_2$ and $^4A_2$ states are very close in energy; also, the vertical excitation energies of these states are drastically underestimated at the SCF level.
5. The calculated excitation energies to the $^2A_2$ state are <u>not</u> in good agreement. However, for the two studies in which correlation was carefully considered (the work of Hay and our results), the $^2A_2$ and $^2B_2$ hypersurfaces are found to be very close for vertical excitation.

To emphasize the improvements of our results over previous theoretical treatments, we point out the following facts: (1) The only calculation which employed a basis set comparable in size to the one we used is that of Schaefer and Rothenberg. However, only an SCF calculation of the ground state at its experimental equilibrium geometry was performed. (2) The only calculation with a comparable treatment of correlation was that of Hay. However, his basis set was much smaller and the correlation was considered only for the ground state equilibrium geometry. (3) The only calculation which also varied both bond angle and bond length was that of Del Bene. However, again the

basis set was quite small and in addition, no correlation effects were treated.

The Determination of the Potential Surfaces

The spectral analysis which we present in Chapter III requires a knowledge of the characteristics of the potential surfaces (i.e., equilibrium bond lengths and bond angles and vibrational frequencies) of the states of interest. In this section we describe the mathematical details of the determination of the potential surfaces from our *ab initio* calculations. The discussion is necessarily limited to the space of C_{2v} geometries.

A convenient set of internal coordinates for describing the symmetric vibrations of the NO_2 molecule is shown in Figure 4, where R_1 is one-half the separation of the two oxygen atoms and R_2 is the distance from the nitrogen atom to the midpoint of the line joining the two oxygen atoms. The classical kinetic energy in terms of these coordinates is given by

$$2T = 2m_O\dot{R}_1^2 + \frac{2m_O m_N}{2m_O+m_N}\dot{R}_2^2 \qquad (4)$$

where the overdot indicates the derivative with respect to time and m_O and m_N are the masses of the oxygen and nitrogen atoms, respectively.

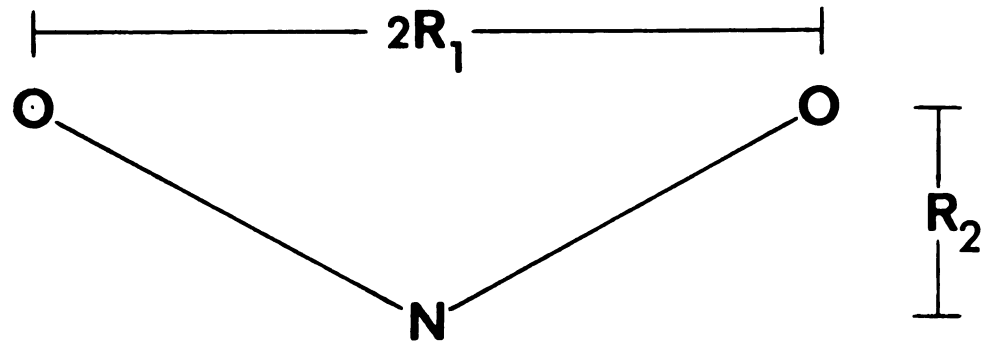

Fig. 4. Internal coordinate system for C_{2v} geometries in NO_2.

The generalized quadratic potential in R_1 and R_2 is

$$2(V-E_e) = f_{11}(R_1-R_1^e)^2 + f_{22}(R_2-R_2^e)^2 + 2f_{12}(R_1-R_1^e)(R_2-R_2^e) \quad (5)$$

From the ab initio calculations we have the electronic energies for the several electronic states of NO_2 at various values of R_1 and R_2. The electronic energies, which provide the potential for nuclear motion in the Born-Oppenheimer approximation, were least-squares fit to the functional form of equation (5). The six variable parameters, namely the three force constants, f_{11}, f_{22}, and f_{12}, the two equilibrium geometrical parameters, R_1^e and R_2^e, and the energy at the equilibrium geometry, E_e, were determined by least-squares optimization, using the STEPIT subroutine available from the Quantum Chemistry Program Exchange,

Indiana University. In general, those points with bond lengths within $\pm$ 0.10 bohrs and angles within $\pm$ 10° of the equilibrium geometry for a given state were used in the determination.

As described in Wilson, Decius, and Cross [29], equations (4) and (5) lead to the secular determinant

$$|F-G^{-1}\lambda| = \begin{vmatrix} f_{11}-2m_O\lambda & f_{12} \\ f_{12} & f_{22}-\frac{2m_Om_N}{2m_O+m_N}\lambda \end{vmatrix} = 0 \qquad (6)$$

which yields two roots, λ_1 and λ_2, related to the harmonic frequencies of the symmetric vibrations by

$$\lambda_i = (2\pi c\omega_i)^2 \qquad (7)$$

where ω_i is in cm^{-1} if λ_i has units of sec^{-2}.

Successive substitution of the roots λ_i into the matrix $F-G^{-1}\lambda$ and solution of

$$(F-G^{-1}\lambda_i)\begin{pmatrix} A_{1i} \\ A_{2i} \end{pmatrix} = \begin{pmatrix} 0 \\ 0 \end{pmatrix} \qquad (8)$$

yields the amplitude ratios of A_{1i} to A_{2i}.

The internal coordinates are related to the normal coordinates, Q_1 and Q_2, by

$$R_j-R_j^e = \eta_1 A_{j1} Q_1 + \eta_2 A_{j2} Q_2 \qquad j = 1,2 \qquad (9)$$

where the η_k are chosen to satisfy the relation

$$\eta_k^2[f_{11}A_{1k}^2 + f_{22}A_{2k}^2 + 2f_{12}A_{1k}A_{2k}] = \lambda_k \qquad (10)$$

Inversion of equations (9) gives the normal coordinates in terms of displacements in the internal coordinates:

$$\begin{aligned} Q_1 &= b_{11}(R_1-R_1^e) + b_{12}(R_2-R_2^e) \\ Q_2 &= b_{21}(R_1-R_1^e) + b_{22}(R_2-R_2^e) \end{aligned} \qquad (11)$$

The coefficients b_{ij} have the dimensionality $mass^{1/2}$ to give the normal coordinates in $mass^{1/2}$ length. The normal coordinates thus defined cast the classical expressions for the kinetic and potential energy into the simple forms

$$2T = \dot{Q}_1^2 + \dot{Q}_2^2 \qquad (12)$$

$$2(V-E_e) = \lambda_1 Q_1^2 + \lambda_2 Q_2^2. \qquad (13)$$

Table XX summarizes the pertinent results for the low-lying doublet states of NO_2 obtained with the methods of this section. We note that the OVC wavefunctions were used for this analysis; as will be shown in the following section, the higher accuracy OVC-CI wavefunctions change the characteristics of the potential surfaces to a negligible extent.

TABLE XX

THE OVC EQUILIBRIUM GEOMETRIES, VIBRATIONAL FREQUENCIES, AND NORMAL COORDINATES FOR THE LOW-LYING DOUBLET STATES OF NO_2

	$^2A_1$	$^2B_1$	$^2B_2$	$^2A_2$
R_e(Å)	1.186	1.197	1.252	1.273
θ_e(degrees)	135.2	179.5	101.4	109.6
ω_1(cm^{-1})	1356	1192	1464	1360
ω_2(cm^{-1})	771	960*	741	798
R_1^e(bohrs)	2.073	2.261	1.831	1.966
R_2^e(bohrs)	0.853	0.011	1.500	1.388
f_{11}(hartrees/$bohr^2$)**	1.545	1.708	1.076	1.116
f_{22}(")	0.427	0.088	0.665	0.577
f_{12}(")	0.414	0.070	0.436	0.344
b_{11}($amu^{1/2}$)	4.184	5.635	2.608	2.741
b_{12}($amu^{1/2}$)	2.100	0.275	2.769	2.730
b_{21}($amu^{1/2}$)	3.807	0.498	5.020	4.948
b_{22}($amu^{1/2}$)	-2.308	-3.109	-1.439	-1.512

*Calculated in the bent molecule formalism.

**1 hartree/$bohr^2$ = 15.57 mdyne/Å

The Accuracy of the Computed Spectroscopic Constants

Because of the complex and severely perturbed absorption spectra of NO_2, not enough excited state spectroscopic constants are known for a rigorous test of the accuracy of the theoretical constants. Comparison with ab initio studies on other, better understood molecules is not helpful either; to the best of our knowledge, there are no previous calculations of excited state spectroscopic constants for a polyatomic molecule of this size at the level reported here. We must, therefore, rely on the $\tilde{X}^2A_1$ constants for our analysis. We do note that tentative vibrational frequencies have been suggested from experiment for the $^2B_2$ excited state and estimates of its equilibrium geometry have been given. However, there are great complexities involved with the data for this state and we defer a detailed discussion to Chapter III.

In Table XXI are tabulated the ab initio spectroscopic constants for the $\tilde{X}^2A_1$ and $^2B_2$ states at both the OVC and OVC-CI level along with the experimentally known ground state parameters. The data amply support our contention that the OVC and OVC-CI wavefunctions give nearly identical descriptions of the potential surfaces. As is the case for diatomics, there is a clear implication that a small set of carefully selected configurations (i.e., the OVC configurations) yields the vast majority of the dominant coorelation effects; at present, though, the

TABLE XXI

COMPARISON OF THE OVC AND OVC-CI AB INITIO SPECTROSCOPIC PARAMETERS FOR THE $\tilde{X}^2A_1$ AND $^2B_2$ STATES OF NO_2

	R_e(Å)	θ_e(degrees)	ω_1(cm^{-1})	ω_2(cm^{-1})	μ(debyes)
$\tilde{X}^2A_1$ (OVC)	1.186	135.2	1356	771	0.38
$\tilde{X}^2A_1$ (OVC-CI)	1.199	134.5	1351	758	0.37
$\tilde{X}^2A_1$ (Experimental)	1.1934*	134.1*	1358**	757**	0.316***
$^2B_2$ (OVC)	1.252	101.4	1464	741	0.47
$^2B_2$ (OVC-CI)	1.263	101.7	1461	739	0.46

*Reference 31.

**Reference 32.

***Reference 33.

selection of these configurations in a priori fashion is less well-defined in polyatomics than for diatomics. (However, see Appendix D for a description of straightforward configuration selection in some molecules other than NO_2.) Because the OVC and OVC-CI surfaces are so nearly the same for the $\tilde{X}^2A_1$ and $^2B_2$ states, no great effort was expended in computing OVC-CI surfaces for the $^2B_1$ and $^2A_2$ states; rather, the OVC-CI energies were calculated for only a few points near the minimum of these states for improved values of the (0-0) transition energies.

Perhaps the most significant difference in the OVC and OVC-CI spectroscopic parameters is the longer bond lengths observed at the OVC-CI level. For both the $\tilde{X}^2A_1$ and $^2B_2$ states, as well as the $^2B_1$ state (see Table XI), the computed equilibrium bond length is 0.01 to 0.015 Å longer for the OVC-CI wavefunctions. This trend might well be expected from the experience with diatomic molecules. Hartree-Fock quality basis set SCF calculations on diatomics generally give bond lengths shorter than experiment [30]; the computed bond lengths then increase as correlation is introduced.

At both the OVC and OVC-CI levels, the theoretical $\tilde{X}^2A_1$ geometrical parameters are in very good agreement with the accurate microwave determinations [31], the errors being less than 1%. The harmonic symmetrical vibrational frequencies, as given by Arakawa and Nielsen [32], are also well reproduced by the ab initio surfaces but in this case

the near coincidence must be regarded as somewhat fortuitous. The ab initio energies were computed on a relatively wide-spaced grid of geometries and the energy at each point was only converged to 1×10^{-5} hartrees. Thus, for the 14 OVC-CI points used in the $\tilde{X}^2A_1$ surface determination, the standard deviation of the ab initio and fitted energies was 1.3×10^{-4} hartrees (29 cm^{-1}) and for one point as large as 2×10^{-4} hartrees (44 cm^{-1}) with the sign and magnitude of the deviation at each point distributed in what appears to be random fashion. Although these residuals do not translate directly into an uncertainty for the vibrational frequencies, we estimate that a more compact grid of geometries and higher convergence of the wavefunctions would not cause a greater than 5% change in the values of ω_1 and ω_2 which we report.

The very small differences between the OVC and OVC-CI dipole moments indicate that the dominant molecular correlation configurations are also those which figure most prominently in determining the dipole moment, consistent with what was found in OVC studies of the diatomic hydrides and CO. This is in contrast to more standard CI treatments of dipole moments which often require careful selection of very lengthy configuration lists in order to obtain good results.

The computed dipole moments were least-squares fit as a function of linear and quadratic displacements in the previously determined normal coordinates. The ground state

dipole moment at the computed equilibrium geometry is 0.37 debyes (polarity $N^{-}O_2^{+}$), only slightly larger than the most accurate experimental determination [33]. In contrast, the STO-3G and [4s3p] basis sets give moments of -0.06 debyes and 1.02 debyes, respectively, at the experimental equilibrium geometry. In the harmonic approximation, the intensity of a fundamental vibration is proportional to the square of the first derivative of the dipole moment with respect to the normal coordinate of that vibration, evaluated at zero displacement in the coordinates. Our fit indicates that on this basis, the bending fundamental for NO_2 should be roughly three orders of magnitude more intense than the symmetric stretch, qualitatively consistent with the experimental observation [34] that the rotational structure of the bend is easily analyzed under conditions in which the stretch is not seen at all. We suggest that the magnitude of the theoretical intensity ratio not be given too much emphasis, however, since the dipole moment expansion contains large second derivative contributions (i.e., $\left(\frac{\partial^2 \mu}{\partial Q_1^2}\right)_0 Q_1^2$, etc.) which do not contribute to the fundamental intensities in first order.

An Unusual Feature of the $^2\Sigma_g^+$ State of NO_2

Several years ago, Mulliken [35] proposed that certain excited states of ostensibly symmetric AB_2 triatomic molecules might actually exhibit two unequal A-B bond

lengths at the minimum of the potential energy hypersurface. He further suggested that such behavior is most likely for states in which the $2b_1$ molecular orbital is occupied in the RHF configuration, his premise being that distortion from the equal bond length situation would reduce the anti-bonding character of this orbital. Prompted by these remarks, Coon and coworkers have examined band systems in NO_2 [36], SO_2 [37, 38], and ClO_2 [38, 39] and have found evidence for the existence of unequal equilibrium bond length states. Their arguments are primarily based on the apparent necessity of a double-minimum potential along the Q_3 normal coordinate in order to explain the unusual isotopic origin shifts and anomalously strong $\Delta v_3=2$ transitions in absorption.

We have not theoretically studied the 2491 Å band system of NO_2 discussed by Coon et al.; the upper state of this system is the <u>second</u> excited $^2B_2$ state in NO_2 and there are conceptual difficulties involved in treating such cases by our approach. However, we do comment on this system in Chapter III in an analysis of predissociative mechanisms in NO_2.

We did find evidence, though, for a non-symmetrical equilibrium structure of the $^2\Sigma_g^+$ state, when examined at the double-zeta basis set level. Further study in the [4s3pld] basis has verified this behavior. Attention was first restricted to $D_{\infty h}$ geometries; configuration lists were optimized and a parabolic interpolation of three

equal bond length points gave a symmetric minimum bond length of 1.302 Å. Further points were then obtained in which one bond length was contracted and the other lengthened by equal amounts. A lowering of the energy was found with a minimum for $\Delta Q_3 = \pm 0.11$ Å, and a barrier to inversion of approximately 800 cm^{-1} as depicted in Figure 5.

Several comments are in order regarding the theoretical technique and results.

1. The configuration lists were optimized at a $D_{\infty h}$ geometry and hence included only $^2\Sigma_g^+$ contributors. Once the symmetry is broken, those configurations of $^2\Sigma_u^+$ symmetry in the equal bond length case will also be involved and should be considered. However, they will only serve to magnify the asymmetry.
2. The wavefunction has not been analyzed in enough detail for an explanation of the asymmetry, although we do note that the RHF SC energies strongly favor unequal bond lengths. An avoided crossing mechanism [40] is improbable, since the first excited state of $^2\Sigma_u^+$ symmetry in NO_2 is most likely that analyzed by Ritchie and Walsh [41]. The origin of this $^2\Sigma_u^+$ state is more than 7 eV above the ground state, and hence, better than 2.5 eV above the $^2\Sigma_g^+$ state.

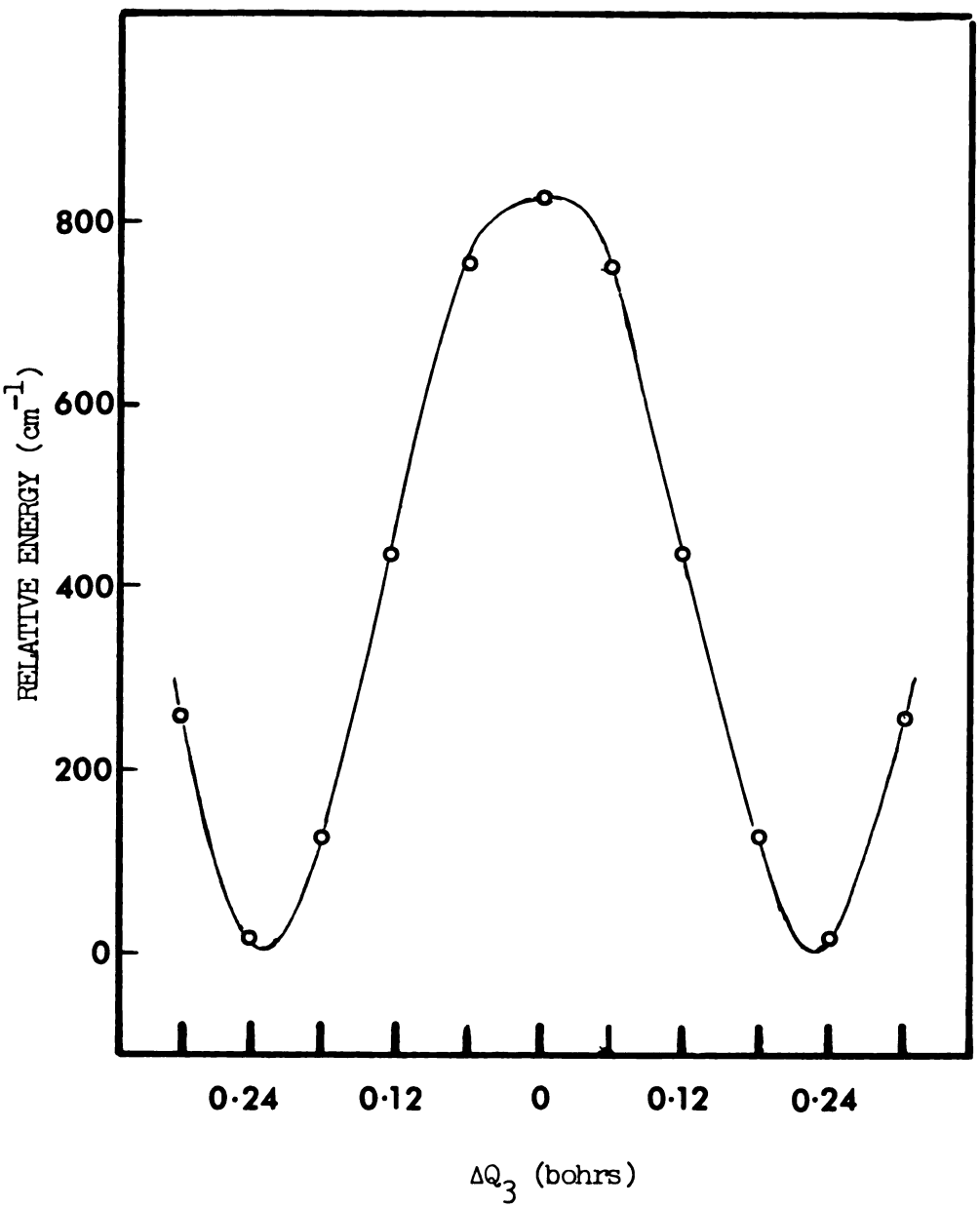

Fig. 5. The Q_3 potential of the $^2\Sigma_g^+$ state of NO_2 as computed at the OVC-CI level.

The displacements are expressed relative to the equal bond length minimum for R = 2.46 bohrs.

3. The $^2\Sigma_g^+$ state is more than 1 eV above the NO($^2\Pi$) + O(^{3}P) asymptote to which it adiabatically correlates. We therefore suggest that the apparent double-minimum character along the asymmetric stretch normal coordinate may be simply a manifestation of the essentially dissociative nature of this state.

CHAPTER III

SPECTRAL INTERPRETATION

A Qualitative Discussion of the Electronic Spectroscopy of NO_2

Despite a voluminous amount of experimental data, many of the details regarding the spectroscopy of NO_2 remain uncertain. The best understood electronic transition is the $^2B_1 \leftarrow \tilde{X}^2A_1$ absorption from 4600 to 3700 Å, analyzed by Douglas and Huber [1], but it is not without its complexities. Less well characterized are the $^2B_2 \leftarrow \tilde{X}^2A_1$ absorption in the visible and near-infrared and the 2491 Å band system to a different $^2B_2$ excited state, hereafter referred to as the 2^2B_2 state. In addition, $^2A_2$, $^4B_2$, $^4A_2$, 2^2A_2 and $2^2A_1(^2\Sigma_g^+)$ states have been suggested to be of importance for excitation energies less than 5 eV. None of these states has as yet been found experimentally, although some of them may be responsible for the two striking predissociations observed at 3979 Å [1] and in the 2491 Å band system. It has been proposed in various analyses that one or more of $^2A_2$, $^4B_2$, or $^4A_2$ contribute to the $NO(^2\Pi)$ + $O(^3P)$ chemiluminescence; again, however, firm experimental confirmation is lacking.

The ab initio calculations presented in Chapter II are a great aid in sorting out the possibilities. For the $\tilde{X}^2A_1$, $^2B_2$, and $^2B_1$ states, the extensive theoretical potential surfaces allow a detailed discussion of the $^2B_2 \leftarrow \tilde{X}^2A_1$ and $^2B_1 \leftarrow \tilde{X}^2A_1$ absorption systems; these are described in the last two sections of this chapter. Here we confine our attention to some of the more qualitative features and attempt to formulate an interpretation which is consistent with as much experimental data as possible. A definitive resolution is not attainable at this time for every experiment, but a significant truncation in the number of possible explanations is achieved. Hopefully, this will enable an efficient approach to the planning of future experimental studies and will also expedite the analysis.

An adiabatic correlation diagram (ACD) relating the molecular states with those of the various dissociative asymptotic products is a useful adjunct to our discussion. As the name implies, the ACD is valid within the regime of adiabatic potential surfaces and it is derivable entirely from group theoretic principles and a knowledge of the electronic energy levels of the states. Figure 6 contains the ACD for dissociation into NO + O and Figure 7 displays the ACD for N + O_2 products. The asymptotic energy levels are placed relative to the $\tilde{X}^2A_1$ ground state of NO_2 from the thermodynamic dissociation energies and the spectroscopic excitation energies of the atoms and diatomic fragments. All of the NO_2 levels up to the 2^2A_2 state,

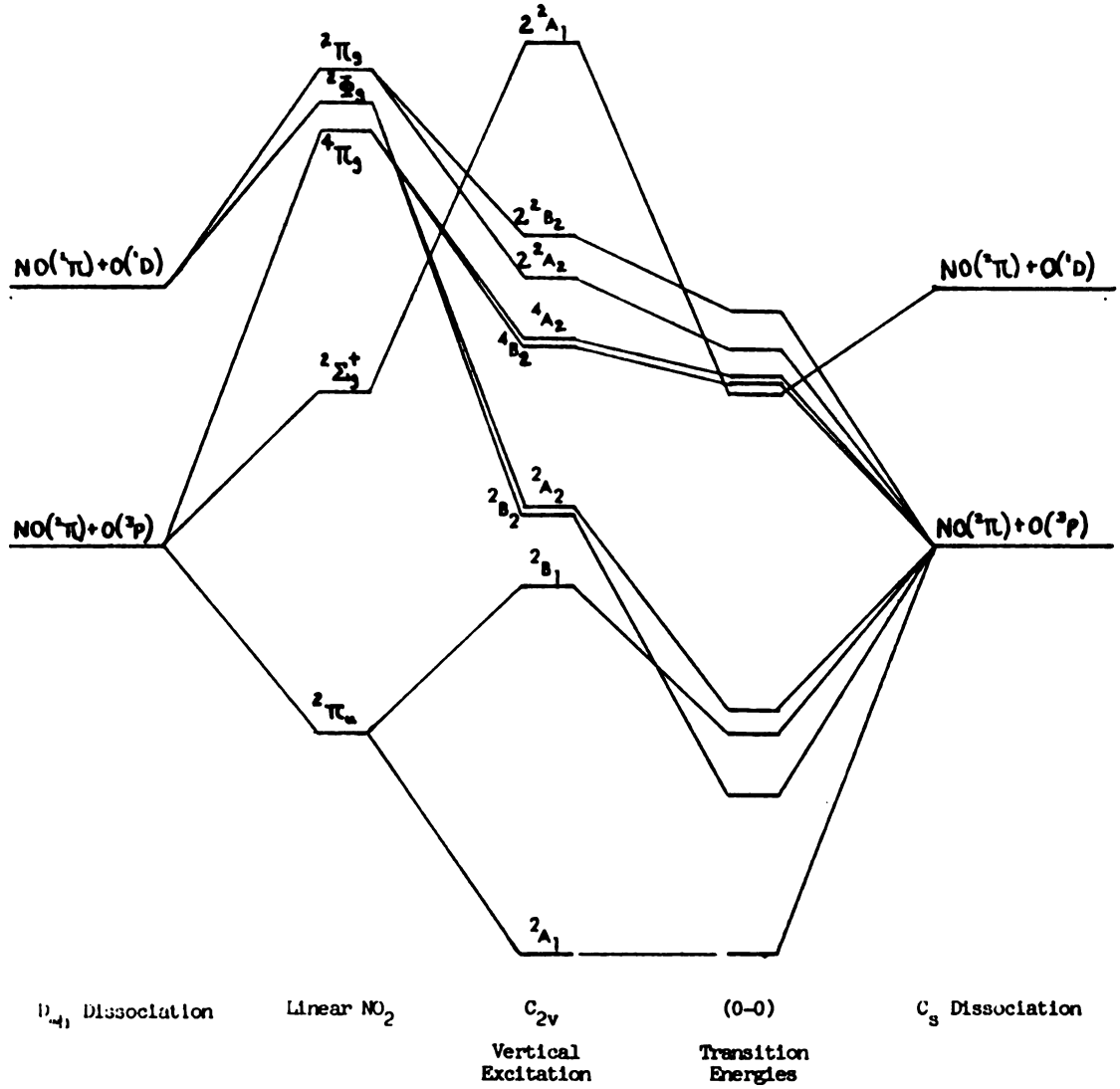

Fig. 6. The adiabatic correlation diagram (ACD) for dissociation of NO_2 into NO + O.

The energies of the asymptotes relative to the ground state of NO_2 are 3.11 eV for $NO(^2\Pi) + O(^3P)$ and 5.08 eV for $NO(^2\Pi) + O(^1D)$.

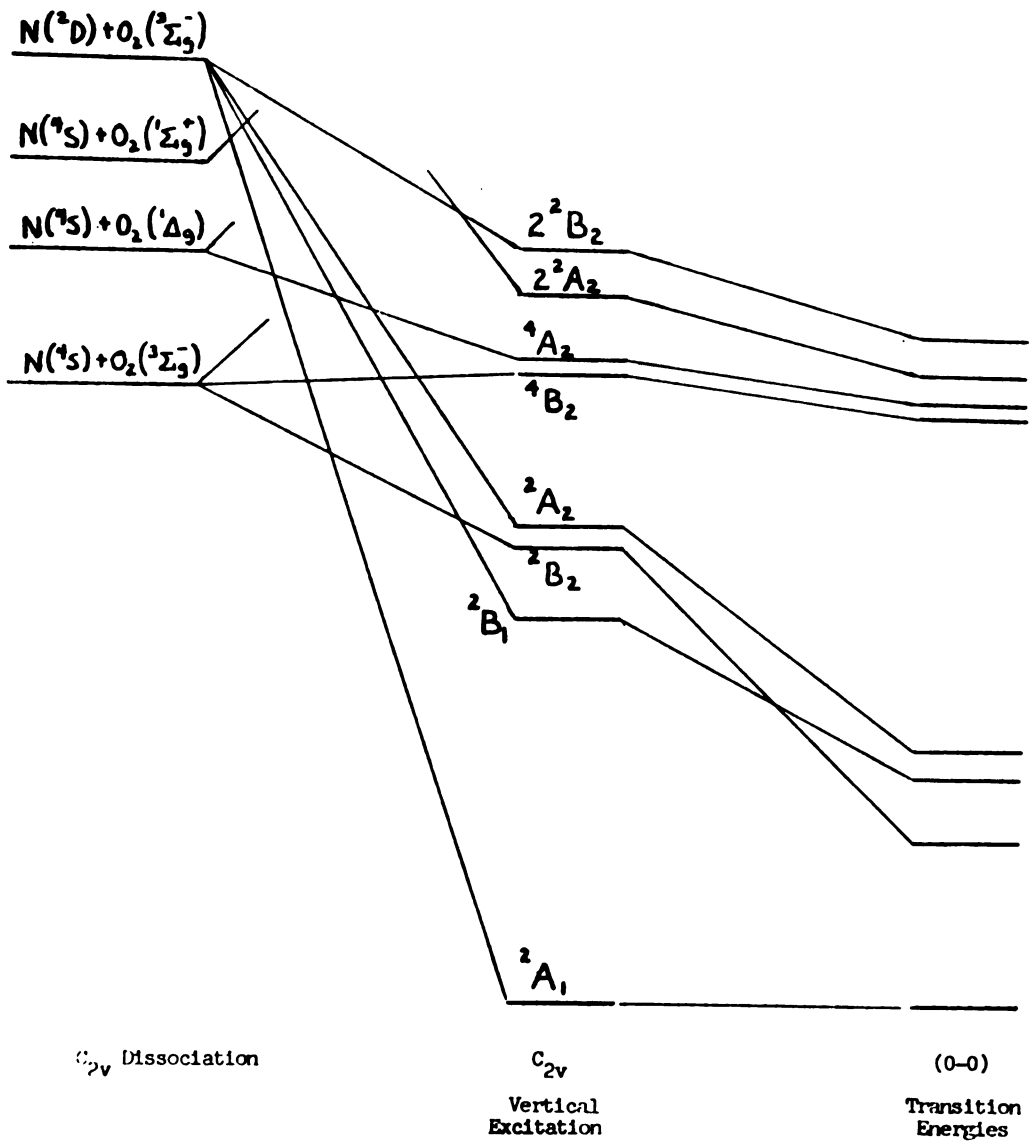

Fig. 7. The ACD for dissociation of NO_2 into N + O_2.

The energies of the asymptotes relative to the ground state of NO_2 are 4.50 eV for $N(^4S) + O_2(^3\Sigma_g^-)$ and 6.88 eV for $N(^2D) + O_2(^3\Sigma_g^-)$

plus the $^4\Pi_g$ level, are from the OVC-CI calculations in the [4s3pld] basis reported in Chapter II. The (0-0) excitation energy of the 2^2B_2 state is known from experiment [36,42,43] and its vertical excitation energy has been estimated. No experimental information is available for the 2^2A_2 state and it was not treated in our calculations; however, Hay [15] computed that it is 0.36 eV below the 2^2B_2 state for vertical excitation and we have used this separation for both the vertical and (0-0) excitation energies. It is quite possible that the order is actually reversed in one or both of these cases. Although neither the $^2\Phi_g$ or $^2\Pi_g$ states were included in the calculations of Chapter II, the RHF configuration of each arises from the same $(1\pi_u)^4(1\pi_g)^3(2\pi_u)^2$ orbital occupancy as the $^4\Pi_g$ RHF configuration. Hund's rules would predict the ordering $E(^4\Pi_g)<E(^2\Phi_g)<E(^2\Pi_g)$ and OVC-CI calculations in the double-zeta quality basis confirm this. The separations of that study were employed here and the position of the 2^2A_1 state for vertical excitation was likewise deduced. Although there is a substantial uncertainty in the energies of these highly excited states, it is of little consequence for the purposes to which we shall apply the ACD. Similarly, the influence of Rydberg states, which probably begin in the vicinity of 6.5 eV, are not of importance here.

Before proceeding to a systematic discussion of the predissociation, chemiluminescence, fluorescence, and other

aspects of NO_2 electronic spectroscopy, we offer the following historical perspective.

In 1957, Robinson, McCarty, and Keelty [44] examined the absorption spectrum between 7000 and 3400 Å of monomeric NO_2 isolated in an argon matrix at liquid helium temperatures. Most of the strong room temperature bands were also seen at low temperature, which eliminated hot bands as the major source of complexity in the visible absorption. These authors also reported a sharp decrease in intensity to the red of 6200 Å, which prompted them to suggest that two electronic transitions might be present. The first would correspond to the weak absorption from 10 000 A to 6200 Å; a second stronger system then covers the remainder of the visible region. On the basis of the matrix isolation studies at 4.2°K and 1.5°K, it was also proposed that the visible absorption is to a bent upper state, since the effect of rotational depopulation between the two temperatures expected for a linear upper state was not observed.

In 1964, Atherton, Dixon, and Kirby [45] γ-irradiated single crystals of $NaNO_2$, which generated NO_2 in the crystal. After the identity and orientation of the NO_2 molecules were established by ESR spectroscopy, the polarization of the optical absorption between 5500 and 4000 Å was examined. The polarization was found to be predominately along the O-O internuclear axis, consistent with a $^2B_2$ upper state. It was noted that deviations from

theoretical polarization ratios might be due to an overlapping and weaker $^2B_1 \leftarrow \tilde{X}^2A_1$ absorption, which is the first transition in the isoelectronic CO_2^- species.

The first successful rotational analysis in the visible and near-infrared appeared in 1965 when Douglas and Huber [1] identified $K_a=0 \leftarrow K_a=1$ subbands of a $^2B_1 \leftarrow \tilde{X}^2A_1$ absorption from 4600 to 3700 Å. According to the qualitative arguments of Walsh [2], the $^2B_1$ state is expected to be linear or nearly so. Although the observed lines are fairly strong, they only account for a small fraction of the total number of lines and intensity in this region. It was proposed that other subbands of the $^2B_1 \leftarrow \tilde{X}^2A_1$ system are severly perturbed by Renner-Teller [46,47] interaction and that these are the source of much of the unanalyzed intensity. Douglas and Huber could not reconcile their observations with those of Atherton et al. Additionally, a linear $^2B_1$ excited state would be in conflict with the Robinson et al. suggestion of a bent upper state in this spectral region.

In 1971, Gangi and Burnelle [13] presented a spectral interpretation based on their ab initio calculations which has since been employed in numerous experimental analyses. They computed that the (0-0) and vertical transition energies to the $^2B_1$ state are 1.2 eV and 1.75 eV, respectively; the corresponding energies for $^2B_2 \leftarrow \tilde{X}^2A_1$ are 2.1 eV and 3.33 eV. Potential curves for bending at a fixed bond length gave bond angles of 180° for $^2B_1$ and

approximately 105° for the $^2B_2$ state. With the exception of the Douglas and Huber analysis, the results of Gangi and Burnelle quite satisfactorily explained the existing experimental data. The long wavelength end of the spectrum was assigned as $^2B_1 \leftarrow \tilde{X}^2A_1$ and the stronger transition to a bent upper state with origin near 6200 Å (2.0 eV) and maximum at roughly 3900 Å (3.2 eV) was well accounted for by the calculated $^2B_2$ excitation energies; the computed oscillator strengths predicted $^2B_2 \leftarrow \tilde{X}^2A_1$ to be about 4 times more intense than $^2B_1 \leftarrow \tilde{X}^2A_1$.

Despite the seemingly high degree of correlation between experiment and theory, the analysis of Gangi and Burnelle must be for the most part discarded. The only contrary evidence at the time of their presentation was that of the Douglas and Huber study; however, it carries great weight because of its quantitative nature as opposed to the more qualitative character of the other experimental results. Furthermore, the much more accurate ab initio calculations we described in Chapter II, in conjunction with many recent experiments, force an entirely different interpretation.

Hardwick and Brand [48] have extended the Douglas and Huber $^{14}N^{16}O_2$ and $^{15}N^{16}O_2$ study to include the $^{14}N^{18}O_2$ isotopic species. Since the $^2B_1$ and $\tilde{X}^2A_1$ bond angles are substantially different (180° versus 134°), it will be very difficult to experimentally observe the $^2B_1 \leftarrow \tilde{X}^2A_1$ origin due to extremely small Franck-Condon factors. In order to

locate the $^2B_1$ origin, Hardwick and Brand employed a hamiltonian specifically designed by Hougen, Bunker, and Johns [49] to treat large amplitude bending vibrations. The force constants which determine the potential function of the hamiltonian were varied to give the best least-squares fit to the observed vibronic levels. The origin for $^{14}N^{16}O_2$ is predicted to be at 1.83 eV (6780 Å) in their analysis, but with an uncertainty of one quantum in their vibrational level numbering. In the third section of this chapter we shall present evidence in favor of such a reassignment, which reduces the predicted origin to 1.71 eV (7250 Å). Our ab initio adiabatic separation of the $\tilde{X}^2A_1$ and $^2B_1$ hypersurfaces is 1.66 eV which yields an origin of 1.69 eV once the correction for differential zero point energy in the two states is included. The calculation of Gangi and Burnelle also severely underestimated the $^2B_1$ vertical excitation energy. Rather than 1.75 eV, we find 2.8 eV (4430 Å); in good agreement, Hardwick and Brand predict, on the basis of computed Franck-Condon factors, that the maximum intensity in the $^2B_1 \leftarrow \tilde{X}^2A_1$ absorption is at 2.84 eV.

Absorption in NO_2 at room temperature is observed past 11 000 Å into the near-infrared [50] and it is no longer possible to assign these features as arising from a $^2B_1 \leftarrow \tilde{X}^2A_1$ transition. Brand, Chan, and Hardwick [50] have found a cold band near 8350 Å (1.48 eV) for which a partial rotational analysis shows that the transition is $^2B_2 \leftarrow \tilde{X}^2A_1$.

Since examination further to the red revealed only hot bands, Brand et al. have associated the 8350 Å band with the $^2B_2 \leftarrow \tilde{X}^2A_1$ origin. The ab initio calculations predict a slightly lower origin, uncorrected for differential zero point energy, of 1.18 eV, which is to be compared with the Gangi and Burnelle value of 2.1 eV. Again we feel that there is strong evidence supporting an origin lower than the present experimental assignment and this is discussed at some length in the final section of this chapter. At any rate, though, it is now firmly established that the $^2B_2$ state is the first excited state in NO_2, and henceforth it will be referred to as the $\tilde{A}^2B_2$ state; likewise, the lowest $^2B_1$ and $^2A_2$ states will be designated as the $\tilde{B}$ and $\tilde{C}$ states, respectively. The vertical excitation energy to the $\tilde{A}^2B_2$ state is computed to be 3.4 eV in the present study which implicates the $\tilde{A}^2B_2$ state as a contributor to the NO_2 absorption throughout the near-infrared, visible, and near-ultraviolet regions of the spectrum. We also note here that the comment of Robinson et al. concerning a sharp change in intensity at 6200 Å is incorrect. As will be shown in the discussion of the $\tilde{A}^2B_2 \leftarrow \tilde{X}^2A_1$ absorption, the bands in either side of 6200 Å join together smoothly in intensity.

Various laser-induced fluorescence studies [3-7] have now confirmed that absorption features to both the $\tilde{A}^2B_2$ and $\tilde{B}^2B_1$ excited states are interspersed at least within the 5145 to 3700 Å region. Thus the once apparently

contradictory observations of Douglas and Huber and Atherton et al. are now understood in terms of a $\tilde{B}^2B_1 \leftarrow \tilde{X}^2A_1$ transition and a stronger, but more highly perturbed, $\tilde{A}^2B_2 \leftarrow \tilde{X}^2A_1$ absorption which overlap. A quantitative ratio of the strengths of the two transitions is not known at this time; in the future oscillator strengths will be computed from the accurate ab initio wavefunctions. It is clear, though, that to the red of 7000 Å only the $\tilde{A}^2B_2 \leftarrow \tilde{X}^2A_1$ transition need be considered in absorption.

A suggestion made by Burnelle, May, and Gangi [11] has also caused considerable confusion in the literature regarding the NO + O states to which the $\tilde{A}^2B_2$ state correlates. In a discussion of the dissociation of NO_2, they noted that both the $\tilde{A}^2B_2$ and $\tilde{C}^2A_2$ states correlate to $NO(^2\Pi) + O(^1D)$, not $NO(^2\Pi) + O(^3P)$, for a colinear dissociation. Although they also remarked that avoided crossings for bent (C_s) dissociation might affect this correlation, their conclusion states "A result which also seems established with certainty is that . . . $^2B_2$ and $^2A_2$ must [emphasis added] dissociate into $NO(^2\Pi) + O(^1D)$." The idea that the $\tilde{A}^2B_2$ state cannot directly yield ground state products has been invoked in the literature to an unfortunate extent, despite numerous comments to the contrary. It is not necessary that avoided crossings be present for the $\tilde{A}^2B_2$ state to correlate with $NO(^2\Pi) + O(^3P)$; such a correlation follows directly from the Wigner-Witmer coupling rules [51] upon which the concept of an ACD is based.

Furthermore, it is highly improbable that states with deep potential wells for bending, such as $\tilde{A}^2B_2$ and $\tilde{C}^2A_2$, would dissociate through a linear intermediate conformation. Because of the neglect of C_s reaction paths along the $\tilde{A}^2B_2$ electronic hypersurface, the existence of an important possible predissociation mechanism has been almost totally ignored; of even greater consequence has been the frequent elimination of the $\tilde{A}^2B_2$ state from consideration as an emitter in the $NO(^2\Pi) + O(^3P)$ chemiluminescence.

On the basis of various broad band excitation fluorescence, photolysis, and quenching experiments, and a semi-empirical LCAO-MO calculation [52], Broida, Schiff, and Sugden [53] proposed a set of potential curves for NO_2 dissociation. The primary feature of their analysis was the suggestion that the diffuseness observed in absorption at ~3700 Å arises from an electronic predissociation of a bound electronic state by a higher lying 2^2A_1 linear excited state. The predissociated state was assumed to be the second excited state, and the first excited state was correlated with the excited products $NO(^2\Pi) + O(^1D)$.

Later Pitts, Sharp, and Chan [54] proposed state labels for the curves of Broida *et al.* and modified that for the 2^2A_1 state so that it was slightly bound. The $^2B_1$ state was suggested as the first excited state and the one which connects with $NO(^2\Pi) + O(^1D)$, while $^2B_2$ was considered to be the state predissociated by 2^2A_1. To explain NO_2 dissociation by light quanta of wavelength 4047 Å, which is

of lower energy (70.61 kcal/mole) than the thermodynamic dissociation energy of 71.78 kcal/mole, they determined that the Boltzmann distribution of rovibronic levels in the ground state would supply the remaining necessary energy. However, Pitts et al. thought it important to explain the conversion of rotational energy in the ground state into energy available for bond dissociation in the excited state and submitted that this was accomplished via: (1) excitation into the $^2B_2$ state; (2) crossing over into the linear 2^2A_1 state; (3) conversion of rotational energy about the least moment of inertia into degenerate bending modes of the linear state; and (4) Coriolis interaction of these bending modes with the antisymmetric stretching mode of the linear state. Despite its extreme complexity, this mechanism required that the "flow" of rotational energy into that available for bond dissociation be about 70% efficient.

In their study of the $\tilde{B}^2B_1 \leftarrow \tilde{X}^2A_1$ absorption, Douglas and Huber established that all bands at shorter wavelengths than 3979 Å exhibit diffuse rotational structure. The vibronic structure was unaffected by the onset of diffuseness, which corresponds to within a few cm^{-1} to the first NO_2 dissociation limit, as inferred from both the thermodynamic data [55] and the breaking-off in intensity of the magnetic rotation spectrum [56]. Because of the continuing vibronic structure through the dissociation limit, the diffuseness must arise from predissociation and not direct dissociation. Douglas and Huber proposed that

the observed bands correspond to excitation of bending modes in the linear $\tilde{B}^2B_1$ state; the diffuseness was thought to arise from a radiationless transition into the continuum associated with dissociation roughly along the asymmetric stretch normal coordinate. The data were shown by Herzberg [57] to satisfy all of the characteristics expected for what he terms case II predissociation (predissociation by vibration) with the following possible exception: predissociation by vibration requires that the dissociation limit be consistent with a reasonable binding energy of the excited state. At the time of Herzberg's discussion it was not clear that the $\tilde{B}^2B_1$ state was sufficiently bound to satisfy this criterion.

Finally, the 1971 theoretical study and spectral interpretation of Gangi and Burnelle [13] for the most part ignored the suggestion of Douglas and Huber and discussion by Herzberg. Instead, these authors revised the curves of Pitts et al. to correlate $\tilde{B}^2B_1$ with $NO(^2\Pi) + O(^3P)$ and $\tilde{A}^2B_2$ with $NO(^2\Pi) + O(^1D)$ but retained the interpretation of an electronic predissociation of the $\tilde{A}^2B_2$ state by 2^2A_1. Much as in the case of the positions of the excited states, this description of NO_2 dissociation has been extensively used in subsequent discussions, while the firm experimental analysis of Douglas and Huber has been largely disregarded. However, again the interpretation of Gangi and Burnelle is inaccurate and must be substantially revised.

As established previously, the $\tilde{A}^2B_2 \leftarrow \tilde{X}^2A_1$ and $\tilde{B}^2B_1 \leftarrow \tilde{X}^2A_1$ absorption features overlap in the 5200 to 3700 Å region. Thus the diffuseness found for <u>all</u> bands at shorter wavelengths than 3979 A requires that predissociation mechanisms be found for both excited states. Three possibilities will be considered:

(1) Electronic predissociation of either or both of the $\tilde{A}^2B_2$ and $\tilde{B}^2B_1$ states by the $2^2A_1(^2\Sigma_g^+)$ state. This mechanism, much favored in previous analyses, is clearly untenable. Since the energy of the 2^2A_1 state at its equilibrium geometry is more than 1 eV above the $NO(^2\Pi) + O(^3P)$ asymptotic energy, any intersections with the $\tilde{A}^2B_2$ or $\tilde{B}^2B_1$ hypersurfaces will be well above the dissociation limit. Thus, any predissociation arising from such an intersection would begin at wavelengths significantly shorter than 3979 Å.

(2) Electronic predissociation of either or both of $\tilde{A}^2B_2$ or $\tilde{B}^2B_1$ by high vibrational levels of the $\tilde{X}^2A_1$ electronic state. As shown in Figure 3, those portions of the $\tilde{B}^2B_1$ hypersurface reached in absorption have negligible Franck-Condon overlap with the ground state, which eliminates an electronic predissociation in this case. However, the $\tilde{X}^2A_1$ and $\tilde{A}^2B_2$ states will exhibit substantial overlap over a large portion of their hypersurfaces and an electronic predissociation is likely. Support is supplied by the existence of strong vibronic coupling [50] between the two states, as will be discussed in the final section

of this chapter. Although $\tilde{A}^2B_2 - \tilde{X}^2A_1$ vibronic coupling has been discussed many times [58-61] in the context of the anomalous fluorescence lifetime, apparently the first (and only) suggestion of such coupling giving rise to predissociation in NO_2 is that of Busch and Wilson [62].

(3) Predissociation by vibration. This seems to be the only satisfactory explanation for the diffuseness of the $\tilde{B}^2B_1$ rotational levels. In the absence of detailed hypersurface calculations for dissociation, the possibility must be entertained that the $\tilde{A}^2B_2$ predissociation also falls into this category. It appears unadvisable at this time to give this mechanism either more or less weight than the previous one; possibly both are quite important.

The chemiluminescent recombination of $NO(^2\Pi)$ + $O(^3P)$ will proceed on the same surfaces as the dissociation and predissociation and we now address this topic. As is shown in Figure 6, only the $\tilde{X}^2A_1$, $\tilde{A}^2B_2$, $\tilde{B}^2B_1$, and $\tilde{C}^2A_2$ states are adiabatically accessible from the lowest NO + O asymptote; contrary to previous speculations, the $^4B_2$ and $^4A_2$ states of NO_2 will not contribute to the NO + O chemiluminescent emission. At moderate pressures (~1 torr), the emission commences [63] at the dissociation limit, peaks at about 6500 Å, and then monotonically decreases in intensity as far into the infrared as 3.7 μm. (We do note that Paulsen, Sheridan, and Hoffman [64] have reported recombination emission at wavelengths as short as 3832 Å for very long photographic exposures.) Although once

though to be continuous, the emission does show weak, but discrete, structure in the visible and near infrared regions and also exhibits a "peak" at 3.7 μm [65] which is approximately 250 cm^{-1} wide at half height. At lower pressures the maximum intensity in the visible is shifted more to the blue but the overall spectral distribution is much the same.

The thermal emission spectrum [64] and the emission from the $NO(^2\Pi) + O_3(^1A_1)$ chemiluminescent recombination [66] are similar to the NO + O chemiluminescence in that each exhibits discrete structure superimposed on a stronger continuum. Furthermore, a sizeable number of the discrete features can be correlated with the stronger bands in absorption. The evidence is quite strong that the same state (or states) of NO_2 is emitting in each of these experiments.

Measurements of intensity versus pressure have established that the chemiluminescent recombination derives nearly all of its intensity via termolecular collisions

$$NO + O + M \rightarrow NO_2^* + M$$

which result in a stabilized collision complex, followed by vibrational relaxation and emission from a large number of excited electronic state vibrational levels [61]. Thus, the apparently continuous emission is actually a quasi-continuum composed of many densely packed lines. It is expected that most of the emission arises from $\tilde{A}^2B_2 \rightarrow \tilde{X}^2A_1$

and $\tilde{B}^2B_1 \rightarrow \tilde{X}^2A_1$ electric-dipole allowed transitions, as are seen in absorption; however, there is also the possibility of $\tilde{C}^2A_2 \rightarrow \tilde{A}^2B_2$ and $\tilde{C}^2A_2 \rightarrow \tilde{B}^2B_1$ allowed transitions in chemiluminescence. In Figure 3, the accessible $\tilde{C}^2A_2$ levels are seen to have very unfavorable Franck-Condon factors with the $\tilde{B}^2B_1$ state, but a $\tilde{C}^2A_2 \rightarrow \tilde{A}^2B_2$ transition appears to be quite feasible.

We suggest that such a mechanism may be responsible for the 3.7 μm peak observed by Stair and Kennealy [65], who proposed that it represented an electronic transition to or from a low-lying excited electronic state. Clough and Thrush [67] found a similar feature centered at 3.6 μm in the NO + O_3 chemiluminescence. In their study, a 10-fold increase in the concentration of N_2 buffer gas reduced the electronic transition emission intensity at 1.5 μm by a factor of 6, but the intensity of the 3.6 μm peak scarcely changed. Also, under a wide variety of conditions, the intensity of the 3.6 μm feature paralleled that of the NO_2 ν_3 fundamental observed at 6.2 μm. Clough and Thrush interpreted the 3.6 μm peak as a $\Delta v_1 = \Delta v_3 = -1$ transition from high vibrational levels of the ground electronic state; the $\tilde{X}^2A_1$ vibrational constants indicate that for this interpretation the maximum of the 3.6 μm peak corresponds to emission primarily from the (311) and (301) levels. Since the 3.6 μm and 1.5 μm emissions have the same temperature coefficient, it was necessary to assume that the high vibrational levels of the ground state are

efficiently populated by radiative transitions from excited electronic states and not by direct reaction; this is quite unexpected as at room temperature, 93% of the NO_2 molecules are formed in the ground state and only 7% in excited electronic states in the NO + O_3 reaction [66]. Furthermore, since the radiative transitions are expected to strongly excite the bending vibration in the ground state, it was also necessary to postulate a rapid redistribution of vibrational energy from the bending mode to the stretching modes within the ground state. An additional interesting feature is that the Clough and Thrush mechanism requires that as much as 30% of the exothermicity of the NO + O_3 reaction appear as vibrational excitation.

Recently Golde, Roche, and Kaufman [68] have examined the kinetics of the NO + O chemiluminescence at 1.5 μm and in the 3.7 μm peak and have found a deviation from a simple [NO][O] dependence. As the O-atom concentration is increased 10-fold, the intensity ratio $I_{3.7}/I_{1.5}$ drops by about 40% whereas it increases by a factor of 2 when the total pressure is increased from 0.8 to 3.0 torr. They concur with the Clough and Thrush mechanism of population of high vibrational levels of the ground state via radiative transitions followed by $\Delta v_1 = \Delta v_3 = -1$ vibrational emission. To explain their kinetic data, they suggest that the long-lived emitting vibrational levels are depopulated both by collisional quenching and the chemical reaction

$$O + NO_2^{\ddagger} \rightarrow NO + O_2$$

of the vibrationally excited levels; the two competing relaxation mechanisms could then give rise to the complicated kinetic behavior.

We contend that assignment of the 3.7 μm peak to a $\tilde{C}^2A_2 \rightarrow \tilde{A}^2B_2$ electronic transition explains the experimental data equally well and does not require invoking the unusual mechanism of Clough and Thrush in order to obtain population of high vibrational levels in the ground electronic state. In the chemiluminescent recombinations, all adiabatically accessible levels are populated, with the highly excited vibrational levels in each electronic state rapidly deactivated by collisions. The radiative decay of the $\tilde{C}^2A_2$ state is unlikely to be faster than the collisional decay from these highly excited levels. But lower in the $\tilde{C}^2A_2$ manifold, the collisional quenching will be less efficient and the electric-dipole allowed transition $\tilde{C}^2A_2 \rightarrow \tilde{A}^2B_2$ can occur. The calculated vertical energy separation between the minimum of the $\tilde{C}^2A_2$ surface and the $\tilde{A}^2B_2$ surface is about 0.5 eV with an estimated error of $\pm$ 0.3 eV; the observed energy difference of 0.33 eV is within this range. Also, the increase in the intensity ratio $I_{3.7}/I_{1.5}$ with increasing total pressure is understood on the basis that once collisional relaxation has brought the population in the $\tilde{C}^2A_2$ manifold to the lowest levels, further relaxation can only occur through electronic

emission (or chemical reaction with O-atoms or O_3 molecules). On the other hand, the $\tilde{A}^2B_2$ and $\tilde{B}^2B_1$ populations can be collisionally relaxed to low vibrational levels from which electronic emission is not possible (see Figure 3).

Although our calculations did not encompass the 2^2B_2 state, we wish to comment on the predissociation in the 2491 Å $2^2B_2 \leftarrow \tilde{X}^2A_1$ band system. A high resolution spectrum, as given in Herzberg [57], shows that the origin at 2491 Å is sharp, the next band at 2459 Å is somewhat diffuse, and all higher energy cold bands are completely diffuse. Ritchie, Walsh, and Warsop [43] have rotationally analyzed the (0-0) band and, under the assumption of C_{2v} symmetry in the upper state, have deduced a 2^2B_2 equilibrium geometry of $R_0 = 1.314$ Å, $\theta_0 = 121°$. To the observed intervals of 524, 713, and 1156 cm^{-1} were assigned the upper state fundamentals ν_2', ν_3', and ν_1'. Coon, Cesani, and Huberman [36] extended the measurements to the $^{14}N^{18}O_2$ isotopic species at somewhat lower resolution than that of Ritchie *et al.* On the basis of an unusually large origin isotopic shift and the unexpected intensity associated with excitation of the presumed asymmetric stretch in the upper state, Coon *et al.* proposed that the 2^2B_2 state exhibits a double minimum potential along the Q_3' normal coordinate and that the 713 cm^{-1} interval actually corresponds to $2\nu_3'$. They estimate that the two unequal bond lengths at equilibrium are displaced $\pm$ 0.112 Å from the C_{2v} geometry of Ritchie *et al.* and that the inversion barrier is 722 cm^{-1}.

However, although the variation of the bond length distortion and barrier inversion and shape parameters gives a quite reasonable agreement with the observed origin isotopic shift and $\Delta v_3 = 2$ transition intensities, further experimental data in support of the mechanism are not available at this time. More importantly, the double minimum potential does not account for the diffuseness of the bands.

The diffuseness first appears for energies at least as low as 4.98 eV which is less than the $NO(^2\Pi) + O(^1D)$ asymptotic energy of 5.08 eV. Thus this second predissociation limit must correspond to dissociation into either $NO(^2\Pi) + O(^3P)$ or $N(^4S) + O_2(^3\Sigma_g^-)$. From Figure 7 we note that the $N(^4S) + O_2(^3\Sigma_g^-)$ asymptote correlates with the $\tilde{A}^2B_2$, $^4B_2$, and lowest $^6B_2$ states of NO_2. The $N(^4S) + O_2(^3\Sigma_g^-) \rightarrow NO(^2\Pi) + O(^3P)$ reaction [69] has an activation energy of 6 to 7 kcal/mole (0.26 to 0.30 eV) and the NO product vibrational distribution [70,71] indicates the reaction proceeds on a surface with a deep well. For a C_{2v} approach of the N-atom, these data suggest the following possibility: Assume that the $N(^4S) + O_2(^3\Sigma_g^-)$ doublet reaction surface proceeds initially toward the 2^2B_2 state of NO_2 whereas the $\tilde{A}^2B_2$ state is zeroth order correlated with the $N(^2D) + O_2(^3\Sigma_g^-)$ asymptote. The avoided crossing of the two $^2B_2$ hypersurfaces could account for the barrier in the $N(^4S) + O_2(^3\Sigma_g^-)$ reaction and the $\tilde{A}^2B_2$ state certainly exhibits a deep well. The saddle point of the

barrier is then within 0.2 eV of the minimum of the 2^2B_2 state; thus, once the 2^2B_2 state is reached in absorption, it could "surface hop" to the dissociative portion of the lower $^2B_2$ hypersurface, as is schematically illustrated in Figure 8. Similar avoided-crossings would occur for non-C_{2v} approaches; however, in C_s symmetry the $\tilde{X}^2A_1$ state of NO_2 does adiabatically correlate with the $N(^4S) + O_2(^3\Sigma_g^-)$ asymptote and the avoided crossing description becomes quite complicated.

Consider on the other hand a predissociation which yields the products $NO(^2\Pi) + O(^3P)$ to which the 2^2B_2 state also adiabatically correlates. Since the minimum of the 2^2B_2 state is greater than 1.8 eV above this NO + O asymptote, it is not unreasonable to suggest that it is an essentially dissociative state with perhaps a barrier of a few hundred cm^{-1} for dissociation along the Q_3' normal coordinate. Harris, King, Benedict, and Pearse [4] originally proposed that all cold bands of the 2491 Å system could be understood in terms of the upper state fundamentals $\nu_1' = 714\ cm^{-1}$ and $\nu_2' = 523\ cm^{-1}$. On this basis we postulate that the diffuseness observed in the bands is due to predissociation by vibration and the sharp rotational structure of the origin of the band system occurs because the zero-point level in the upper state is below the barrier for dissociation. In such a situation, the hypersurface of the 2^2B_2 state would be far from harmonic in each of its "normal coordinates" which could explain the

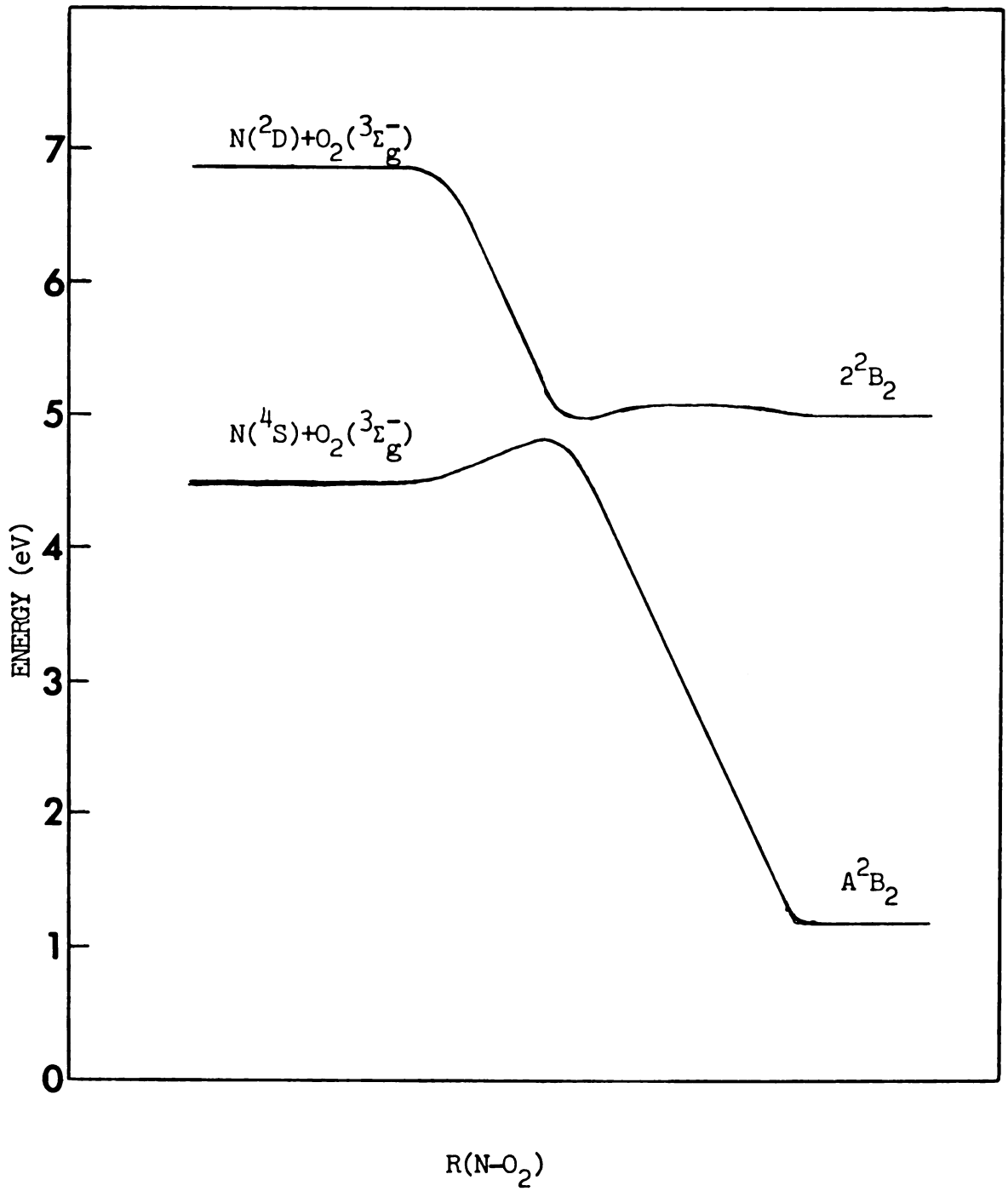

Fig. 8. Schematic potential curves which could give rise to predissociation of the 2^2B_2 state of NO_2 into $N(^4S) + O_2(^3\Sigma_g^-)$.

large anharmonicities, unusual origin isotopic shift, and irregular intensity pattern.

Clearly our suggestions concerning predissociation in the $2^2B_2 \leftarrow \tilde{X}^2A_1$ band system are of a speculative nature. Our purpose is only to identify possible predissociative mechanisms which have to this time been given little attention. We also note that an electronic predissociation by, or an avoided crossing with, the 2^2A_1 state is unlikely. The 2^2A_1 state rises sharply in energy as the bond angle is reduced from linearity and any intersection will be far above the minimum of the 2^2B_2 hypersurface.

Gerstmayr, Harteck, and Reeves [72] have reported the photodissociation of NO_2 by the 6943 Å line of a pulsed ruby laser, although the energy of a single photon at this wavelength only accounts for 57% of the NO_2 dissociation energy. These authors have interpreted their results in terms of two consecutive single photon absorptions rather than the alternative explanations of a simultaneous two photon absorption or a single photon absorption followed by chemical reaction of the initially produced excited electronic state. From their data they infer that the absorption coefficient of the second transition is some 20 times greater than that of the first. As is shown in the potential curves of Figure 3, the state expected to be reached following the absorption of the first photon is $\tilde{A}^2B_2$. The energetically accessible candidates for the upper state of the subsequent transition are $\tilde{X}^2A_1$, $\tilde{A}^2B_2$,

$\tilde{B}^2B_1$, and $\tilde{C}^2A_2$. The middle two can be eliminated since a $^2B_1 \leftarrow {}^2B_2$ transition is electric-dipole forbidden, while the transition within the $^2B_2$ manifold would have very small Franck-Condon factors. The most likely final state appears to be $\tilde{C}^2A_2$, again on the basis of probable Franck-Condon factors. The computation of electronic transition moments would be useful in evaluating the various possibilities.

In a laser photodetachment study of NO_2^-, Herbst, Patterson, and Lineberger [73] observed two distinct processes for photon bombardment of an ion beam produced in a plasma source from O_2 and a trace of N_2 precursors. The first process gave neutral species when the ion beam was intersected by photons of energy $\geq$1.8 eV, while the second required photons of energy $\geq$2.2 eV; either process could be made the predominant one by appropriate selection of the experimental conditions. When NO_2 was employed as the ion precursor, only the higher energy process was found. The common feature for the two different ion beams was shown to arise from

$$NO_2^-(\tilde{X}^1A_1) + h\nu \rightarrow NO_2(\tilde{X}^2A_1) + e$$

and an NO_2 electron affinity of 2.36 $\pm$ 0.10 eV was extracted from the data. It was further suggested that the lower energy photodetachment could be attributed to

$$NO_2^{-*} + h\nu \rightarrow NO(^2\Pi) + O(^3P) + e$$

where NO_2^{-*} denotes a peroxy isomer of NO_2^- of approximate geometry $[N\!\!\swarrow\!\!\searrow O]^-$.

We would like to offer an alternative interpretation, namely

$$NO_2^-(^1A_1, \text{Ring}) + h\nu \rightarrow NO_2(^2B_1, \text{Ring}) + e$$

where "Ring" denotes an electronic state of C_{2v} equilibrium geometry and a nearly equilateral triangle conformation, $[O\!\!\underset{N}{\rightleftharpoons}\!\!O]$. Ab initio calculations of NO_2 [15] and O_3 [74] (isoelectronic with NO_2^-) have predicted the existence of such small angle states. In NO_2 the ring state is of electronic symmetry $^2B_1$; an 18 configuration OVC calculation in the double-zeta quality basis set placed this state adiabatically 1.8 eV above the minimum of the $\tilde{X}^2A_1$ ground state and separated by a barrier of approximately 1.5 eV from the large angle portion of the $\tilde{B}^2B_1$ hypersurface. (We note that the very flat $^2B_1$ potential curve for bond angles in the range $60° \leq \theta \leq 180°$ as deduced by Hay [15] can be attributed to the use of only a two configuration MC-SCF wavefunction and fixed bond lengths in the large and small angle regions.) In a similar study of O_3, Hay and Goddard [75] find that the ring state is again close in energy to the ground state and also separated by a substantial barrier from the large angle portion of the hypersurface.

The pertinent, schematic potential curves to illustrate this mechanism are given in Figure 9. A careful

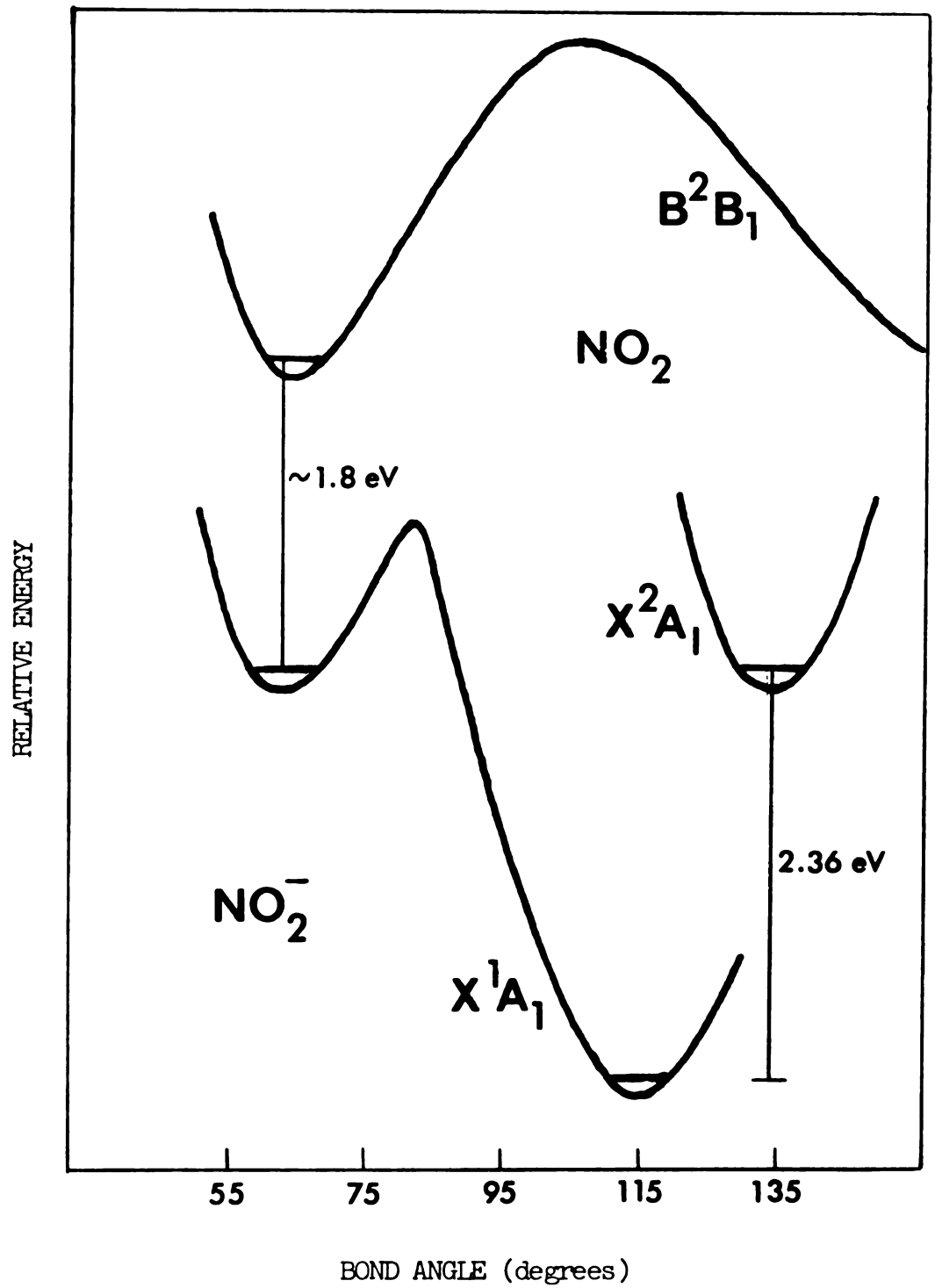

Fig. 9. Schematic potential curves describing the ring states of NO_2^- and NO_2 which could account for the unusual photodetachment process observed by Herbst, Patterson, and Lineberger [73].

theoretical study which includes polarization functions in the basis set and extensive treatment of correlation for both NO_2^- and NO_2 will be necessary for a critical evaluation of the viability of our suggestion.

Perhaps more attention has been devoted to the radiative lifetime controversy than any other aspect of the electronic spectroscopy of NO_2. The most celebrated feature is the "anomalously long fluorescence lifetime." Beginning with the 1954 study of Neuberger and Duncan [76], nearly all lifetime observations [60,76-79] led to values more than 100 times greater than the 0.26 μsec result derived from the integrated absorption coefficient. This issue was further complicated by side disputes concerning the dependence of the lifetime on cell geometry [60,77,78] and excitation wavelength [77] and the question of whether or not the decay is exponential [59,60,77,78]. More recently, studies utilizing laser excitation have revealed that (1) there may be some features which decay in a lifetime of the order of magnitude indicated by the integrated absorption coefficient [80]; and (2) some of the apparently non-exponential decays are actually due to the overlapping of two exponentially decaying transitions of different lifetime [4].

Douglas [58] has discussed four reasons why a fluorescence lifetime might appear anomalously long when compared with that determined from the integrated absorption coefficient. The last of these, level dilution arising

from vibronic coupling of the emitting state with a different electronic state, has received the most attention in NO_2. This proposal was prompted by the realization that if the Born-Oppenheimer levels of the emitting state were sufficiently "diluted" by other levels not optically connected to the ground state of the absorption, the experimental emissive lifetime would be lengthened. The electronic ground state was perforce identified as the source of the diluting levels since only the ground state would provide the requisite high level density.

Now that accurate potential surfaces exist for the low-lying electronic states of NO_2, it is possible to more critically examine this mechamism. As discussed by Kaufman [61], two conditions must be met to substantiate the importance of level dilution: (a) the two states must interact strongly; and (b) their level density ratio must be sufficiently large. Condition (a) seems likely to be met for the $\tilde{A}^2B_2$ state, since, as indicated in Figure 3, the $\tilde{X}^2A_1$ hypersurface intersects very near the minimum of the $\tilde{A}^2B_2$ hypersurface. Further evidence supporting the existence of strong $\tilde{A}^2B_2$ - $\tilde{X}^2A_1$ vibronic coupling will be presented in a later section of this chapter. Unfortunately, condition (b) does not seem to be satisfied, at least to the degree necessary to account for the two-order-of-magnitude discrepancy. Using a semi-classical density of states expression [81], Kaufman [61] calculated for an excited $^2B_1$ state with origin around 12 000 cm^{-1} that the

level density ratio would be less than 4 for absorption in the 20 000 - 25 000 cm^{-1} region, where many of the experimental determinations have been made. Relying on older theoretical calculations [13] which suggested a $^2B_2$ origin around 18 000 cm^{-1}, he found a more suitable density ratio of between 10 and 100 for this state. However, the $\tilde{A}^2B_2$ origin is now known experimentally [50] to be at least as low as 12 000 cm^{-1} and our theoretical results suggest that this may even be as much as 2000 cm^{-1} too high. Consequently, level dilution does not seem capable of accounting for more than a fraction of the lifetime anomaly.

Two recently developed experimental techniques show great promise for clearing up at least part of the lifetime mystery. Stevens, Zare, and coworkers [4,7] have employed a tunable dye laser to selectively excite individual rovibronic levels which eliminates the complication of two overlapping decays of different lifetime; extension of this approach over a wide spectral range may be very informative. Also, Smalley, Ramakrishna, Levy, and Wharton [82] have obtained rotational temperatures of approximately 3°K for a supersonic beam of 5% NO_2 seeded in argon gas, which results in a dramatically simplified fluorescence excitation spectrum.

In addition to the spectral disruption expected from $\tilde{A}^2B_2 - \tilde{X}^2A_1$ vibronic interaction, the regularity of absorption features will be affected by other perturbing mechanisms. The lowest linear $^2\Pi_u$ state is split by

Renner-Teller interaction into the bent $\tilde{X}^2A_1$ ground state and the linear $\tilde{B}^2B_1$ excited state. The form of this interaction is such that all K>0 vibronic levels are determined by the Born-Oppenheimer potentials of both Renner components. This is of little consequence for low vibrational levels of the ground electronic state as there are no perturbing, isoergic $^2B_1$ zeroth-order levels. However, the $\tilde{B}^2B_1$ rovibronic manifold is severely affected as evidenced by the absence of any apparent K'>0 features in absorption.

The same type of behavior is possible for the $\tilde{A}^2B_2$, $\tilde{C}^2A_2$ Renner-split pair of the linear $^2\Phi_g$ state. As shown in Figure 3, these two states are very close in energy over much of their hypersurfaces. For bond angles near 180°, this proximity is due to the ρ^6 dependence of the Renner splitting of a Φ state, where ρ is the supplement of the bond angle. However, in the region of experimental observation, these states are so far from linearity that it is very doubtful that the proximity can still be attributed to Renner-Teller coupling [46,47]. The thrust of this argument is that for small bond angles, the electronic angular momentum of the Φ state is so effectively quenched that it is no longer valid to apply the Renner-Teller formalism. Instead, the closeness of the hypersurfaces is much more likely due to the similar bonding properties of the $4b_2$ and $1a_2$ molecular orbitals, which are respectively in-plane and out-of-plane non-bonding orbitals with

electron density almost entirely on the oxygen atoms. The RHF configurations of the $\tilde{A}^2B_2$ and $\tilde{C}^2A_2$ states differ only in the single occupancy of these two orbitals; an analogous explanation holds for the closeness of the $^4B_2$ and $^4A_2$ states which arise from the linear $^4\Pi_g$ state.

Franck-Condon Factor Calculations

The large differences in the equilibrium geometries of the ground and excited electronic states suggest that rapid change of Franck-Condon factors with excitation wavelength may be responsible in part for the complexity of the absorption of NO_2. To examine this possibility, we have computed vibrational overlap integrals for various values of symmetric vibration quantum numbers in the upper and lower electronic states.

Under the Born-Oppenheimer approximation, the wavefunction separates into a product of an electronic wavefunction and a vibrational wavefunction.

$$\Psi_{as}(q,Q) = \Phi_a(q,Q)\,\chi_{as}(Q) \qquad (14)$$

where q indicates the totality of electronic coordinates, and Q symbolizes the nuclear coordinates. The electronic wavefunction Φ_a is determined for fixed nuclei and thus is parametrically dependent on the nuclear coordinates. The labels on the vibrational wavefunction denote the s^{th} vibrational level of the electronic state Φ_a; reference to explicit vibrational quantum numbers is deferred.

For each absorption band of an electronic transition it is possible to define [83] a "partial oscillator strength." For the electric-dipole allowed transition $\Psi_{bt} \leftarrow \Psi_{as}$, this is given by

$$f_{bt,as} = C\tilde{\nu}_{bt,as}\left|\left\langle\psi_{bt}(q,Q)\left|\hat{\mu}\right|\psi_{as}(q,Q)\right\rangle_{q,Q}\right|^2 \qquad (15)$$

where $C = 4\pi m_e c/3\hbar$, $\tilde{\nu}_{bt,as} = (E_{bt}-E_{as})/h$, $\hat{\mu}$ is the dipole moment operator, and the subscripts denote integration over all electronic and nuclear coordinates.

Substitution of equation (15) into equation (14) and integration over the electronic coordinates yields

$$f_{bt,as} = C\tilde{\nu}_{bt,as}\left|\left\langle\chi_{bt}(Q)\left|P_{ab}(Q)\right|\chi_{as}(Q)\right\rangle_{Q}\right|^2 \qquad (16)$$

where the electronic transition matrix element is

$$P_{ab}(Q) = \left\langle\Phi_b(q,Q)\left|\hat{\mu}\right|\Phi_a(q,Q)\right\rangle_q \qquad (17)$$

It is usually assumed that the electronic transition matrix element varies slowly enough about some point Q_O in the region of significant overlap of Ψ_{bt} and Ψ_{as} such that $P_{ab}(Q)$ may be replaced by $P_{ab}(Q_O)$. This simplifies equation (16) to

$$f_{bt,as} = C\tilde{\nu}_{bt,as}\left|P_{ab}(Q_O)\right|^2\left|\left\langle\chi_{bt}(Q)\left|\chi_{as}(Q)\right\rangle_{Q}\right|^2 \qquad (18)$$

The squared overlap integral is the Franck-Condon factor of the wavefunctions Ψ_{as} and Ψ_{bt}.

Before describing the actual evaluation of the Franck-Condon factors, we note that the replacement of

$P_{ab}(Q)$ by $P_{ab}(Q_0)$ and its subsequent removal from the integration over the nuclear coordinates may introduce error in the case of very weakly overlapping vibrational wavefunctions, as has been discussed by Nicholls [84]. In the future we shall directly compute the electronic transition matrix elements from the ab initio wavefunctions for NO_2 and examine the nuclear coordinate dependence.

Our treatment is predicted upon the vibrations being harmonic which leads to great mathematical simplification. Although inclusion of anharmonicity would change the Franck-Condon factors somewhat, the effect will be small for low quantum numbers. Within this approximation, the vibrational wavefunction factors into a product of one-dimensional harmonic oscillators along the normal coordinates. For the particular case of a non-linear AB_2 triatomic

$$\chi_{as}(Q) = \psi_{v_1}(\alpha_1^{1/2}Q_1)\psi_{v_2}(\alpha_2^{1/2}Q_2)\psi_{v_3}(\alpha_3^{1/2}Q_3) \qquad (19)$$

where

$$\psi_{v_i}(\alpha_i^{1/2}Q_i) = N_{v_i}H_{v_i}(\alpha_i^{1/2}Q_i)\exp(-\alpha_i Q_i^2/2) \qquad (20)$$

and

$$N_{v_i}^2 = \left(\frac{\alpha_i}{\pi}\right)^{1/2}\frac{1}{2^{v_i}(v_i)!}\,. \qquad (21)$$

The H_{v_i} are Hermite polynomials of order v_i and α_i are related to the λ_i of equation (7) by

$$\alpha_i = \lambda_i^{1/2}/\hbar \tag{22}$$

Similar relations can be written for χ_{bt} with the α_i, Q_i, and v_i replaced by β_i, Q_i', and v_i'. In general the normal coordinates will not be the same in the two different electronic states. As pointed out by Duschinsky [85], the two sets are related by

$$Q_i = \sum_k a_{ik} Q_K' + \Delta_i \tag{23}$$

where the a_{ik} are the elements of a rotation matrix A in normal coordinate space, and the Δ_i are displacements determined by the different equilibrium geometries of the two states.

The normal coordinates for each electronic state transform as the irreducible representations of an appropriate point group. If both electronic states in question belong to the same (non-degenerate) point group, two general rules follow from the symmetry transformation properties of the normal coordinates:

(1) a_{ij} is identically zero unless Q_i and Q_j belong to the same irreducible representation.

(2) Δ_i is identically zero unless Q_i transforms as the totally symmetric irreducible representation.

The further requirement of invariance of the kinetic energy

$$2T = \sum_i \dot{Q}_i^2 = \sum_i \dot{Q}_i'^2 \qquad (24)$$

under the transformation of equation (23) forces the A matrix to be orthogonal. For the specific case of an AB_2 triatomic, in which Q_1 and Q_2 transform as a_1 in the C_{2v} point group and Q_3 as b_2, equation (23) expands to

$$\begin{pmatrix} Q_1 \\ Q_2 \\ Q_3 \end{pmatrix} = \begin{pmatrix} \cos\theta & \sin\theta & 0 \\ -\sin\theta & \cos\theta & 0 \\ 0 & 0 & 1 \end{pmatrix} \begin{pmatrix} Q_1' \\ Q_2' \\ Q_3' \end{pmatrix} + \begin{pmatrix} \Delta_1 \\ \Delta_2 \\ 0 \end{pmatrix} \qquad (25)$$

which leads to the following expression for the Franck-Condon overlap integral

$$\langle \chi_{bt} | \chi_{as} \rangle = \int dQ_1' dQ_2' \{ \psi_{v_1'}(\beta_1^{1/2} Q_1') \psi_{v_2'}(\beta_2^{1/2} Q_2') \psi_{v_1} [\alpha_1^{1/2} (\cos\theta Q_1' + \sin\theta Q_2' + \Delta_1)]$$

$$\times \psi_{v_2} [\alpha_2^{1/2} (-\sin\theta Q_1' + \cos\theta Q_2' + \Delta_2)] \} \int dQ_3' \psi_{v_3'}(\beta_3^{1/2} Q_3') \psi_{v_3}(\alpha_3^{1/2} Q_3') \qquad (26)$$

The integral over Q_3' is straightforward and will be discussed later. Although the remaining two-dimensional integral can be evaluated in closed form, clearly the integrations will be extremely tedious for all but the very lowest vibrational quantum numbers.

In a procedure which is in some sense the reverse of the one we are following, Coon, DeWames, and Loyd [86] approximated the two-dimensional integral by assuming that the symmetric normal coordinates in one state could be chosen parallel to those in the other state. Thus the rotation angle θ of equation (25) was arbitrarily chosen

as 0°. Their goal was to extract the Δ_i from ratios of Franck-Condon factors determined by the experimental band intensities; the Δ_i were then combined with the known ground state geometrical parameters to give excited state geometries. In the examples they cited, the changes in geometry were small and good results were obtained. However, for large differences in the equilibrium geometries of the two states, the approximation $\theta = 0°$ becomes inadequate.

The present needs are somewhat different since the normal coordinates, and hence the Δ_i, are already known from the ab initio potential functions. Faced with a similar problem in calculating Franck-Condon factors between the $\tilde{X}^2A_1$ state of NO_2 and the $\tilde{X}^1A_1$ state of NO_2^-, Herbst, Patterson, and Lineberger [73] resorted to numerical integration for evaluation of the two-dimensional integral. We describe here an alternative method which is perhaps simpler, especially when only a few vibrational levels are of interest in one of the two states.

Similar to Coon et al. [86], we choose coordinates for the ground state which are parallel to and displaced from the normal coordinates of the upper state, i.e., the b_{ij} of equation (11) are chosen to be those of the upper state, but R_1^e and R_2^e are those appropriate to the ground state. These two coordinates satisfy the relations

$$X_1 = b'_{11}(R_1-R_1^e) + b'_{12}(R_2-R_2^e) = Q'_1 - \Delta_1 \qquad (27)$$

$$X_2 = b'_{21}(R_1-R_1^e) + b'_{22}(R_2-R_2^e) = Q'_2 - \Delta_2 \qquad (28)$$

Because X_1 and X_2 are <u>not</u> normal coordinates, the potential energy expression in terms of them contains cross terms

$$2(V-E_e) = k_{11}X_1^2 + k_{22}X_2^2 + 2k_{12}X_1X_2 \qquad (29)$$

although the kinetic energy expression is identical in form to equation (12)

$$2T = \dot{Q}_1^2 + \dot{Q}_2^2 = \dot{Q}'^2_1 + \dot{Q}'^2_2 = \dot{X}_1^2 + \dot{X}_2^2 \qquad (30)$$

Because of the cross term in the potential, the vibrational eigenfunctions for symmetric vibration are no longer the product of one-dimensional harmonic oscillators as in the normal coordinate system. Instead, the eigenfunctions are linear combinations of such products along the coordinates X_1 and X_2

$$\psi_{v_1}(\alpha_1^{1/2}Q_1)\ \psi_{v_2}(\alpha_2^{1/2}Q_2) = \sum_{m,n} C_{mn}^{(v_1,v_2)} \psi_m(\gamma_1^{1/2}\chi_1)\psi_n(\gamma_2^{1/2}\chi_2) \qquad (31)$$

where

$$\gamma_i = k_{ii}^{1/2}/\hbar \qquad (32)$$

The expansion coefficients are found by transformation of equations (29) and (30) to the quantum mechanical hamiltonian, and construction and diagonalization of a truncated, infinite matrix whose elements are those of the

hamiltonian operator between the harmonic oscillator product basis functions along X_1 and X_2. The range of indices m and n is increased until the lower eigenvalues of interest have converged. It is important to note that this procedure gives the identical description as the normal coordinate treatment as was verified by comparison of the eigenvalues of the matrix diagonalization with those obtained from the ground state normal coordinate analysis. Naturally the basis set must be made larger to converge higher eigenvalues, but only the first few are necessary to treat the cold bands and prominent hot band absorptions in our study. If the interest is instead in Franck-Condon factors for emission from a few vibrational levels in the upper state to many levels in the ground state, it is more convenient to reverse the process and expand the upper state wavefunction using displaced ground state normal coordinates.

The integral over Q_1' and Q_2' has now been reduced to

$$\langle\psi_{v_1'}(\beta_1^{1/2}Q_1')\psi_{v_2'}(\beta_2^{1/2}Q_2')|\psi_{v_1}(\alpha_1^{1/2}Q_1)\psi_{v_2}(\alpha_2^{1/2}Q_2)\rangle = \tag{33}$$

$$\sum_{m,n} C_{mn}^{(v_1,v_2)} \langle\psi_{v_1'}(\beta_1^{1/2}Q_1')|\psi_m[\gamma_1^{1/2}(Q_1'-\Delta_1)]\rangle\langle\psi_{v_2'}(\beta_2^{1/2}Q_2')|\psi_n[\gamma_2^{1/2}(Q_2'-\Delta_2)]\rangle$$

The resulting one-dimensional integrals of displaced harmonic oscillators are easily evaluated with the aid of relations developed by Henderson, Muramoto, and Willett [87].

For a given one-dimensional integral, these authors defined two dimensionless parameters (in our notation)

$$\delta_i = (\beta_i/\gamma_i)^{1/2} \tag{34}$$

$$D_i = \beta_i^{1/2}\Delta_i \tag{35}$$

and gave the following expression

$$R_{00}^{(i)} = \langle\psi_0(\beta_i^{1/2}Q_i')|\psi_0[\gamma_i^{1/2}(Q_1'-\Delta_i)]\rangle = \left[\frac{2\delta_i}{1+\delta_i^2}\right]^{1/2} e^{-\rho_i^2/2} \tag{36}$$

where

$$\rho_i = D_i/(1+\delta_i^2)^{1/2} \tag{37}$$

for the overlap integral when both quantum numbers are zero. Further, they developed the following two recursion relations which enable the rapid computation of the overlap for all other combinations of the quantum numbers.

$$2\delta_i D_i R_{mn}^{(i)} + (1+\delta_i^2)[2(n+1)]^{1/2}R_{m,n+1}^{(i)} + (2n)^{1/2}(\delta_i^2-1)R_{m,n-1}^{(i)} = 2\delta_i(2m)^{1/2}R_{m-1,n} \tag{38}$$

$$2D_i R_{mn}^{(i)} + 2\delta_i(2n)^{1/2}R_{m,n-1}^{(i)} + (2m)^{1/2}(\delta_i^2-1)R_{m-1,n}^{(i)} = (\delta_i^2+1)[2(m+1)]^{1/2}R_{m+1,n}^{(i)} \tag{39}$$

The integral over Q_3' could also be evaluated with equations (34) through (39). However, except for two linear states, only equal bond length geometries were studied and no information was obtained about the asymmetric stretching frequencies of most of the excited states. In many cases, though, the Q_3' integral is essentially unity if $v_3 = v_3'$ and zero otherwise, as is shown by the following analysis.

The symmetry properties of a harmonic, non-totally symmetric vibration require that its quantum number not change by an odd number for an electronic transition. Consider then the overlap integral over Q_3' for $v_3 = 0$ and $v_3' = 0,2,4,$etc. Since there is no displacement along Q_3', $D_3 = 0$, and equation (38) yields

$$\frac{R^{(3)}_{0,n+1}}{R^{(3)}_{0,n-1}} = -\sqrt{\frac{n}{n+1}}\ \frac{\delta_3^2-1}{\delta_3^2+1} \tag{40}$$

The ratio of $R^{(3)}_{02}$ to $R^{(3)}_{00}$ is therefore less than 0.1 for $0.75 \leq \delta_3^2 \leq 1.32$. The Franck-Condon factor is the square of the overlap integral, so if δ_3 is in the specified range, the $\Delta V_3 = 2$ transition has less than 0.01 the intensity of the $\Delta V_3 = 0$ transition. Now

$$\delta_3{}^2 = (\beta_3/\alpha_3)^2 = \omega_3'/\omega_3 \tag{41}$$

and unless the asymmetric stretching frequencies are greater than 30% different in the two states of the transition, the square of the Q_3' overlap integral is unity for $v_3' = 0 \leftarrow v_3 = 0$ and zero for $v_3' \neq 0 \leftarrow v_3 = 0$ to less than 1% error. The overlap is similarly diagonal for transitions from $v_3 \neq 0$ levels.

In summary of this section: we invoked the Born-Oppenheimer approximation and assumed that the electronic transition matrix element is independent of nuclear geometry in order to obtain an expression involving Franck-Condon factors and related to the transition oscillator strength. A set of (non-normal) coordinates were defined for the ground state which enabled the ground state vibrational wavefunction to be expanded in products of harmonic oscillators along the upper state normal coordinates. Consequently, the three-dimensional overlap integral was reduced to a linear combination of products of one-dimensional integrals which are easily evaluated.

The $\tilde{B}^2B_1 \leftarrow \tilde{X}^2A_1$ Absorption System

The first published rotational analysis in the visible region of the absorption spectrum of NO_2 is that of Douglas and Huber [1], who assigned a series of bands in the region 4600 to 3700 Å as perpendicular $K'=0 \leftarrow K''=1$ transitions to a $^2B_1$ excited electronic state. The observed bands form a nearly harmonic progression in an upper state vibration, thought to be the bending mode, of

about 900 cm^{-1}. From the qualitative arguments of Walsh [2], the $^2B_1$ excited state is expected to be low-lying and to have a substantially larger bond angle than that in the $\tilde{X}^2A_1$ ground state. Both the $^2B_1$ and $\tilde{X}^2A_1$ states arise from Renner-Teller splitting of the lowest linear $^2\Pi_u$ state; it was suggested by Douglas and Huber that the absence of any K'>0 features was likely due to perturbations created by the Renner-Teller interaction, which will disrupt all but the K'=0 upper state levels. The magnitude of the band isotope shifts of the $^{14}N^{16}O_2$ and $^{15}N^{16}O_2$ isotopic species indicate a system origin between 8500 and 6500 Å (1.46 to 1.91 eV). Since the observed bands are far removed from the system origin, it is not possible to determine the $^2B_1$ equilibrium geometry from the Douglas and Huber data.

Hougen, Bunker, and Johns [49] have developed a hamiltonian, later extended by Bunker and Stone [88], which employs a curvilinear bending coordinate to account explicitly for the effects of large amplitude bending vibrations. After enlarging the Douglas and Huber absorption study to include the $^{14}N^{18}O_2$ species, Hardwick and Brand [48] used this hamiltonian to mathematically extrapolate to the system origin of the $^2B_1$ state. For each of the three isotopic species, the parameters of the hamiltonian were varied to give the best least squares fit to the observed Σ_g^- vibronic levels of the excited state. The experimental band origins were best reproduced for a linear $^2B_1$ state. The remaining three parameters,

quadratic and quartic force constants of the potential function and the system origin T_0, were determined separately for each isotopic species by Hardwick and Brand and are given in Table XXII.

TABLE XXII

SYSTEM ORIGINS AND POTENTIAL CONSTANTS OF THE $^2B_1$ STATE OF NO_2 AS DETERMINED BY HARDWICK AND BRAND*

	$^{14}N^{16}O_2$	$^{15}N^{16}O_2$	$^{14}N^{18}O_2$
T_0 (cm^{-1})	14743.5	14722.3	14717.9
K_{22} (md-Å/rad^2)	0.46228	0.46595	0.46218
K_{2222} (md-Å/rad^4)	0.050054	0.051105	0.042047

*Reference 48.

It was suggested by these authors that there is a possible uncertainty of one in their vibrational quantum number assignments. We have analyzed the results of Hardwick and Brand on the basis of origin isotopic shifts and find strong evidence in support of a revisement of the system origin to one quantum of the bend further to the red. Our reasoning is detailed in the next several paragraphs.

The form of the normal coordinates of an AB_2 triatomic lead to the following relationships of the harmonic vibrational frequencies for the normal and isotopically substituted species [57]

$$\text{Bent } NO_2 \begin{cases} \left(\frac{\omega_1^*\omega_2^*}{\omega_1\omega_2}\right)^2 = \frac{m_O^2 m_N}{m_O^{*2} m_N^*} \frac{(m_N^* + 2m_O^*)}{(m_N + 2m_O)} & (42) \\ \left(\frac{\omega_3^*}{\omega_3}\right)^2 = \frac{m_O m_N}{m_O^* m_N^*} \frac{(m_N^* + 2m_O^* \sin^2\alpha)}{(m_N + 2m_O \sin^2\alpha)} & (43) \end{cases}$$

$$\text{Linear } NO_2 \begin{cases} \left(\frac{\omega_1^*}{\omega_1}\right)^2 = \frac{m_O}{m_O^*} & (44) \\ \left(\frac{\omega_2^*}{\omega_2}\right)^2 = \left(\frac{\omega_3^*}{\omega_3}\right)^2 = \frac{m_O m_N}{m_O^* m_N^*} \frac{(m_N^* + 2m_O^*)}{(m_N + 2m_O)} & (45) \end{cases}$$

where m_O and m_N are the masses of the oxygen and nitrogen atoms, respectively, 2α is the equilibrium bond angle, and the asterisks denote the isotopically substituted species.

Our analysis requires the harmonic vibrational frequencies in the $\tilde{X}^2A_1$ ground state for the isotopic modifications of interest and these are listed in Table Table XXIII. The $^{14}N^{16}O_2$ and $^{15}N^{16}O_2$ data are from the infrared study of Arakawa and Nielsen [32] and ω_3^* for $^{14}N^{18}O$ results from the substitution of the $^{14}N^{16}O_2$ value of ω_3 into equation (43). In order to obtain ω_1 and ω_2 for $^{14}N^{18}O_2$, we use the Coon, Cesani, and Huberman [36] measurement of ν_1 and ν_2, assume that the difference in ν_2 and ω_2 is essentially the same as for the other isotopic species, and choose ω_1 to satisfy equation (42).

If anharmonicity is neglected, the origin of an electronic transition is given by

$$\sigma_o = (T_e' - T_e'') + \frac{1}{2}(\omega_1' + \omega_2' + \omega_3') - \frac{1}{2}(\omega_1'' + \omega_2'' + \omega_3'') \qquad (46)$$

TABLE XXIII

HARMONIC FREQUENCIES OF ISOTOPIC MODIFICATIONS IN THE $^2A_1$ STATE OF NO_2

	$^{14}N^{16}O_2$ [a]	$^{15}N^{16}O_2$ [a]	$^{14}N^{18}O_2$ [b]
ω_1 (cm^{-1})	1357.8	1342.5	1308 ± 2
ω_2 (cm^{-1})	756.8	747.1	728 ± 1
ω_3 (cm^{-1})	1665.5	1628.0	1633.7

[a] Reference 32.

[b] Coon, Cesani, and Huberman [36] measured $\nu_1'' = 1268.6 \pm 0.4$ cm^{-1}, $\nu_2'' = 721.0 \pm 0.4$ cm^{-1} for $^{14}N^{18}O_2$

The quantity $(T_e' - T_e'')$ is independent of isotopic substitution so that the origin isotopic shift is

$$\Delta\sigma_0 = \sigma_0 - \sigma_0^* = \frac{1}{2}\sum_{j=1}^{3}[(\omega_j' - \omega_j'^*) - (\omega_j'' - \omega_j''^*)] \qquad (47)$$

For the isotopes $^{14}N^{16}O_2$ and $^{15}N^{16}O_2$, the ground state change in zero point energy is 31.2 cm^{-1}. If the excited $^2B_1$ state is linear, then $\omega_1' = \omega_1'^*$, and application of equation (45) reduces equation (47) to

$$\Delta\sigma_0 = \frac{1}{2}(0.0234)(\omega_2' + \omega_3') - 31.2 \qquad (48)$$

The Hardwick and Brand analysis gives $\Delta\sigma_0 = 21.2$ cm^{-1} and predicts an ω_2' in the neighborhood of 925 cm^{-1}. The origin

shift then requires an ω_3' of 3500 cm^{-1}, which is certainly much too large for such relatively heavy atoms.

In Figure 10 we have plotted the isotope shift relative to the $\sigma(^{14}N^{16}O_2)$ of the Hardwick and Brand calculated band origins versus $\sigma(^{14}N^{16}O_2)$ and have extrapolated one quantum of the bend further to the red. A revised value of $\Delta\sigma_0 = 3 \pm 1$ cm^{-1} for $^{14}N^{16}O_2$ and $^{15}N^{16}O_2$ results which reduces the estimate of ω_3' to 2000 ± 200 cm^{-1}. From a comparison with the $^1\Sigma_g^+$ ground state of CO_2, this seems to be reasonable. The asymmetric stretching fundamental of CO_2 is 2349 cm^{-1} and addition of an electron into the $2\pi_u$ antibonding orbital to give the electronic configuration of the $\tilde{B}^2B_1(^2\Pi_u)$ state of NO_2 will reduce this somewhat.

The accurate OVC and OVC-CI theoretical data also strongly support the proposed revisement of the origin. As has been the case in all other <u>ab initio</u> studies, the $\tilde{B}^2B_1$ state is again found to be linear. Very encouraging is the agreement of the <u>ab initio</u> $\omega_2' = 960$ cm^{-1} and $\omega_3' = 2040$ cm^{-1} with the experimental harmonic bending frequency of 925 ± 10 cm^{-1} and the asymmetric stretching frequency of 2000 ± 200 cm^{-1} derived from the revised assignment of the system origin. The consistency seems good enough to warrant the use of these numbers in conjunction with the theoretical $\omega_1' = 1192$ cm^{-1} to examine the origin isotope shift for $^{14}N^{16}O_2$ and $^{14}N^{18}O_2$. From the <u>ab initio</u> upper state vibrational frequencies and the experimental ground state frequencies the predicted origin

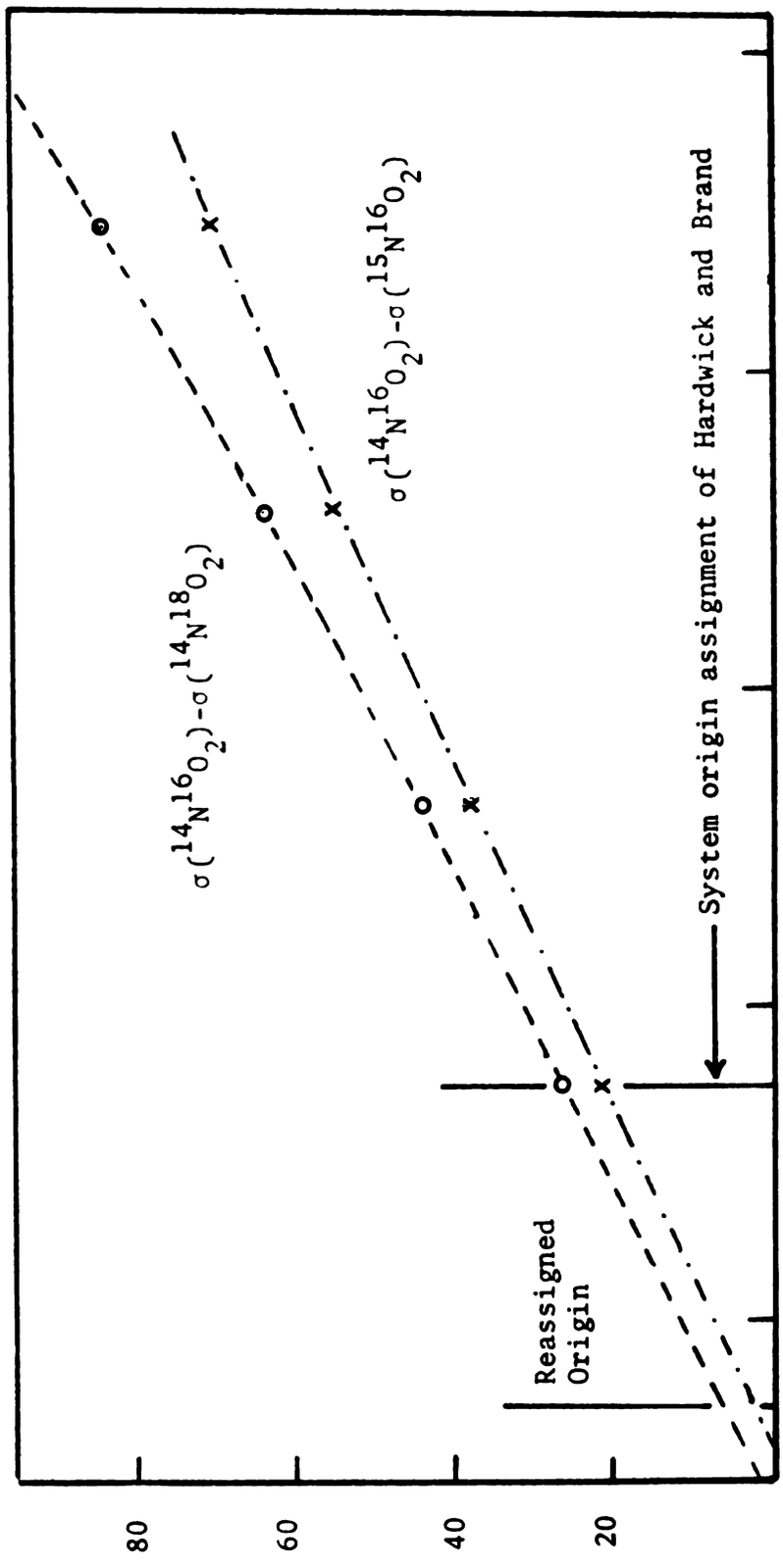

Fig. 10. Band origin isotope shifts in the $B^2B_1 \leftarrow X^2A_1$ absorption system as calculated by Hardwick and Brand [48].

The position of the reassigned origin as predicted by our isotope shift analysis is indicated.

shift is 5.6 cm^{-1} to the red; the analysis of Hardwick and Brand gives 25.6 cm^{-1} which is reduced to about 5 cm^{-1} for the proposed reassignment of the origin. The OVC-CI adiabatic separation of the $\tilde{X}^2A_1$ and $\tilde{B}^2B_1$ hypersurfaces is 1.66 eV. For the $\tilde{B}^2B_1$ state, the zero point energy is calculated to be 2100 cm^{-1}; when this is combined with the experimental $\tilde{X}^2A_1$ zero point energy of 1840 cm^{-1}, a $\tilde{B}^2B_1 \leftarrow \tilde{X}^2A_1$ origin of 1.69 eV is obtained. The Hardwick and Brand $^{14}N^{16}O_2$ origin is 1.83 eV which drops to 1.71 eV for the proposed vibrational quantum number reassignment. However, we do note that the OVC-CI origin has an estimated uncertainty of $\pm$ 0.3 eV and is therefore consistent with either the Hardwick and Brand or revised origins.

Three remarks concerning the validity of the isotope shift analysis are in order:

(1) The least squares fit will be distorted if a local perturbation affects a given band origin more in one isotopic species than in the others and this distortion would be magnified in the long extrapolation to the system origin.

(2) Although the force constants obtained in the reduction of the data for each isotopic species are very similar, they do vary slightly and hence must represent effective potential constants. A simultaneous fit of all three isotopic species is desirable, but requires knowledge of the anharmonicities associated with the stretching vibrations, which have as yet not been observed.

(3) We have assumed that the origin isotope shifts for the proposed reassignment of vibrational quantum numbers follow directly from an extrapolation of the calculated band origins obtained with the Hardwick and Brand quantum numbering. The possibility exists that recalculation of the least squares fit for the revised quantum numbering would substantially affect the computed band origins, necessitating changes in our analysis.

Nevertheless, despite these caveats, there is a strong suggestion that the origin of the $\tilde{B}^2B_1 \leftarrow \tilde{X}^2A_1$ absorption in NO_2 is about 925 cm^{-1} to the red of the value given by Hardwick and Brand.

Hardwick and Brand also employed the numerical vibrational wavefunctions which they obtained to correct the experimentally observed B'_{v_2} for the effects of large amplitude bending in order to yield extrapolated values of B'_0 and hence r'_0. They suggest that an equilibrium bond length of 1.23 Å for the $\tilde{B}^2B_1$ state, or a lengthening of nearly 0.04 Å from the ground state, is indicated. However, we favor the <u>ab initio</u> prediction of a less than 0.01 Å increase in bond length and cite the following evidence:

(1) The <u>ab initio</u> bond length calculations are expected to be accurate to 0.02 Å and no worse than this for predicting trends.

(2) The $\tilde{X}^2A_1$ and $\tilde{B}^2B_1$ states are Renner-Teller split components of a linear $^2\Pi_u$ state and as such are expected to have very similar bond lengths.

(3) No spectral features assignable to excitation of the symmetric stretching mode have been observed in the $\tilde{B}^2B_1 \leftarrow \tilde{X}^2A_1$ system. Computed Franck-Condon factors, based on a change in the bond length of 0.01 Å, predict that absorption to $(1,v_2',0)$ upper state levels should occur with intensities comparable to absorption to $(0,v_2',0)$ levels in the region of experimental observation. If the change in bond length between the two states is actually as large as 0.04 Å, the stretching features should be quite prominent.

(4) There is a trend in the data of Hardwick and Brand in that the lower the vibrational level from which the extrapolation from B'_{v_2} to B'_0 is made, the shorter the predicted r'_0. Neglect of the effects due to bond stretching in the hamiltonian of Hougen et al. is the likely cause of this behavior.

The $\tilde{B}^2B_2 \leftarrow \tilde{X}^2A_1$ Absorption System

Although the absorption features associated with the $\tilde{B}^2B_1$ upper state are reasonably strong, they only account for a small number of the observed spectral lines. Polarization studies [45] established that most of the visible absorption intensity arises from a transition with moment parallel to the axis joining the two oxygen atoms, indicating a $^2B_2$ upper state; the presence of the $\tilde{A}^2B_2$

low-lying excited state of NO_2 has since been verified by rotational analyses [3-9] obtained through several diverse experimental techniques. However, the analyzed bands are in widely separated regions of the spectrum and there is no clear relationship among the various sets of rotational constants which have been extracted. Consequently, there is no precise determination of the $\tilde{A}^2B_2$ equilibrium geometry or vibrational frequencies. Brand and coworkers have suggested tentative vibrational quantum number assignments [5] for the strongest cold bands in the 8500 to 6000 Å spectral region and have associated the origin of the $\tilde{A}^2B_2 \leftarrow \tilde{X}^2A_1$ transition with a feature near 8350 Å [50]. However, as pointed out by these authors, separations of consecutive members of the assigned progressions show a several percent variation in the upper state vibrational frequencies. Their value for the system origin is based on the temperature variation of the absorption; isotope substitution studies were inconclusive due to abnormally large and highly irregular band shifts.

In view of the present uncertainties concerning the $\tilde{A}^2B_2$ state, the <u>ab initio</u> calculations which we have presented are of significant value because of the reliable zeroth description they provide. To be sure, the theoretical vibrational frequencies and origin are not of a sufficient accuracy for a definitive assignment of the experimental spectral features. However, they are expected to be very useful for prediction of trends and evaluation

of possible interpretations. On the other hand, the ab initio equilibrium geometries should be quite representative of the $\tilde{A}^2B_2$ Born-Oppenheimer state. Thus, if there are large deviations in the theoretical and observed rotational constants (as there are), these must be attributed to the influence of perturbations and not to any inherent deficiencies of the theoretical approach. With the existence of these perturbations firmly established, the ab initio results further serve to assess the significance of various candidates for such a perturbing role. Although this aspect is only discussed in a qualitative fashion here, it does not seem unreasonable to anticipate direct evaluation of perturbation matrix elements from the ab initio wavefunctions in the future.

In this section we discuss the ab initio potential surface for the lowest $^2B_2$ state of NO_2 in the space of C_{2v} geometries. From this surface and that of the $\tilde{X}^2A_1$ ground state, Franck-Condon factors (FCF) are computed using the techniques previously described. A theoretical absorption spectrum is then constructed from the FCF and a correlation with the experimental spectrum attempted. After the successes of the theoretical spectrum in reproducing experiment are examined in some detail, we conclude this section with an analysis of the vibronic perturbation most likely responsible for the spectral disruption.

The computed equilibrium geometry of the $\tilde{A}^2B_2$ state is R_e = 1.26 Å, θ_e = 102° which represents an increase of 0.06 Å and a decrease of 32° from the respective $\tilde{X}^2A_1$ parameters. The $\tilde{A}^2B_2$ state at its minimum is calculated to be only 1.18 eV above the minimum of the ground state, but some 3.4 eV above $\tilde{X}^2A_1$ for vertical excitation. The theoretical prediction is therefore for the absorption to commence in the vicinity of 10 000 Å, with progressions of increasing intensity in both the symmetric stretching mode and the bending mode, especially the latter, toward 4000 Å and beyond. The experimental spectrum does in fact steadily increase in intensity to a maximum around 3900 Å (3.2 eV) [89] from an assumed origin at 8350 Å (1.48 eV). The agreement of the qualitative features of theory and experiment is pleasing but not a very stringent test of the reliability of the calculations. However, with the aid of the FCF from which an absorption spectrum is generated, more detailed comparisons are possible.

The theoretical spectrum has been constructed under the assumption that only excitation of the symmetric vibrational modes in the upper state is important. Although this is largely dictated since only C_{2v} geometries were considered in the ab initio calculations, any transitions with $\Delta V_3 \neq 0$ are expected to be quite weak, as discussed previously. Nevertheless, Brand, Hardwick, Pirkle, and Seliskar [5] found a strong ν_3 hot band in their absorption

study, which indicates the presence of vibronically allowed bands. This is supported in turn by the laser induced fluorescence study of Abe, Myers, McCubbin and Polo [3]. The fluorescence induced by the 4800 Å Ar^+ line consists of bands displaced to lower energy from the exciting radiation by frequencies corresponding to ν_1, ν_2, and $2\nu_2$ in the ground electronic state. However, additional lines were seen for which the displacement was close but not equal to ν_3 in the ground state. These somewhat unexpected lines were explained by Abe *et al.* on the following basis: the laser excitation is from the $\tilde{X}^2A_1$ vibrationless level of vibrational symmetry A_1 to a level which has B_2 (v_3' odd) vibrational symmetry in the $\tilde{A}^2B_2$ excited electronic state. This transition, which is vibronically $A_1 \leftarrow A_1$, obeys perpendicular rotational selection rules ($\Delta K = \pm 1$ in the limit of a prolate symmetric top) and hence is electronically forbidden but vibronically allowed. The fluorescence, however, returns to the (001) vibrational level of the ground electronic state, and is fully allowed, corresponding to an $A_1 \rightarrow B_2$ vibronic transition obeying parallel rotational selection rules ($\Delta K = 0$). In a later microwave-optical double resonance (MODR) study, Solarz, Levy, Abe, and Curl [8] deduced the rotational quantum numbers involved in both the upper and lower states and confirmed this interpretation.

The observance of $\Delta_{v_3} = \pm 1$ transitions does not *a priori* vitiate our neglect of asymmetric stretching

features in generating the theoretical absorption spectrum. As pointed out by Brand et al.[5], in a fixed frequency laser study, very weak transitions may appear with apparently appreciable intensity if the narrow laser line matches the bandwidth of the weak transition but does not significantly overlap the bandwidth of stronger, more allowed transitions. This appears to be the case for the 4880 Å laser line; however, in emission the totally allowed parallel fluorescence is observed, but not the perpendicular, electronically forbidden, resonance fluorescence. Use of a tunable laser in this spectral region would reveal the relative intensities of the "unusual" transitions vis a vis the stronger, fully allowed transitions which are nearby in energy. On the other hand, the ν_3 hot band found by Brand et al. in a straightforward absorption experiment does indicate that such ostensibly weak transitions are fairly strong, and may in fact be competitive in intensity with the fully allowed transitions in certain regions of the spectrum. The appearance of these unexpected transitions could also be taken as evidence supporting the existence of vibronic perturbations in the excited state.

The FCF necessary for construction of the theoretical absorption spectrum were computed strictly on the basis of the ab initio equilibrium geometries, normal coordinates, and harmonic vibrational frequencies of the $\tilde{X}^2A_1$ and $\tilde{A}^2B_2$ electronic states. The pertinent parameters have been given previously in Tables XX and XXI. Consistent with

the large differences in the equilibrium geometries of the two states, the FCF for low vibrational levels in each state are very small, as shown in Table XXIV.

Once the FCF have been calculated, the theoretical absorption spectrum is easily generated. From the upper state T_e, the vibrational frequencies of the two states, and the appropriate vibrational quantum numbers, the ν frequency factor is calculated for each vibronic transition. Each FCF, multiplied by its frequency factor and a Boltzmann factor for the chosen temperature, results in the partial oscillator strength of that transition. Plots of the partial oscillator strengths versus the transition frequencies comprise the theoretical absorption spectrum.

The *ab initio* $\tilde{A}^2B_2 \leftarrow \tilde{X}^2A_1$ spectrum for a temperature of 300°K is shown in Figure 11. In the computation of the transition frequencies, the *ab initio* value of ω_1' was reduced from 1461 cm^{-1} to 1410 cm^{-1}; without this modification, many of the absorption features would be nearly indistinguishable at the resolution of Figure 11 since ω_1' is so close to $2\omega_2'$ (1461 cm^{-1} vs. 2 x 738 = 1476 cm^{-1}). The choice of the modified ω_1' smaller than $2\omega_2'$ was prompted by a comparison of the experimental and theoretical spectra. We also point out that the direction of the adjustment of ω_1' is consistent with the probable effect of the introduction of anharmonicities. (The x_{11} anharmonicity constant is an order of magnitude larger than x_{22} for the $\tilde{X}^2A_1$ ground state [32].)

TABLE XXIV

SOME COMPUTED FRANCK-CONDON FACTORS FOR $\tilde{A}^2B_2 \leftrightarrow \tilde{X}^2A_1$ TRANSITIONS IN NO_2

$(v_1' \; v_2' \; v_3')$	$(v_1'' \; v_2'' \; v_3'')$	FCF*	Relative FCF
000	000	3.82×10^{-9}	1.0
010	000	5.04×10^{-8}	13.2
020	000	3.30×10^{-7}	86.4
100	000	1.80×10^{-8}	4.7
200	000	4.37×10^{-8}	11.4
110	000	2.43×10^{-7}	63.6
120	000	1.63×10^{-6}	427.
060	000	2.51×10^{-5}	6570.
140	000	2.39×10^{-5}	6260.
000	010	7.41×10^{-8}	19.4
010	010	8.68×10^{-7}	227.
020	010	5.00×10^{-6}	1310.
020	020	3.71×10^{-5}	9710.
000	100	5.45×10^{-9}	1.4

*Computed from the OVC-CI potential surfaces.

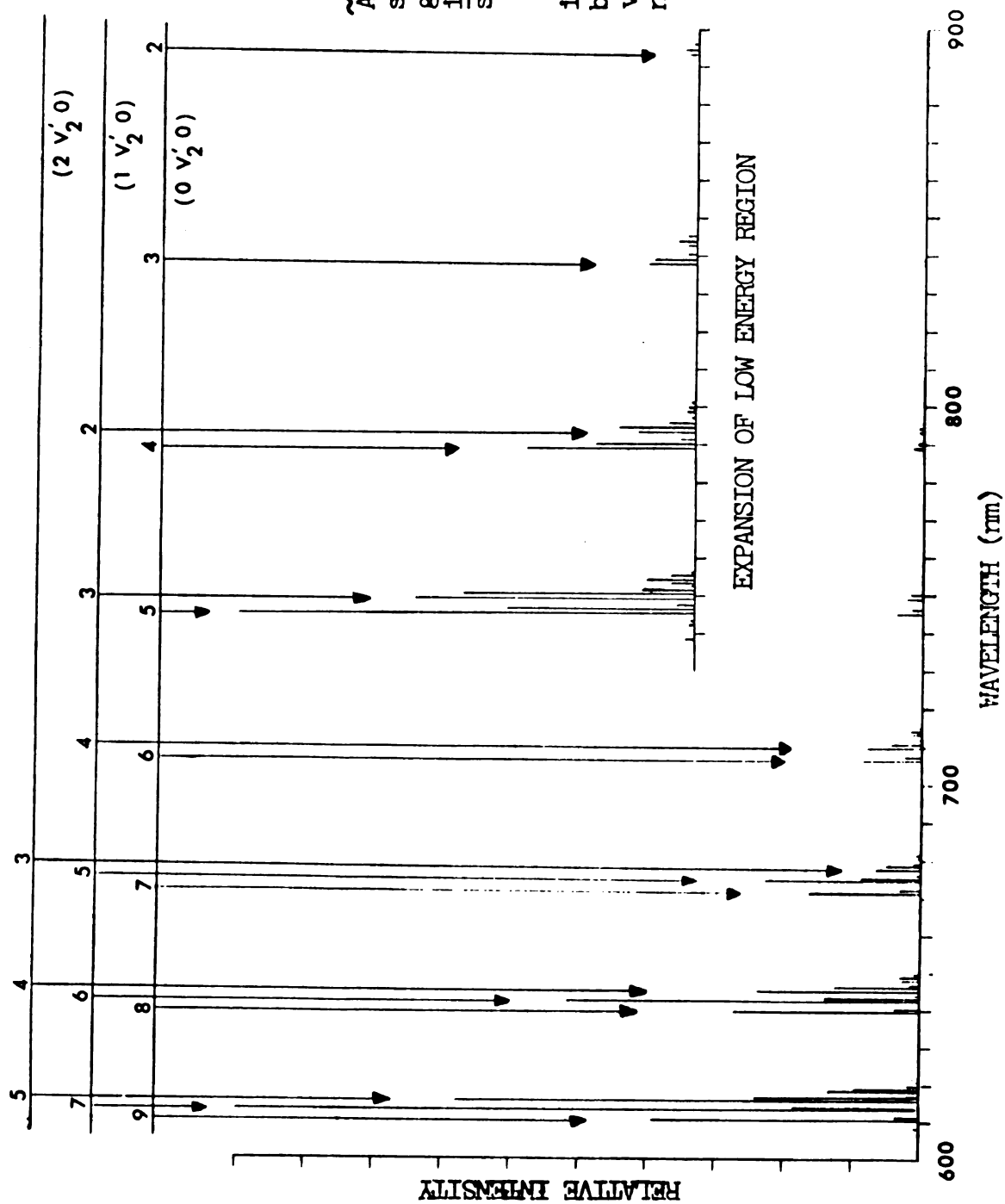

Fig. 11. The $\tilde{A}^2B_2 \leftarrow \tilde{X}^2A_1$ absorption spectrum at 300°K generated from the ab initio potential surfaces.

Cold bands are indicated and labelled by the upper state vibrational quantum numbers.

Some of the features of the theoretical spectrum which we feel are worthy of comment include:

(1) The origin of the $\tilde{A}^2B_2 \leftarrow \tilde{X}^2A_1$ absorption is very weak relative to higher energy portions of the spectrum. The FCF for vertical excitation are probably on the order of 0.1, so that the origin is some seven orders of magnitude weaker.

(2) The low energy region is going to be considerably complicated by unusually strong hot bands, even at room temperature. The transition (010) ← (010) will occur at almost the same frequency as (000) ← (000) since the bending frequency is nearly the same in the two electronic states. The computed FCF for this particular hot band is larger than that for the origin by a factor of 227 which outweighs the Boltzmann factor of 0.027 at a temperature of 300°K. At 500°K, for which the Boltzmann factor for a ν_2 hot band is increased to 0.11, the origin will be almost completely buried under this hot band. We have identified the cold bands in Figure 11 by labelling them by the upper state vibrational quantum numbers. We note that although the hot bands are relatively less prominent higher in the $\tilde{A}^2B_2$ manifold, their effect is by no means negligible.

(3) The intensity of the cold bands increases rapidly near the origin. On the basis of the FCF, the intensities of the cold bands (020) ← (000), (010) ← (000), and (000) ← (000) are in the proportion 86:13:1.

(4) Higher in the $\tilde{A}^2B_2$ manifold, spectral features involving simultaneous excitation of both bending and symmetric stretching modes become relatively more intense than those in which only the bending mode is excited.

Before proceeding to an actual comparison of the theoretical and experimental absorption spectra, we summarize some limitations of our approach.

(1) The theoretical spectra are stick plots of intensity versus wavelength for the idealized case of a non-rotating molecule and the effects of rotational motion (K and N structure in the limit of a prolate symmetric top, Hönl-London line strength factors, rotational selection rules, etc.) have been neglected. Thus in the normalization of the most intense line of the theoretical spectrum to the most intense "peak" of the experimental spectrum, some error is introduced since other background transitions are undoubtedly contributing some of the apparent intensity of the most intense peak. This error will be minimized if each dominant spectral feature is equally affected by the background intensity on a percentage basis.

(2) The variation of the electronic transition moment with nuclear geometry has been ignored in order to obtain an expression relating intensity to Franck-Condon factors.

(3) The vibrational frequencies and normal modes have been found for infinitesimal amplitudes of the vibrations, yet the FCF of interest are primarily those for

transitions in which several quanta are excited, either in the upper or lower states, or both. Certainly as the domain of large amplitude vibrations is entered, the use of harmonic wavefunctions for computing the FCF becomes less satisfactory. Similarly, neglect of anharmonicity will affect the computed transition frequencies.

(4) The final complication is more a peculiar property of NO_2 than it is a limitation of our approach. As will be discussed, the evidence is indisputable that the $\tilde{A}^2B_2$ state is severely perturbed by high vibrational levels of the ground state. The consequences of this interaction are almost completely unknown in more than a qualitative sense and it is not possible to account for them in the generation of the ab initio absorption spectrum.

Although these caveats are not inconsequential, the theoretical spectrum is quite successful in reproducing many of the qualitative features of the low resolution experimental absorption spectrum as shown in Figures 12 and 13. We would suggest that the experimental spectrum be viewed in terms of groups of bands, with the groups roughly centered at the wavelengths 892, 836, 791, 747, 710, 671, 647, and 615 cm^{-1}. The existence of groups of bands arises from the near coincidence and overlapping of cold bands to the upper state levels $(0,v_2',0)$, $(1,v_2'-2,0)$, $(2,v_2'-4,0)$, etc. Complications are introduced by vibronic interaction with the ground state, the prominent hot bands at low energies, and the likely occurrence of Fermi

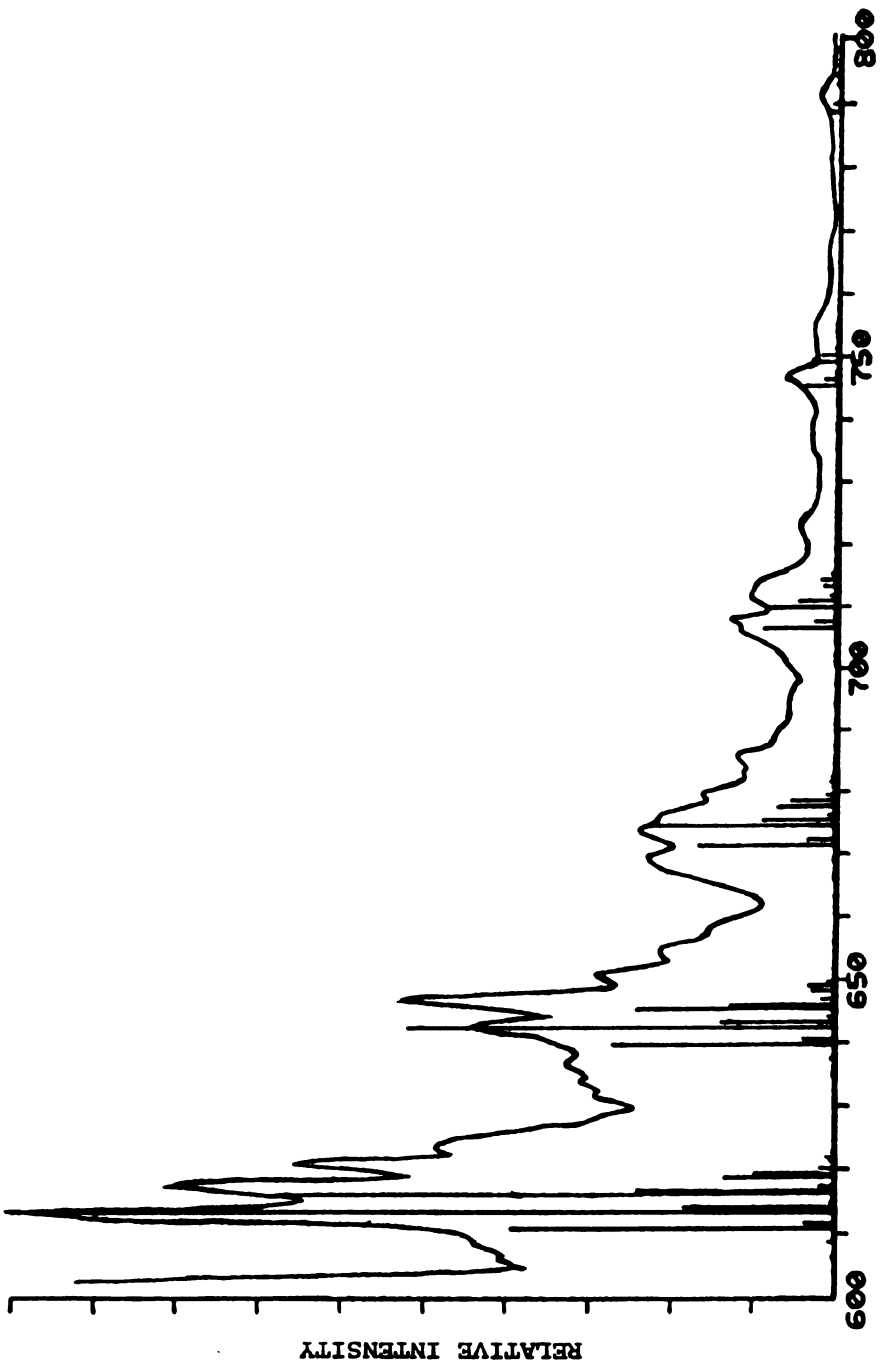

Fig. 12. Superposition of a low resolution (~10 Å) experimental NO_2 absorption spectrum between 800 and 600 nm on the $\tilde{A}^2B_2 \leftarrow \tilde{X}^2A_1$ spectrum generated from the ab initio potential surfaces.

The experimental spectrum has been measured on a Cary 17 operated in the infrared detection mode. The theoretical spectrum is normalized to the strongest experimental band.

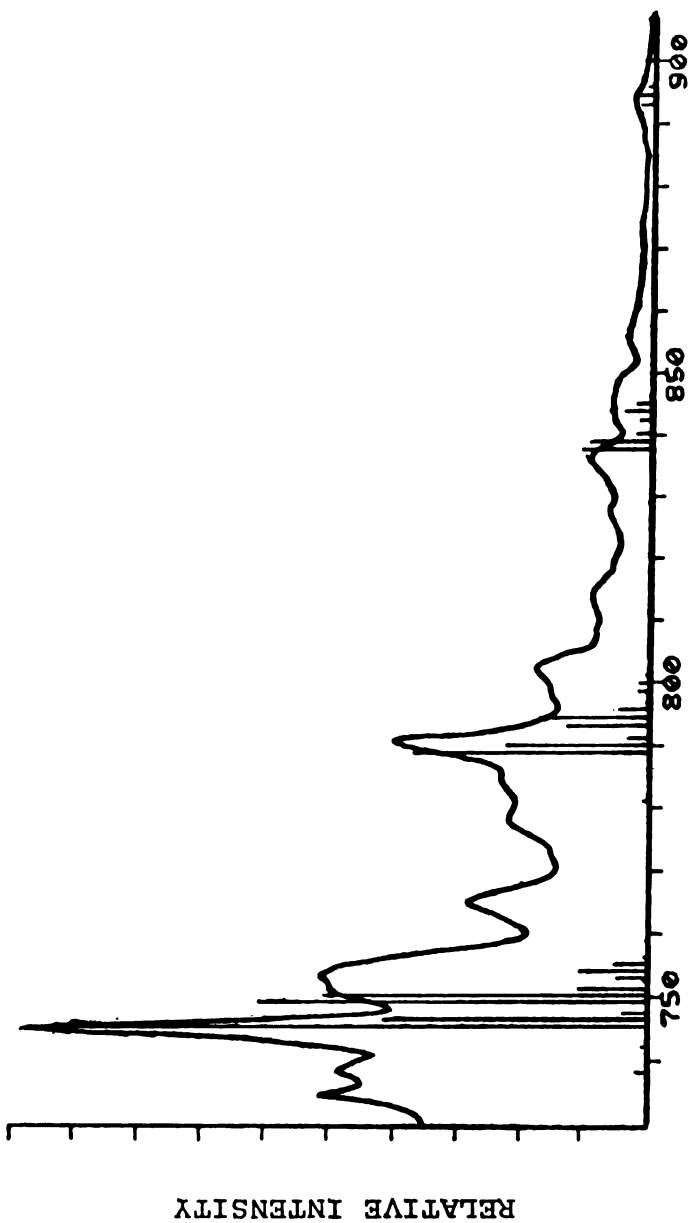

Fig. 13. Superposition of a low resolution NO_2 absorption spectrum between 900 and 730 nm on the $A^2B_2 \leftarrow X^2A_1$ spectrum generated from the ab initio potential surfaces.

resonance and significant anharmonicity. The very different contours of the various band groups can be attributed to the presence of strong hot bands at low energies and the increasing prominence of symmetric stretching features higher in the $\tilde{A}^2B_2$ manifold.

We feel that the support for our qualitative interpretation is strong and that we have achieved a satisfactory zeroth-order description. Such a description is of prime importance if we are to hope to unravel the complexities of the electronic spectroscopy of NO_2. At this point we must await further studies by Smalley, Ramakrishna, Levy, and Wharton [82] for a more precise evaluation of our interpretation. These authors have achieved rotational temperatures of 3°K for a supersonic beam of argon seeded with NO_2. The NO_2 fluorescence excitation spectrum obtained by irradiating the beam with the output of a tunable dye laser is very close to the hypothetical case of a free, non-rotating molecule assumed in the generation of the ab initio absorption spectrum. At present, their investigation has been limited to the 5800 to 6100 Å region, but hopefully further studies will be made in the red and infrared.

For the construction of the theoretical spectrum, the ab initio $\tilde{A}^2B_2 \leftarrow \tilde{X}^2A_1$ origin of 9700 cm^{-1} was used. Temperature studies by Brand and coworkers [50], however, have not revealed any cold bands at lower energies than one at 11 956 cm^{-1} and it is to this band that they assign the origin. A nearby hot band at 11 895 cm^{-1} is of nearly

equal intensity at 90°C and has been assigned as (010) ← (010). At a more elevated temperature of 220°C, two hot bands at 11 205 cm^{-1} and 11 145 cm^{-1} are found with band contours very similar to the 11 956 cm^{-1} and 11 895 cm^{-1} bands, respectively. A simultaneous partial rotational analysis of the 11 956 cm^{-1} and 11 205 cm^{-1} bands based on combination differences from ground state (000) and (010) infrared studies [90] verified that the 11 205 cm^{-1} band is a ν_2 hot band of the 11 956 cm^{-1} band. From the similar contour and 750 cm^{-1} separation, there is little doubt that the 11 145 cm^{-1} band fits in with the 11 895 cm^{-1} band as a ground state ν_2 progression and it has been assigned as (010) ← (020). The highest frequency member of this progression is a cold band at 12 646 cm^{-1} assigned as (010) ← (000).

Although the upper state bending frequency is not firmly established spectroscopically, on the basis of the theoretical spectrum we are confident that the 12 646 cm^{-1} cold band differs from the 11 956 cm^{-1} cold band in one additional upper state bending quantum as suggested by Brand *et al*. However, we would like to propose that the 11 956 cm^{-1} band may *not* be the origin of the $\tilde{A}^2B_2 \leftarrow \tilde{X}^2A_1$ absorption; for purposes of discussion we identify it as (030) ← (000) which would be consistent with the *ab initio* origin of 9700 cm^{-1}. Revised quantum number assignments for the other bands are given in Table XXV.

With the aid of the computed Franck-Condon factors, we have calculated various band intensity ratios for both the Brand et al. vibrational quantum numbering and for our proposed reassignment. These have then been compared with two experimentally determined ratios from the spectra of Brand, Chan, and Hardwick [50] at the stated temperatures as is shown in Table XXVI. Although it is difficult to extract accurate intensity ratios from the experimental spectra and it would be desirable to have more comparisons, the intensity ratios are much better explained with the revised vibrational quantum number assignments.

It is then necessary to explain the apparent absence of the (020) ← (000) cold band if the assignment of (030) ← (000) for the 11 956 cm^{-1} band is accepted. Again using the ab initio FCF, we find that at 220°C the intensity ratio of (020) ← (000) to (030) ← (010) is 0.16. The (020) ← (000) band should occur at nearly the same frequency as the (030) ← (010) band at 11 205 cm^{-1}, in which case it may be buried underneath. As will be discussed momentarily, one must also consider the possibility that the (020) ← (000) band is drastically shifted by vibronic interaction from its expected position. This shift could be as large as perhaps 200 cm^{-1} in which case the cold band might simply be lost in the noise of the spectrum of Brand et al.

Vibronic interaction between the $\tilde{A}^2B_2$ state and high vibrational levels of the $\tilde{X}^2A_1$ ground state has long been a popular feature in discussions of NO_2 spectroscopy

TABLE XXV

SOME $\tilde{A}^2B_2 \leftarrow \tilde{X}^2A_1$ VIBRATIONAL QUANTUM NUMBER ASSIGNMENTS OF BRAND ET AL. AND A PROPOSED REASSIGNMENT

σ, cm^{-1}	Assignment of* Brand et al.	The Proposed Reassignment
12646	(010)←(000)	(040)←(000)
11956	(000)←(000)	(030)←(000)
11895	(010)←(010)	(040)←(010)
11205	(000)←(010)	(030)←(010)
11145	(010)←(020)	(040)←(020)

*Reference 50.

TABLE XXVI

A COMPARISON OF EXPERIMENTAL BAND INTENSITY RATIOS WITH AB INITIO FRANCK-CONDON RATIOS FOR THE ASSIGNMENTS OF BRAND ET AL. AND THE PROPOSED REASSIGNMENT

	Assignment of Brand et al.	The Proposed Reassignment	Experimental Ratio
$\frac{I(11956)}{I(11895)}$*	0.1	0.6	∿1
$\frac{I(11205)}{I(11145)}$**	0.01	0.6	∿2

*At a temperature of 90°C.

**At a temperature of 220°C.

[58-61], especially in regard to the anomalous fluorescence lifetime. Although the large spectral disruption is strongly supportive of such a perturbation, until quite recently the evidence was primarily of a qualitative nature. However, the several partial rotational analyses which have been lately achieved, in conjunction with the accurate ab initio calculations of this study, now provide compelling proof for the existence of strong $\tilde{A}^2B_2 \leftrightarrow \tilde{X}^2A_1$ vibronic coupling.

In Table XXVII are given experimental $\tilde{A}^2B_2$ rotational constants, the wavelengths at which they were determined, and the experimental techniques which were employed. The final set of constants is that inferred from the ab initio $\tilde{A}^2B_2$ equilibrium geometry. The dissonance of experiment and theory is striking and irreconcilable unless vibronic coupling is invoked. Even very conservative error bars of $\pm$ 0.03 Å in the theoretical bond length and $\pm$ 3° in the bond angle do little to improve the agreement. It is also not possible to explain the differences in experiment and theory on the basis of vibrational-rotational interaction, as the constants of such an interaction would have to be impossibly large.

The recent model calculation of Brand, Chan, and Hardwick provides a most promising first step towards a resolution. These authors have roughly estimated the energies of B_2 vibronic levels (v_3 odd) of the $\tilde{X}^2A_1$ ground state in the vicinity of the $\tilde{A}^2B_2 \leftarrow \tilde{X}^2A_1$ cold band at

TABLE XXVII

VARIOUS DETERMINATIONS OF THE $\tilde{A}^2B_2$ ROTATIONAL CONSTANTS

	Technique	Wavelength of Determination	A(cm^{-1})	B(cm^{-1})	C(cm^{-1})	$\bar{B}$(cm^{-1})
Stevens and Zare*	laser-induced fluorescence	5933 Å	7.85	0.451	0.394	
Abe**	laser-induced fluorescence	5145 Å	7.99			0.477
Brand et al.***	rotational analysis in absorption	5943 Å				0.414
	"	6470 Å				0.423
	"	8350 Å	7.17	0.495	0.436	
This study	ab initio calculation	equilibrium geometry	2.50	0.57	0.46	

*Reference 7.

**Reference 6.

***References 5 and 50.

11 956 cm^{-1}. Further, they estimated the Franck-Condon overlap of the $\tilde{A}^2B_2$ levels with the high vibrational levels of the ground state in which the $\tilde{A}^2B_2$ levels are embedded. Finally they deduce a representative vibronic coupling matrix element from the shift of one of the K sub-bands as indicated by their rotational analysis of the 11 956 cm^{-1} band. From these data, they construct an energy matrix, diagonal in N and K, which describes the vibronic interaction and can be diagonalized to yield estimates of intensity variation due to the coupling and also approximate rotational constants. When these constants are deperturbed to give the estimated rotational constants of the $\tilde{A}^2B_2$ Born-Oppenheimer state, a geometry of R = 1.26 Å, θ = 102° results which is coincident with the ab initio geometry.

The Brand, Chan, and Hardwick treatment is of a model nature and the agreement with the ab initio predictions is probably somewhat fortuitous. However, their analysis is highly significant because it provides a description of vibronic coupling which is not totally dependent on ad hoc assumptions. There no longer appears to be any rational alternative to $\tilde{A}^2B_2 \leftrightarrow \tilde{X}^2A_1$ vibronic coupling which can satisfactorily account for the spectral disruption and highly perturbed $\tilde{A}^2B_2$ rotational constants in NO_2.

Solarz et al. have suggested that their observations in a MODR study could be attributed to an unequal bond length equilibrium geometry of the $\tilde{A}^2B_2$ state [8], although

alternative explanations are possible. Shortly thereafter Hinze, Solarz, and Levy [40] described schematic potential surfaces which could cause an ostensibly C_{2v} electronic state to exhibit a double minimum potential along the asymmetric stretch normal coordinate. Relying on our preliminary ab initio calculations, they proposed that an avoided crossing of the $\tilde{A}^2B_2$ and 2^2A_1 states over certain portions of their hypersurfaces and a subsequent double minimum potential was consistent with the MODR study.

The calculations we have presented in Chapter II now exclude the 2^2A_1 state from such a role, as it is much too high in energy to affect the $\tilde{A}^2B_2$ levels reached in the 4880 Å optical transition in the MODR experiment. However, the Hinze et al. discussion is still relevant for the intersection of the $\tilde{A}^2B_2$ and $\tilde{X}^2A_1$ hypersurfaces. As shown in Figure 3, the $\tilde{X}^2A_1$ surface intersects very near to the minimum of the $\tilde{A}^2B_2$ surface; for various fixed bond lengths, plots of potential energy as a function of bond angle show that the crossing point is on the large angle arm of the $\tilde{A}^2B_2$ curve and within ~0.3 eV of its minimum. Thus the stated conditions of Hinze et al. for the existence of a C_s equilibrium geometry of the $\tilde{A}^2B_2$ state has likely to be satisfied.

As has been pointed out by Brand, Chan, and Hardwick [50], though, it may not be meaningful to even ask whether or not the $\tilde{A}^2B_2$ state has a double minimum potential

along Q_3. For C_s geometries near the intersection with the $\tilde{X}^2A_1$ hypersurface, the Born-Oppenheimer approximation is likely not valid; if so, the concept of the potential function or surface is no longer well defined.

CHAPTER IV

CONCLUSIONS AND RESULTS

The major conclusions and results of this study are tabulated below in the sequence in which they have been discussed.

(1) The orbital basis has been partitioned into core, valence, and virtual spaces and the dominant molecular correlation effects are found to reside in the valence space as expected.

(2) The $4a_1$ orbital has been found to play a significantly different bonding role in the $\tilde{X}^2A_1$ and $\tilde{A}^2B_2$ states, which cannot be simply accounted for in terms of the different bond angles of the two states.

(3) The designation of various configurations as describing molecular extra correlation energy or differential atomic correlation is not as well defined for polyatomic molecules as it is in diatomics.

(4) A technique was described in which various classes of configurations were successively examined; compact final configuration lists were formed on the basis of this procedure.

(5) The basis set used in these calculations is larger and more flexible than any previously employed in an NO_2 ab initio calculation.

(6) Adiabatic excitation energies are estimated to be accurate to $\pm$ 0.3 eV from an analysis of the quality of the basis set and the extent of the inclusion of molecular correlation.

(7) The treatment of molecular correlation is more extensive than in any previous NO_2 ab initio calculation. Better than 95% of the valence (not total) correlation energy is obtained.

(8) The $\tilde{X}^2A_1$ calculated equilibrium geometry is within 0.01 Å and 1° of the experimental values.

(9) The $\tilde{X}^2A_1$ calculated symmetric vibration harmonic frequencies are within 10 cm^{-1} of the experimental ω_1 and ω_2. The estimated accuracy of the computed vibrational frequencies of the lowest doublet states is $\pm$ 10%.

(10) The $\tilde{X}^2A_1$ calculated dipole moment is 0.37 debyes which is only slightly larger than the experimental determination of 0.32 debyes.

(11) The $^2\Sigma_g^+$ (2^2A_1) state exhibits a double minimum potential along Q_3.

(12) The $\tilde{A}^2B_2$ state is the first excited state in NO_2. The long-wavelength absorption in NO_2 ($\lambda \geq 7000$ Å) is only to the $\tilde{A}^2B_2$ upper state and not to $\tilde{B}^2B_1$. The $\tilde{A}^2B_2$ and $\tilde{B}^2B_1$ states overlap at least in the 5200-3700 Å spectral region.

(13) The $\tilde{A}^2B_2$ and $\tilde{C}^2A_2$ states adiabatically correlate to the $NO(^2\Pi) + O(^3P)$ asymptote along C_s paths.

(14) The $^2\Sigma_g^+$ (2^2A_1) state is not responsible for either the 3979 Å or 2491 Å predissociations in NO_2.

(15) Both the $\tilde{A}^2B_2$ and $\tilde{B}^2B_1$ states are predissociated for $\lambda<3979$ Å. In the $\tilde{B}^2B_1$ state, the likely mechanism is predissociation by vibration. Either predissociation by vibration or a heterogeneous predissociation by high vibrational levels of the $\tilde{X}^2A_1$ ground state is possible for the $\tilde{A}^2B_2$ state.

(16) The $NO(^2\Pi) + O(^3P)$ chemiluminescence only involves the $\tilde{X}^2A_1$, $\tilde{A}^2B_2$, $\tilde{B}^2B_1$, and $\tilde{C}^2A_2$ electronic states.

(17) The $^4B_2$ and $^4A_2$ states do not contribute to either the NO+O chemiluminescence or visible absorption of NO_2.

(18) The $NO(^2\Pi) + O(^3P)$ chemiluminescence data regarding the peak at 3.7 μm is consistent with a $\tilde{C}^2A_2 \rightarrow \tilde{A}^2B_2$ electronic transition.

(19) The predissociation in the 2491 Å band system is likely due to either (a) a homogeneous predissociation into $N(^4S) + O_2$ ($^3\Sigma_g^-$); or (b) predissociation by vibration into $NO(^2\Pi) + O(^3P)$.

(20) The photodissociation of NO_2 by the 6943 Å ruby laser line probably involves a $\tilde{A}^2B_2 \leftarrow \tilde{X}^2A_1$ absorption followed by a subsequent $\tilde{C}^2A_2 \leftarrow \tilde{A}^2B_2$ absorption.

(21) The 1.8 eV photodetachment process in NO_2^- may involve the ring states of NO_2^- and NO_2.

(22) Level dilution of the $\tilde{A}^2B_2$ state by high vibrational levels of the $\tilde{X}^2A_1$ ground state can only account for a small portion of the anomalous fluorescence lifetime.

(23) The proximity of the $\tilde{A}^2B_2$ and $\tilde{C}^2A_2$ potential hypersurfaces is due more to the similar properties of the $4b_2$ and $1a_2$ molecular orbitals than it is due to Renner-Teller interaction in the $^2\Phi_g$ linear state.

(24) The origin of the $\tilde{B}^2B_1 \leftarrow \tilde{X}^2A_1$ absorption system is probably near 13 800 cm^{-1}, about 900 cm^{-1} lower than the present assignment of Hardwick and Brand.

(25) The $\tilde{B}^2B_1$ state is linear and has a bond length about 0.01 Å longer than in the $\tilde{X}^2A_1$ ground state.

(26) The $\tilde{A}^2B_2$ equilibrium Born-Oppenheimer geometry is R=1.26 Å, θ=102°. The Franck-Condon factor for the vibrationless levels of the $\tilde{X}^2A_1$ and $\tilde{A}^2B_2$ states is of the order 10^{-8}.

(27) Near the origin of the $\tilde{A}^2B_2 \leftarrow \tilde{X}^2A_1$ transition, ν_2 hot bands will be more intense than cold bands, even at room temperature.

(28) The $\tilde{A}^2B_2 \leftarrow \tilde{X}^2A_1$ absorption between 8500 Å and 6000 Å is qualitatively understood in terms of groups of bands, with successive groups separated by the $\tilde{A}^2B_2$ bending frequency. The members of each group correspond to cold

bands to the $(0,\nu_2',0)$, $(1,\nu_2'-2,0)$, $(2,\nu_2'-4,0)$, etc. upper state levels.

(29) The relative intensities of hot and cold bands indicate that the $\tilde{A}^2B_2 \leftarrow \tilde{X}^2A_1$ origin may be lower than the present assignment of Brand et al. at 11963 cm^{-1}.

(30) The dissonance of the experimental $\tilde{A}^2B_2$ rotational constants with those inferred from the accurate ab initio geometry of this study can only be attributed to strong $\tilde{A}^2B_2 - \tilde{X}^2A_1$ vibronic coupling.

Table XXVIII summarizes the spectroscopic parameters of the low-lying doublet states and includes the most recent experimental determinations.

TABLE XXVIII

A SUMMARY OF THE THEORETICAL SPECTROSCOPIC PARAMETERS OF THE LOW-LYING DOUBLET STATES OF NO_2 *,**

	T_e(eV)	R_e(Å)	θ_e(degrees)	ω_1(cm^{-1})	ω_2(cm^{-1})	μ(debyes)	References
$\tilde{C}^2A_2$	1.84	1.27	110	1360	798	0.05	
$\tilde{B}^2B_1$ ***	1.66 (1.83)	1.20 (1.23)	180 (180)	1192	960 (925)	0.00	1, 48
$\tilde{A}^2B_2$	1.18 (1.48)	1.26	102	1461 (1430)	739 (700)	0.46	5, 50
$\tilde{X}^2A_1$	0.00 (0.00)	1.20 (1.1934)	134 (134.1)	1351 (1358)	758 (757)	0.37 (0.32)	31, 32, 33

*The experimental parameters are included in parentheses. Only those for the ground state are known to a high degree of accuracy experimentally.

**The $\tilde{X}^2A_1$ and $\tilde{A}^2B_2$ theoretical parameters are derived from the OVC-CI calculations, as are also R_e and T_e for $\tilde{B}^2B_1$ and T_e for $\tilde{C}^2A_2$. All remaining values were calculated at the OVC level.

***A value of ω_3 = 2040 cm^{-1} was also calculated for the $\tilde{B}^2B_1$ state.

REFERENCES

REFERENCES

1. A. E. Douglas and K. P. Huber, Can. J. Phys. 43, 74 (1965).

2. A. D. Walsh, J. Chem. Soc. p. 2266 (1953).

3. K. Abe, F. Meyers, T. K. McCubbin, and S. R. Polo, J. Mol. Spectrosc. 38, 552 (1971).

4. C. G. Stevens, M. W. Swagel, R. Wallace, and R. N. Zare, Chem. Phys. Letters 18, 465 (1973).

5. J. C. D. Brand, J. L. Hardwick, R. J. Pirkle, and C. J. Seliskar, Can. J. Phys. 51, 2184 (1973).

6. K. Abe, J. Mol. Spectrosc. 48, 395 (1973).

7. C. G. Stevens and R. N. Zare, J. Mol. Spectrosc, In Press.

8. R. Solarz, D. H. Levy, K. Abe, and R. F. Curl, J. Chem. Phys. 60, 1182 (1974).

9. T. Tanaka, K. Abe, and R. F. Curl, J. Mol. Spectrosc. 49, 310 (1974).

10. W. H. Fink, J. Chem. Phys. 49, 5054 (1968); ibid. 54, 2911 (1971).

11. L. Burnelle, A. M. May, and R. A. Gangi, J. Chem. Phys. 49, 561 (1968).

12. L. Burnelle and K. P. Dressler, J. Chem. Phys. 51, 2758 (1969).

13. R. A. Gangi and L. Burnelle, J. Chem. Phys. 55, 843 (1971); ibid. 55, 851 (1971).

14. J. E. Del Bene, J. Chem. Phys. 54, 3487 (1971).

15. P. J. Hay, J. Chem. Phys. 58, 4706 (1973).

16. G. Das and A. C. Wahl, J. Chem. Phys. 56, 3532 (1972).

17. G. Das and A. C. Wahl, "BISON-MC": A Fortran Computing System for Multi-Configuration Self-Consistent-Field (MCSCF) Calculations on Atoms, Diatoms, and Polyatoms, Argonne National Laboratory Report #ANL-7955 (1972).

18. POLYATOM (VERSION 2), written by D. B. Neumann, H. Basch, R. L. Kornegay, L. C. Snyder, J. W. Moskowitz, C. Hornback, and S. P. Liebmann, available from the Quantum Chemistry Program Exchange, Indiana University.

19. G. Das and A. C. Wahl, J. Chem. Phys. 56, 1769 (1972).

20. F. P. Billingsley II and M. Krauss, J. Chem. Phys. 60, 4130 (1974).

21. W. J. Stevens, G. Das, A. C. Wahl, M. Krauss, and D. Neumann, J. Chem. Phys. 61, 3686 (1974).

22. T. H. Dunning, J. Chem. Phys. 53, 2823 (1970).

23. S. Huzinaga, J. Chem. Phys. 42, 1239 (1965).

24. H. F. Schaefer and S. Rothenberg, J. Chem. Phys. 54, 1423 (1971).

25. T. H. Dunning, J. Chem. Phys. 55, 3958 (1971).

26. C. W. Wilson and A. C. Wahl, Report on Research under ARPA Order No. 2022 (1973).

27. C. R. Brundle, D. Neumann, W. C. Price, D. Evans, A. W. Potts, and D. G. Streets, J. Chem. Phys. 53, 705 (1970).

28. W. J. Hehre, R. F. Stewart, and J. A. Pople, J. Chem. Phys. 51, 2657 (1969).

29. E. B. Wilson, Jr., J. C. Decuis, and P. C. Cross, "Molecular Vibrations," McGraw-Hill, New York, 1955.

30. H. F. Schaefer, "The Electronic Structure of Atoms and Molecules," Addison-Wesley, Reading, Massachusetts, 1972, p. 152.

31. G. R. Bird, J. C. Baird, A. W. Jache, J. A. Hodgeson, R. F. Curl, A. C. Kunkle, J. W. Bransford, J. Rastrup-Andersen, and J. Rosenthal, J. Chem. Phys. 40, 3378 (1964).

32. E. T. Arakawa and A. H. Nielsen, J. Mol. Spectrosc. 2, 413 (1958).

33. J. A. Hodgeson, E. E. Sibert, and R. F. Curl, J. Phys. Chem. 67, 2833 (1963).

34. R. E. Weston, J. Chem. Phys. 26, 1248 (1957).

35. R. S. Mulliken, Can. J. Chem. 36, 10 (1958).

36. J. B. Coon, F. A. Cesani, and F. P. Huberman, J. Chem. Phys. 52, 1647 (1970).

37. J. B. Coon, P. M. Elliott, J. W. Riggs, and S. U. Kim, Bull. Am. Phys. Soc. 12, 182 (1967).

38. P. M. Elliott and J. B. Coon, Bull. Am. Phys. Soc. 9, 145 (1964).

39. J. B. Coon, F. A. Cesani, and C. M. Loyd, Discussions Faraday Soc. 35, 118 (1963).

40. J. Hinze, R. Solarz, and D. H. Levy, Chem. Phys. Letters, 25, 284 (1974).

41. R. W. Ritchie and A. D. Walsh, Proc. Roy. Soc. 267A, 395 (1962).

42. L. Harris, G. W. King, W. S. Benedict, and R. W. B. Pearse, J. Chem. Phys. 8, 765 (1940); L. Harris and G. W. King, J. Chem. Phys. 8, 775 (1940).

43. R. W. Ritchie, A. D. Walsh, and P. A. Warsop, Proc. Roy. Soc. 266A, 257 (1962).

44. G. W. Robinson, M. McCarty, and M. C. Keelty, J. Chem. Phys. 27, 972 (1957).

45. N. M. Atherton, R. N. Dixon, and G. H. Kirby, Trans. Faraday Soc. 60, 1688 (1964).

46. G. Herzberg and E. Teller, Z. phys. Chem. B21, 410 (1933).

47. R. Renner, Z. Physik 92, 172 (1934).

48. J. L. Hardwick and J. C. D. Brand, Chem. Phys. Letters, 21, 458 (1973).

49. J. T. Hougen, P. R. Bunker, and J. W. C. Johns, J. Mol. Spectrosc. 34, 136 (1970).

50. J. C. D. Brand, W. H. Chan, and J. L. Hardwick, to be published.

51. E. Wigner and E. E. Witmer, Z. Physik 51, 859 (1928).

52. M. Green and J. W. Linnett, Trans. Faraday Soc. 57, 1 (1961).

53. H. P. Broida, H. I. Schiff, and T. M. Sugden, Trans. Faraday Soc. 57, 259 (1961).

54. J. N. Pitts, J. H. Sharp, and S. I. Chan, J. Chem. Phys. 40, 3655 (1964).

55. W. F. Gianque and J. D. Kemp, J. Chem. Phys. 6, 40 (1938).

56. W. H. Eberhardt and H. Renner, J. Mol. Spectrosc. 6, 483 (1961).

57. G. Herzberg, "Electronic Structure of Polyatomic Molecules," Van Nostrand Reinhold, New York, 1966.

58. A. E. Douglas, J. Chem. Phys. 45, 1007 (1966).

59. D. B. Hartley and B. A. Thrush, Discussions Faraday Soc. 37, 220 (1964).

60. S. E. Schwartz and H. S. Johnston, J. Chem. Phys. 51, 1286 (1969).

61. F. Kaufman, in "Chemiluminescence and Bioluminescence," ed. Cormier, Hercules, and Lee, Plenum Press, New York, 1973, p. 83.

62. G. E. Busch and K. R. Wilson, J. Chem. Phys. 56, 3638 (1972).

63. K. H. Becker, W. Groth, and D. Thran, Chem. Phys. Letters 15, 215 (1972).

64. D. E. Paulsen, W. F. Sheridan, and R. E. Huffman, J. Chem. Phys. 53, 647 (1970).

65. A. T. Stair and J. P. Kennealy, J. de Chimie Physique 64, 124 (1967).

66. M. A. A. Clyne, B. A. Thrush, and R. P. Wayne, Trans. Faraday Soc. 60, 359 (1964).

67. P. N. Clough and B. A. Thrush, Trans. Faraday Soc. 65, 23 (1969).

68. M. F. Golde, A. E. Roche, and F. Kaufman, J. Chem. Phys. 59, 3953 (1973).

69. M. A. A. Clyne and B. A. Thrush, Proc. Royal Soc. A261, 259 (1969).

70. F. Hushfar, J. W. Rogers, and A. T. Stair, Applied Opt. 10, 1843 (1971).

71. D. A. Hamlin and B. F. Myers, J. Quant. Spectrosc. Radiat. Transfer 13, 293 (1973).

72. J. W. Gerstmayr, P. Harteck, and R. R. Reeves, J. Phys. Chem. 76, 474 (1972).

73. E. Herbst, T. A. Patterson, and W. C. Lineberger, J. Chem. Phys. 61, 1300 (1974).

74. E. F. Hayes and G. V. Pfeiffer, J. Am. Chem. Soc. 90, 4773 (1968).

75. P. J. Hay and W. A. Goddard III, Chem. Phys. Letters 14, 46 (1972).

76. D. Neuberger and A. B. F. Duncan, J. Chem. Phys. 22, 1693 (1954).

77. L. F. Keyser, S. Z. Levine, and F. Kaufman, J. Chem. Phys. 54, 355 (1971).

78. P. B. Sackett and J. T. Yardley, J. Chem. Phys. 57, 152 (1972).

79. K. Sakurai and G. Capelle, J. Chem. Phys. 53, 3764 (1970).

80. P. B. Sackett and J. T. Yardley, Chem. Phys. Letters 9, 612 (1971).

81. R. A. Marcus and O. K. Rice, J. Phys. Colloid. Chem. 55, 894 (1951).

82. R. E. Smalley, B. L. Ramakrishna, D. H. Levy, and L. Wharton, J. Chem. Phys. 61, 4363 (1974).

83. N. Mataga and T. Kubota, "Molecular Interactions and Electronic Spectra," Marcel Dekker, New York, 1970.

84. R. Nicholls, Chem. Phys. Letters 20, 261 (1973).

85. F. Duschinsky, Acta. Physiochimica URSS 7, 551 (1937).

86. J. B. Coon, R. E. DeWames, and C. M. Loyd, J. Mol. Spectrosc. 8, 285 (1962).

87. J. R. Henderson, M. Muramoto, and R. A. Willett, J. Chem. Phys. 41, 580 (1964).

88. P. R. Bunker and J. M. R. Stone, J. Mol. Spectrosc. 41, 310 (1972).

89. T. C. Hall, Jr. and F. E. Blacet, J. Chem. Phys. 20, 1745 (1952).

90. S. C. Hurlock, K. N. Rao, L. A. Weller, and P. K. L. Yin, J. Mol. Spectrosc. 48, 372 (1973).

91. J. L. Gole and E. F. Hayes, J. Chem. Phys. 57, 360 (1972).

92. D. H. Liskow, H. F. Schaeffer, and C. F. Bender, J. Am. Chem. Soc. 93, 6734 (1971).

93. An ab initio calculation of the ground state rotational barrier in HONO was discussed by S. Skaarup and J. E. Boggs at the XXIX Symp. Mol. Struct. and Spectr., Columbus, Ohio (1974).

94. A. P. Cox, A. H. Brittain, and D. J. Finnigan, Trans. Faraday Soc. 67, 2179 (1971).

95. T. K. Ha and U. P. Wild, Chem. Phys. 4, 300 (1974).

APPENDICES

APPENDIX A

THE COMPUTER PROGRAMS AND THE COST OF THE CALCULATION

APPENDIX A

THE COMPUTER PROGRAMS AND THE COST OF THE CALCULATION

Tabulated below are the various programs used in the calculation of the molecular wavefunctions, and the execution time, core requirement, and the cost of each step for a given state at a single geometry. All calculations were performed on the IBM 370/195 machine at Argonne National Laboratory; the estimated costs are based on submission at normal priority and the published Applied Math Division (AMD) charges as of January 1, 1975.

Program	Execution Time (Minutes)	Core Requirement (Kilobytes)	Cost (Dollars)
POLYINT	8	400	25
XSBS	9	950	50
INTMO	2	1200	15
CI	1	750	5
Total	20	. .	95

POLYINT computes the one- and two-electron integrals over the Gaussian-type-orbital (GTO) basis functions and has been abstracted from the POLYATOM [18] system of codes and modified by Mr. A. R. Hinds.

XSBS performs the OVC orbital optimization and is a modification of the BISON-MC [17] system of codes specifically designed to handle large Gaussian basis sets. The contraints on this program are a maximum of 20 configurations, none of which contains more than 5 open shells, and a maximum of 50 contracted basis functions if the molecule has no elements of symmetry other than the identity. If a plane of symmetry exists, a larger number of basis functions can be accommodated due to symmetry blocking of the in-plane and out-of-plane basis functions. For example, 45 in-plane and 21 out-of-plane basis functions are within the present limits of the program.

INTMO transforms the integrals over the contracted basis functions into integrals over the molecular orbitals computed by XSBS. The configuration interaction wavefunctions are then evaluated from the integrals over the molecular orbitals by CI. At the time of our study, CI was limited to a maximum of 99 configurations, none containing more than 6 open shells.

APPENDIX B

THE BASIS SET

APPENDIX B

THE BASIS SET

In Appendix C we shall present the molecular orbitals of the $\tilde{X}^2A_1$, $\tilde{A}^2B_2$, $\tilde{B}^2B_1$, and $\tilde{C}^2A_2$ states of NO_2. Preparatory to that section, we tabulate here the exponents and contraction coefficients of the primitive Gaussian basis functions; also included is a notation for each contracted basis function in terms of which the molecular orbitals will be expressed

	Exponent	Contraction Coefficient	Notation
The Nitrogen Atom	5909.44	0.002004	NS1
	887.451	0.015310	
	204.749	0.074293	
	59.8376	0.253364	
	19.9981	0.600576	
	2.6860	0.245111	
	7.1927	1.0	NS2
	0.7000	1.0	NS3
	0.2133	1.0	NS4
	26.7860	0.038244	NX1
	5.9564	0.243846	
	1.7074	0.817193	
	0.5314	1.0	NX2
	0.1654	1.0	NX3
	1.0	1.0	NXX

The nitrogen p-functions in the y and z directions have the same exponents and contraction coefficients as for those in the X direction; their notation is similarly NY1, NY2, NY3, NZ1, etc. Likewise, the other d-functions have the identical exponent and contraction coefficient as the d_x2 function and are denoted by NYY, NZZ, NXY, NYZ, and NXZ. Note that these are Cartesian d-functions and that the spherically symmetric combination $d_x2 + d_y2 + d_z2$ has not been projected out of the basis.

	Exponent	Contraction Coefficient	Notation
The Oxygen Atom	7816.54	0.002031	
	1175.82	0.015436	
	273.188	0.073771	O1S1
	81.1696	0.247606	(or O2S1)
	27.1836	0.611831	
	3.4136	0.241205	
	9.5322	1.0	O1S2
	0.9398	1.0	O1S3
	0.2846	1.0	O1S4
	35.1832	0.040023	
	7.9040	0.253849	O1X1
	2.3051	0.806841	
	0.7171	1.0	O1X2
	0.2137	1.0	O1X3
	1.35	1.0	O1XX
		etc.	

APPENDIX C

MOLECULAR ORBITALS OF THE OVC WAVEFUNCTIONS FOR THE LOW-LYING DOUBLET STATES OF NO_2

APPENDIX C

MOLECULAR ORBITALS OF THE OVC WAVEFUNCTIONS FOR THE LOW-LYING DOUBLET STATES OF NO_2

Listed in Tables XXIX through XXXII are the molecular orbitals of the $\tilde{X}^2A_1$, $\tilde{A}^2B_2$, $\tilde{B}^2B_1(^2\Pi_u)$, and $\tilde{C}^2A_2$ states of NO_2, respectively, as determined in the OVC orbital optimization. The wavefunctions have been computed near the equilibrium geometry in each state.

For the linear $\tilde{B}^2B_1(^2\Pi_u)$ state, the internuclear axis is the z-axis

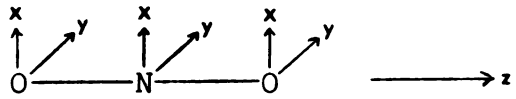

while for the remaining three bent states, the C_{2v} coordinate system is

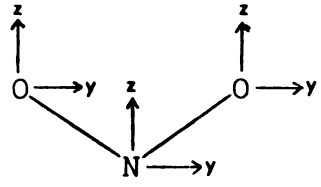

and the x-direction is perpendicular to the plane of the molecule.

TABLE XXIX

THE $\tilde{X}^2A_1$ OVC ORBITALS FOR A GEOMETRY OF R=2.2552 BOHRS, θ=134°

Basis Function		Orbital					
		$1b_2$	$1a_1$	$2a_1$	$3a_1$	$2b_2$	$4a_1$
N	S1	-0.00000	0.00117	0.59360	0.02021	0.00000	-0.10093
	S2	0.00000	0.00158	0.44586	0.03016	0.00000	-0.13307
	S3	0.00000	-0.00316	0.00242	-0.08159	-0.00000	0.41962
	S4	-0.00000	0.00101	0.00184	0.02749	-0.00000	0.17361
	Y1	-0.00087	0.00000	-0.00000	0.00000	0.04238	0.00000
	Y2	-0.00208	-0.00000	0.00000	-0.00000	0.02827	-0.00000
	Y3	0.00096	0.00000	-0.00000	0.00000	-0.00444	0.00000
	Z1	0.00000	0.00004	0.00166	0.00155	-0.00000	0.15070
	Z2	-0.00000	0.00114	-0.00059	0.01672	0.00000	0.20391
	Z3	-0.00000	0.00094	0.00069	0.02483	-0.00000	0.05290
O1	S1	0.41110	0.41597	0.00095	0.07673	0.09870	-0.00032
	S2	0.32654	0.33377	0.00152	0.11866	0.13834	0.00241
	S3	-0.00144	-0.02379	-0.00505	-0.39720	-0.40180	-0.00772
	S4	0.00046	-0.02114	-0.00546	-0.37969	-0.36511	-0.14271
	Y1	0.00218	0.00480	0.00118	0.05483	0.05677	0.17389
	Y2	-0.00008	0.00292	0.00166	0.06112	0.06526	0.21293
	Y3	0.00105	0.00374	0.00060	0.04436	0.05701	0.08137
	Z1	-0.00075	-0.00035	-0.00021	0.00821	-0.01096	0.01976
	Z2	0.00023	0.00092	-0.00021	0.01461	-0.01128	0.03127
	Z3	-0.00035	-0.00018	-0.00016	0.00278	-0.01084	0.02703
O2	S1	-0.41110	0.41597	0.00095	0.07673	-0.09870	-0.00032
	S2	-0.32654	0.33377	0.00152	0.11866	-0.13834	0.00241
	S3	0.00144	-0.02379	-0.00505	-0.39720	0.40180	-0.00772
	S4	-0.00046	-0.02114	-0.00546	-0.37969	0.36511	-0.14271
	Y1	0.00218	-0.00480	-0.00118	-0.05483	0.05677	-0.17389
	Y2	-0.00008	-0.00292	-0.00166	-0.06112	0.06526	-0.21293
	Y3	0.00105	-0.00374	-0.00060	-0.04436	0.05701	-0.08137
	Z1	0.00075	-0.00035	-0.00021	0.00821	-0.01096	0.01976
	Z2	-0.00023	0.00092	-0.00021	0.01461	0.01128	0.03127
	Z3	0.00035	-0.00018	-0.00016	0.00278	0.01084	0.02703
N	XX	0.00000	0.00066	-0.00013	-0.01059	0.00000	-0.00690
	YY	0.00000	-0.00079	-0.00022	-0.01963	0.00000	0.01773
	ZZ	0.00000	0.00079	0.00009	0.01149	0.00000	0.01954
	YZ	-0.00059	-0.00000	-0.00000	0.00000	0.01328	0.00000
O1	XX	-0.00006	0.00019	0.00003	0.00281	0.00258	-0.00461
	YY	-0.00012	0.00009	0.00043	0.00256	0.00150	0.02914
	ZZ	0.00002	0.00014	0.00001	0.00119	0.00173	-0.00725
	YZ	0.00009	0.00023	-0.00013	0.00214	0.00120	-0.00558
O2	XX	0.00006	0.00019	0.00003	0.00281	-0.00258	-0.00461
	YY	0.00012	0.00009	0.00043	0.00256	-0.00150	0.02914
	ZZ	-0.00002	0.00014	0.00001	0.00119	-0.00173	-0.00725
	YZ	0.00009	-0.00023	0.00013	-0.00214	0.00120	0.00558

TABLE XXIX, continued

Basis function		Orbital					
		$3b_2$	$7a_1$	$5b_2$	$5a_1$	$4b_2$	$6a_1$
N	S1	0.00000	-0.10910	0.00000	0.08088	-0.00000	-0.04363
	S2	-0.00000	-0.15992	0.00000	0.10826	-0.00000	-0.06244
	S3	-0.00000	0.73955	-0.00000	-0.33563	-0.00000	-0.17138
	S4	-0.00000	0.29847	0.00000	-0.26179	-0.00000	0.48994
	Y1	0.25346	0.00000	-0.59751	-0.00000	-0.07865	0.00000
	Y2	0.31317	-0.00000	-0.62744	0.00000	-0.10935	-0.00000
	Y3	-0.03645	0.00000	0.06342	-0.00000	-0.06805	0.00000
	Z1	-0.00000	0.27216	-0.00000	0.18597	-0.00000	-0.25680
	Z2	0.00000	0.36310	0.00000	0.25007	-0.00000	-0.33559
	Z3	0.00000	0.07665	0.00000	0.10571	-0.00000	-0.20135
O1	S1	0.01213	0.03648	0.03714	-0.01677	0.00635	0.01086
	S2	0.01480	0.05349	0.05427	-0.02446	0.00999	0.01516
	S3	-0.03223	-0.19198	-0.22885	0.07558	-0.02711	-0.05139
	S4	0.03624	-0.24720	-0.18393	0.10163	-0.10973	-0.06989
	Y1	-0.21868	-0.34339	-0.30312	0.01530	-0.06403	-0.01608
	Y2	-0.26766	-0.36883	-0.31606	0.02473	-0.09444	-0.02521
	Y3	-0.14056	-0.05067	-0.00664	0.02430	-0.09029	-0.01499
	Z1	0.01525	0.01999	0.09230	0.15626	-0.24794	-0.21999
	Z2	0.01042	0.04921	0.16263	0.20201	-0.32606	0.28493
	Z3	-0.01444	0.01683	0.11763	0.10620	-0.21887	0.25185
O2	S1	-0.01213	0.03648	-0.03714	-0.01677	-0.00635	-0.01086
	S2	-0.01480	0.05349	-0.05427	-0.02446	-0.00999	0.01516
	S3	0.03223	-0.19198	0.22885	0.07558	0.02711	-0.05139
	S4	-0.03624	-0.24720	0.18393	0.10163	-0.10973	-0.06989
	Y1	-0.21868	-0.34339	-0.30312	-0.01530	-0.06403	0.01608
	Y2	-0.26766	0.36883	-0.31606	-0.02473	-0.09444	0.02521
	Y3	-0.14056	0.05067	-0.00664	-0.02430	-0.09029	0.01499
	Z1	-0.01525	-0.01999	-0.09230	0.15626	0.24794	0.21999
	Z2	-0.01042	0.04921	-0.16263	0.20201	0.32606	0.28493
	Z3	0.01444	0.01683	-0.11763	0.10620	0.21887	0.25185
N	XX	-0.00000	-0.04155	-0.00000	-0.00642	-0.00000	0.00523
	YY	0.00000	-0.04129	0.00000	-0.03174	0.00000	-0.04930
	ZZ	-0.00000	0.03651	0.00000	0.02340	0.00000	0.01887
	YZ	-0.04419	-0.00000	-0.09454	-0.00000	0.03103	0.00000
O1	XX	0.00963	0.00420	-0.00066	0.00100	-0.00029	0.00202
	YY	-0.02227	-0.00310	-0.00251	0.00673	-0.00236	-0.00733
	ZZ	-0.00597	0.00102	-0.00511	-0.00909	0.01209	0.00092
	YZ	0.01406	0.01394	0.00015	0.01477	-0.01632	0.00409
O2	XX	-0.00963	0.00420	0.00066	0.00100	0.00029	0.00202
	YY	-0.02227	-0.00310	0.00251	0.00673	0.00236	-0.00733
	ZZ	-0.00597	0.00102	0.00511	-0.00909	-0.01209	0.00092
	YZ	0.01406	-0.01394	0.00015	-0.01477	-0.01632	-0.00409

Basis function		Orbital		
		$1b_1$	$1a_2$	$2b_1$
N	X1	-0.24265	0.00000	0.32005
	X2	-0.34042	0.00000	0.42869
	X3	-0.14628	-0.00000	0.19687
O1	X1	-0.16968	0.25971	-0.29212
	X2	-0.22602	0.34233	-0.32477
	X3	-0.11516	0.26187	-0.08560
O2	X1	-0.16968	-0.25971	-0.29212
	X2	-0.22602	-0.34233	-0.32477
	X3	-0.11516	-0.26187	-0.08560
N	XY	0.00000	-0.05439	-0.00000
	XZ	-0.02488	-0.00000	0.01689
O1	XY	-0.02218	0.01712	0.00917
	XZ	0.00891	-0.00724	-0.00446
O2	XY	0.02218	0.01712	-0.00917
	XZ	0.00891	0.00724	-0.00446

TABLE XXX

THE $\tilde{A}^2B_2$ OVC ORBITALS FOR A GEOMETRY OF R=2.40 BOHRS, θ=100°

Basis function		Orbital					
		$1b_2$	$1a_1$	$2a_1$	$3a_1$	$2b_2$	$4a_1$
N	S1	-0.00000	-0.00100	-0.60282	0.01521	0.00000	-0.07871
	S2	0.00000	-0.00179	-0.45970	0.01886	-0.00000	-0.13802
	S3	0.00000	0.00192	0.04438	-0.03025	-0.00000	0.57822
	S4	-0.00000	0.00035	0.04909	0.01758	0.00000	0.55885
	Y1	0.00103	-0.00000	-0.00000	0.00000	-0.02710	-0.00000
	Y2	-0.00037	0.00000	0.00000	-0.00000	-0.01812	0.00000
	Y3	-0.00076	-0.00000	0.00000	0.00000	0.02068	0.00000
	Z1	0.00000	0.00055	-0.01827	-0.01635	-0.00000	-0.16755
	Z2	-0.00000	-0.00053	-0.01658	-0.00954	0.00000	-0.20487
	Z3	-0.00000	-0.00178	-0.01066	0.02306	0.00000	-0.11314
O1	S1	0.41647	-0.41638	0.00108	0.07187	-0.07618	0.00976
	S2	0.33455	-0.33447	0.00152	0.11630	-0.12197	0.01476
	S3	-0.02663	0.02621	-0.00450	-0.39731	0.41516	-0.04556
	S4	-0.02267	0.02297	-0.01038	-0.37333	0.38242	-0.11444
	Y1	0.00352	-0.00339	0.00067	0.03227	-0.03437	0.01037
	Y2	0.00197	-0.00188	-0.00012	0.03538	-0.03505	0.00807
	Y3	0.00266	-0.00215	-0.00138	0.02497	-0.03211	-0.01510
	Z1	-0.00366	0.00406	-0.00215	-0.04871	0.03820	-0.02824
	Z2	-0.00290	0.00338	-0.00239	-0.05636	0.04552	-0.03484
	Z3	-0.00278	0.00335	0.00262	-0.04545	0.03375	0.02675
O2	S1	-0.41647	-0.41638	0.00108	-0.07187	-0.07618	-0.00976
	S2	-0.33455	-0.33447	0.00152	0.11630	0.12197	0.01476
	S3	0.02663	0.02671	-0.00450	-0.39731	-0.41516	-0.04556
	S4	-0.02267	0.02297	-0.01038	-0.37333	-0.38242	-0.11444
	Y1	0.00352	0.00339	-0.00067	-0.03227	-0.03437	-0.01037
	Y2	0.00197	0.00188	0.00012	-0.03538	-0.03505	-0.00807
	Y3	0.00266	0.00215	0.00138	-0.02497	-0.03211	0.01510
	Z1	0.00366	0.00406	-0.00215	-0.04871	-0.03820	-0.02824
	Z2	0.00290	0.00338	-0.00239	-0.05636	-0.04552	-0.03484
	Z3	0.00278	0.00335	0.00262	-0.04545	-0.03375	0.02675
N	XX	0.00000	-0.00061	0.00048	0.00882	-0.00000	0.00514
	YY	0.00000	-0.00030	0.00089	-0.00316	-0.00000	0.00961
	ZZ	0.00000	-0.00019	-0.00122	-0.00403	-0.00000	-0.01093
	YZ	0.00063	-0.00000	0.00000	0.00000	-0.01999	0.00000
O1	XX	0.00018	-0.00032	-0.00004	0.00300	-0.00186	-0.00033
	YY	0.00009	-0.00009	-0.00048	0.00176	-0.00134	-0.00134
	ZZ	0.00023	-0.00029	0.00061	0.00263	-0.00285	0.00852
	YZ	0.00017	-0.00001	-0.00042	-0.00056	-0.00104	-0.00841
O2	XX	-0.00018	-0.00032	-0.00004	0.00300	0.00186	-0.00033
	YY	-0.00009	-0.00009	-0.00048	0.00176	0.00134	-0.00134
	ZZ	-0.00023	-0.00029	0.00061	0.00263	0.00285	0.00852
	YZ	0.00012	0.00001	0.00042	0.00056	-0.00104	0.00841

TABLE XXX, continued

Basis function		Orbital					
		$3b_2$	$7a_1$	$5b_2$	$5a_1$	$4b_2$	$6a_1$
N	S1	0.00000	-0.08855	-0.00000	-0.01862	0.00000	-0.04114
	S2	0.00000	-0.12718	0.00000	-0.02571	0.00000	-0.05005
	S3	-0.00000	0.55769	0.00000	-0.06747	-0.00000	0.17765
	S4	0.00000	0.30598	-0.00000	0.15692	0.00000	-0.16059
	Y1	0.24105	0.00000	-0.49517	-0.00000	-0.03114	0.00000
	Y2	-0.32571	-0.00000	-0.58287	-0.00000	-0.03898	-0.00000
	Y3	0.02588	0.00000	-0.05771	0.00000	0.00875	-0.00000
	Z1	-0.00000	0.42136	-0.00000	-0.00702	0.00000	0.26244
	Z2	-0.00000	-0.46137	-0.00000	-0.00668	0.00000	0.35022
	Z3	0.00000	0.05213	-0.00000	-0.04608	0.00000	0.11736
O1	S1	0.01005	0.03479	0.03385	0.01439	-0.00713	-0.00812
	S2	-0.01203	-0.05129	-0.04959	-0.02026	-0.00976	-0.00857
	S3	-0.03069	-0.18781	-0.18969	-0.06944	0.03269	0.02833
	S4	0.04488	-0.23898	-0.19528	-0.07893	0.04087	-0.07663
	Y1	-0.12283	-0.23356	-0.18354	-0.16005	0.23273	0.12471
	Y2	-0.15037	-0.28431	-0.21450	0.20466	0.30918	0.16063
	Y3	-0.08432	-0.10782	-0.03016	0.14335	0.20070	0.05363
	Z1	-0.16698	-0.20239	-0.23280	0.19157	0.17206	-0.13934
	Z2	0.21012	0.21088	0.25391	0.25654	0.22219	-0.17685
	Z3	0.10524	-0.00205	0.04515	0.19416	0.14674	-0.11758
O2	S1	-0.01005	0.03479	-0.03385	-0.01439	0.00713	-0.00812
	S2	-0.01203	0.05129	-0.04959	0.02026	0.00976	-0.00857
	S3	0.03069	-0.18781	0.18969	-0.06944	-0.03269	0.02833
	S4	-0.04488	-0.23898	0.19528	-0.07893	-0.04087	-0.07663
	Y1	-0.12283	0.23356	-0.18354	-0.16005	0.23273	-0.12471
	Y2	-0.15037	0.28431	-0.21450	-0.20466	0.30918	-0.16063
	Y3	-0.08432	0.10782	-0.03016	-0.14335	0.20070	-0.05363
	Z1	-0.16698	0.20239	-0.23280	0.19157	-0.17206	-0.13934
	Z2	-0.21012	0.21088	-0.25391	0.25654	-0.22219	-0.17685
	Z3	-0.10524	-0.00205	-0.04515	0.19416	-0.14674	-0.11758
N	XX	-0.00000	-0.02685	0.00000	0.00967	0.00000	-0.01176
	YY	-0.00000	-0.00703	0.00000	-0.03772	0.00000	0.02397
	ZZ	-0.00000	0.04427	0.00000	0.03271	0.00000	0.03672
	YZ	0.04911	0.00000	-0.06553	0.00000	-0.02257	-0.00000
O1	XX	0.00656	0.00359	-0.00101	-0.00363	-0.00013	-0.00444
	YY	-0.00417	0.00164	-0.00207	0.01293	0.01184	0.02090
	ZZ	-0.01061	0.00388	0.00620	-0.01318	-0.00697	0.00367
	YZ	0.01861	0.00004	0.00198	0.00498	-0.00466	-0.01836
O2	XX	-0.00656	0.00359	0.00101	-0.00363	0.00013	-0.00444
	YY	0.00417	0.00164	0.00207	0.01293	-0.01184	0.02090
	ZZ	0.01061	0.00388	-0.00620	-0.01318	0.00697	0.00367
	YZ	0.01861	-0.00004	0.00198	-0.00498	-0.00466	0.01836
N	X1	-0.21943	-0.00000	0.31739			
	X2	-0.31491	0.00000	0.43575			
	X3	-0.14210	-0.00000	0.21979			
O1	X1	-0.17845	0.26724	-0.26420			
	X2	-0.23581	0.35239	-0.31281			
	X3	-0.13953	0.26180	-0.08051			
O2	X1	-0.17845	-0.26724	-0.26420			
	X2	-0.23581	-0.35239	-0.31282			
	X3	-0.13953	-0.26180	-0.08051			
N	XY	0.00000	-0.03733	-0.00000			
	XZ	-0.03935	-0.00000	0.03172			
O1	XY	-0.01741	0.01132	0.01224			
	XZ	0.01289	-0.01081	-0.00096			
O2	XY	0.01741	0.01132	-0.01224			
	XZ	0.01289	0.01081	-0.00096			

TABLE XXXI

THE $\tilde{A}^2B_1$ OVC ORBITALS FOR A GEOMETRY
R=2.25 BOHRS, θ=180°

Basis function		Orbital								
		$1\sigma_u$	$1\sigma_g$	$2\sigma_g$	$3\sigma_g$	$2\sigma_u$	$4\sigma_g$	$3\sigma_u$	$5\sigma_g$	$4\sigma_u$
N	S1	-0.00000	0.00095	-0.59269	0.02118	-0.00000	-0.13147	0.00000	-0.12757	0.00000
	S2	0.00000	0.00171	-0.44470	0.02942	-0.00000	-0.17182	-0.00000	-0.18564	-0.00000
	S3	0.00000	-0.00184	-0.00642	-0.07393	0.00000	0.52803	-0.00000	0.84524	-0.00000
	S4	-0.00000	0.00208	-0.00364	0.05147	-0.00000	0.28816	0.00000	0.33525	0.00000
	Z1	-0.00118	-0.00000	0.00000	-0.00000	-0.05453	-0.00000	0.26886	0.00000	-0.61008
	Z2	-0.00229	0.00000	-0.00000	0.00000	-0.03572	0.00000	0.32383	-0.00000	-0.64211
	Z3	0.00167	0.00000	-0.00000	0.00000	0.00087	0.00000	-0.03787	0.00000	0.01434
O1	S1	0.41075	0.41562	-0.00064	0.07919	-0.10046	0.00838	0.00515	0.03198	0.03339
	S2	0.32608	0.33318	-0.00109	0.12369	-0.13962	0.01458	0.00449	0.04543	0.04833
	S3	-0.00012	-0.02190	0.00383	-0.40729	0.40334	-0.04729	0.00221	-0.14306	-0.17541
	S4	0.00169	-0.01898	0.00494	-0.38160	0.35869	-0.17358	0.06810	-0.23023	-0.28602
	Z1	0.00233	0.00424	-0.00161	0.03949	-0.04838	0.15509	-0.20815	-0.33809	-0.32425
	Z2	-0.00024	0.00171	-0.00201	0.04527	-0.05129	0.18212	-0.25600	-0.38676	-0.37320
	Z3	0.00089	0.00268	-0.00065	0.03185	-0.05341	0.06760	-0.11950	-0.06597	-0.05286
O2	S1	-0.41075	0.41562	-0.00064	0.07919	0.10046	0.00838	-0.00515	0.03198	-0.03339
	S2	-0.32608	0.33318	-0.00109	0.12369	0.13962	0.01458	-0.00449	0.04543	-0.04833
	S3	0.00012	-0.02190	0.00383	-0.40729	-0.40334	-0.04729	-0.00221	-0.14306	0.17541
	S4	-0.00169	-0.01898	0.00494	-0.38160	-0.35869	-0.17358	-0.06810	-0.23023	0.28602
	Z1	0.00233	-0.00424	0.00161	-0.03949	-0.04838	-0.15509	-0.20815	0.33809	-0.32425
	Z2	-0.00024	-0.00171	0.00201	-0.04527	-0.05129	-0.18212	-0.25600	0.38676	-0.37320
	Z3	0.00089	-0.00268	0.00065	-0.03185	-0.05341	-0.06760	-0.11950	0.06597	-0.05286
N	XX	0.00000	0.00065	0.00051	0.01161	0.00000	-0.00063	-0.00000	0.00711	-0.00000
	YY	0.00000	0.00069	0.00013	0.01334	0.00000	-0.00174	-0.00000	-0.03443	-0.00000
	ZZ	0.00000	-0.00009	0.00004	-0.02938	-0.00000	0.04433	0.00000	-0.03335	-0.00000
O1	XX	-0.00062	0.00015	-0.00000	0.00312	-0.00247	-0.00463	0.01060	0.00421	-0.01102
	YY	0.00011	0.00029	0.00005	0.00318	-0.00263	-0.00602	0.01154	0.00235	-0.00294
	ZZ	-0.00004	-0.00013	-0.00045	0.00359	0.00233	0.02191	-0.03305	-0.01924	0.00227
O2	XX	0.00062	0.00015	-0.00000	0.00312	0.00247	-0.00463	-0.01060	0.00421	0.01102
	YY	-0.00011	0.00029	0.00005	0.00318	0.00263	-0.00602	-0.01154	0.00235	0.00294
	ZZ	0.00004	-0.00013	-0.00045	0.00359	-0.00233	0.02191	0.03305	-0.01924	-0.00227

TABLE XXXI, continued

Basis function		Orbital		
		$1\pi_u^{(x)}$	$1\pi_g^{(x)}$	$2\pi_u^{(x)}$
N	X1	0.23829	0.00000	0.32753
	X2	0.33451	0.00000	0.43385
	X3	0.15252	-0.00000	0.19096
O1	X1	0.17269	0.25916	-0.29439
	X2	0.23216	0.33830	-0.31544
	X3	0.11203	0.25880	-0.08974
O2	X1	0.17269	-0.25916	-0.29439
	X2	0.23216	-0.33830	-0.31544
	X3	0.11203	-0.25880	-0.08974
	XZ	0.00000	-0.05876	-0.00000
	XZ	0.02457	0.01850	0.01149
	XZ	-0.02457	0.01850	-0.01149
		$1\pi_u^{(y)}$	$1\pi_g^{(y)}$	$2\pi_u^{(y)}$
N	Y1	0.23156	0.00000	0.33969
	Y2	0.31376	0.00000	0.47604
	Y3	0.12345	-0.00000	0.35480
O1	Y1	0.18655	0.26338	-0.21236
	Y2	0.26696	0.34181	-0.27157
	Y3	0.12465	0.25222	-0.28364
O2	Y1	0.18655	-0.26338	-0.21236
	Y2	0.26696	-0.34181	-0.27157
	Y3	0.12465	-0.25222	-0.28364
	YZ	0.00000	-0.05166	-0.00000
	YZ	0.02219	0.01593	0.00990
	YZ	-0.02219	0.01593	-0.00990

TABLE XXXII

THE $\tilde{X}^2A_2$ OVC ORBITALS FOR A GEOMETRY OF R=2.40 BOHRS, θ=110°

Basis function		Orbital					
		$1b_2$	$1a_1$	$2a_1$	$3a_1$	$2b_2$	$4a_1$
N	S1	-0.00000	-0.00001	-0.59394	0.01474	0.00000	-0.12797
	S2	0.00000	-0.00005	-0.44632	0.01864	-0.00000	-0.17451
	S3	0.00000	-0.00021	-0.00079	-0.03170	-0.00000	0.52208
	S4	-0.00000	0.00160	0.00198	0.01930	0.00000	0.56952
	Y1	-0.00044	0.00000	-0.00000	-0.00000	-0.02041	-0.00000
	Y2	-0.00127	-0.00000	0.00000	0.00000	-0.00859	0.00000
	Y3	0.00068	-0.00000	0.00000	0.00000	0.01876	0.00000
	Z1	0.00000	-0.00063	-0.00450	-0.01451	-0.00000	-0.17553
	Z2	-0.00000	-0.00117	0.00017	-0.00746	0.00000	-0.21539
	Z3	-0.00000	0.00014	-0.00138	0.02327	0.00000	0.14413
O1	S1	0.41080	-0.41086	0.00019	0.09908	-0.10142	0.01050
	S2	0.32614	-0.32626	0.00017	0.13830	-0.14151	0.01583
	S3	-0.00022	0.00046	-0.00032	-0.40055	0.41139	-0.04938
	S4	0.00167	-0.00120	-0.00023	-0.37770	0.37916	-0.12308
	Y1	0.00116	-0.00132	-0.00047	0.03877	-0.03993	0.01538
	Y2	-0.00056	0.00033	-0.00112	0.04256	-0.04222	0.01404
	Y3	0.00045	-0.00056	-0.00024	0.03023	-0.03890	-0.01515
	Z1	-0.00102	0.00087	0.00047	-0.04453	0.04418	-0.02462
	Z2	0.00014	-0.00017	0.00078	-0.05111	0.05426	-0.02943
	Z3	-0.00058	0.00044	0.00061	-0.04325	0.03759	0.03296
O2	S1	-0.41080	-0.41086	0.00019	0.09908	0.10142	0.01050
	S2	-0.32614	-0.32626	0.00017	0.13830	0.14151	0.01583
	S3	0.00022	0.00046	-0.00032	-0.40055	-0.41139	-0.04938
	S4	0.00167	-0.00120	-0.00023	-0.37770	-0.37916	-0.12308
	Y1	0.00116	0.00132	-0.00047	-0.03877	-0.03993	-0.01538
	Y2	-0.00056	-0.00033	0.00112	-0.04256	-0.04222	-0.01404
	Y3	0.00045	0.00056	0.00024	-0.03023	-0.03890	0.01515
	Z1	0.00102	0.00087	0.00047	-0.04453	-0.04418	-0.02462
	Z2	-0.00014	-0.00017	0.00078	-0.05111	-0.05426	-0.02943
	Z3	0.00058	0.00044	0.00061	-0.04325	-0.03759	0.03296
N	XX	0.00000	-0.00005	0.00011	0.00864	-0.00000	0.00727
	YY	0.00000	-0.00056	0.00009	-0.00549	-0.00000	0.00869
	ZZ	0.00000	-0.00035	-0.00030	-0.00121	-0.00000	-0.01205
	YZ	-0.00058	-0.00000	0.00000	0.00000	-0.01792	0.00000
O1	XX	-0.00015	0.00007	-0.00001	0.00293	-0.00251	-0.00079
	YY	0.00004	-0.00012	-0.00044	0.00129	-0.00077	0.00020
	ZZ	0.00014	-0.00021	-0.00005	0.00200	-0.00278	0.00721
	YZ	0.00018	-0.00013	0.00027	-0.00038	0.00063	-0.00912
O2	XX	0.00015	0.00007	-0.00001	0.00293	0.00251	-0.00079
	YY	-0.00004	-0.00012	-0.00044	-0.00129	0.00077	0.00020
	ZZ	-0.00014	-0.00021	-0.00005	0.00200	0.00278	0.00721
	YZ	0.00018	0.00013	-0.00027	0.00038	0.00063	0.00912

TABLE XXXII, continued

Basis function		Orbital					
		$3b_2$	$7a_1$	$5b_2$	$5a_1$	$4b_2$	$6a_1$
N	S1	0.00000	-0.09080	-0.00000	-0.01684	-0.00000	-0.04479
	S2	0.00000	-0.13285	0.00000	-0.02373	-0.00000	-0.05462
	S3	-0.00000	0.58150	0.00000	0.05715	0.00000	0.18946
	S4	0.00000	-0.28118	-0.00000	0.19915	-0.00000	-0.15656
	Y1	0.24137	-0.00000	-0.52962	-0.00000	0.02479	-0.00000
	Y2	0.32398	-0.00000	-0.59466	0.00000	0.03782	0.00000
	Y3	-0.00157	0.00000	-0.01783	0.00000	0.03417	0.00000
	Z1	-0.00000	0.42851	0.00000	-0.01085	0.00000	0.26306
	Z2	0.00000	0.41735	-0.00000	0.00301	-0.00000	0.34910
	Z3	0.00000	0.02160	-0.00000	-0.04211	-0.00000	0.12933
O1	S1	0.01380	0.03673	0.03533	0.01313	-0.00056	-0.00867
	S2	0.01748	0.05455	0.05242	0.01850	-0.00116	-0.00930
	S3	-0.04803	-0.20370	-0.20621	-0.05954	0.00580	0.03152
	S4	0.02369	-0.19923	-0.17981	-0.08525	0.04159	-0.07157
	Y1	-0.18018	-0.26867	-0.22348	0.13625	0.17082	-0.14166
	Y2	-0.22647	-0.30730	-0.23757	0.16794	0.23026	0.18261
	Y3	-0.12961	-0.08664	-0.02496	0.10990	0.17084	0.06774
	Z1	0.10841	0.15388	0.19337	0.21889	-0.21344	-0.11939
	Z2	-0.13363	0.15513	0.22937	0.28857	0.27744	-0.15291
	Z3	0.05895	0.01446	0.06737	0.21824	0.18878	-0.11109
O2	S1	-0.01380	0.03673	-0.03533	0.01313	-0.00056	-0.00867
	S2	-0.01748	0.05455	-0.05242	0.01850	0.00116	-0.00930
	S3	0.04803	-0.20370	0.20621	-0.05954	-0.00580	0.03152
	S4	-0.02369	-0.19923	0.17981	-0.08525	-0.04159	-0.07157
	Y1	-0.18018	-0.26867	-0.22348	-0.13625	0.17082	-0.14166
	Y2	-0.22647	0.30730	-0.23757	-0.16794	0.23026	-0.18261
	Y3	-0.12961	0.08664	-0.02496	-0.10990	0.17084	-0.06774
	Z1	-0.10841	0.15388	-0.19337	0.21889	-0.21344	-0.11939
	Z2	-0.13363	0.15513	-0.22937	0.28857	-0.27744	-0.15291
	Z3	-0.05895	0.01446	-0.06737	0.21824	-0.18878	-0.11109
N	XX	-0.00000	-0.03654	0.00000	-0.00032	0.00000	-0.01171
	YY	-0.00000	0.00551	0.00000	-0.03718	-0.00000	0.02748
	ZZ	-0.00000	0.01510	0.00000	0.02909	-0.00000	-0.03095
	YZ	-0.05317	-0.00000	-0.09905	0.00000	-0.01569	-0.00000
O1	XX	0.00706	0.00566	0.00177	-0.00123	0.00061	-0.00395
	YY	-0.01156	-0.00636	0.00237	0.00962	-0.01068	-0.02397
	ZZ	-0.00447	0.01096	0.00349	-0.01041	-0.01064	0.00043
	YZ	0.01862	0.00545	0.00527	0.00581	0.00308	-0.01580
O2	XX	-0.00706	0.00566	-0.00177	-0.00123	-0.00061	-0.00395
	YY	-0.01156	-0.00636	-0.00237	0.00962	-0.01068	0.02397
	ZZ	0.00447	0.01096	-0.00349	-0.01041	0.01064	0.00043
	YZ	0.01862	-0.00545	0.00527	-0.00581	-0.00308	-0.01580
N	X1	-0.21969	-0.00000	0.35153			
	X2	-0.31380	0.00000	0.45529			
	X3	-0.14726	-0.00000	0.17135			
O1	X1	-0.17830	0.27045	-0.24769			
	X2	-0.23746	0.36114	-0.30760			
	X3	-0.13850	0.23740	-0.09555			
O2	X1	-0.17830	-0.27045	-0.24769			
	X2	-0.23746	-0.36114	-0.30760			
	X3	-0.13850	-0.23740	-0.09555			
N	XY	-0.00000	-0.03539	-0.00000			
	XZ	-0.03663	-0.00000	0.03047			
O1	XY	-0.01826	0.01370	0.00108			
	XZ	0.01107	-0.00989	0.00065			
O2	XY	0.01826	0.01370	-0.00108			
	XZ	0.01107	0.00989	0.00065			

APPENDIX D

CONFIGURATION SELECTION IN "WELL-BEHAVED" POLYATOMIC MOLECULES

APPENDIX D

CONFIGURATION SELECTION IN "WELL-BEHAVED" POLYATOMIC MOLECULES

In those molecules for which a "good" valence-bond type wavefunction may be written, the dominant molecular correlation configurations are easily identified in a priori fashion. A valence-bond type wavefunction is understood to denote a case in which the molecular binding is well described by localized σ and π bonding and anti-bonding orbitals, in addition to core and lone-pair orbitals; this is in contrast to the necessarily delocalized orbital structure of NO_2.

In these "well-behaved" molecules, the most important correlating configurations relative to the RHF configuration fall into three classes:

(1) Diagonal bond correlation configurations. Such configurations are generated by $\sigma^2_{A-B} \rightarrow \sigma^{*2}_{A-B}$ and $\pi^2_{A-B} \rightarrow \pi^{*2}_{A-B}$ excitations from localized bonding orbitals into the corresponding anti-bonding orbitals.

(2) Split-shell multiple bond correlations. This class is of the form $\sigma_{A-B}\pi_{A-B} \rightarrow \sigma^{*}_{A-B}\pi^{*}_{A-B}$ where the σ and π orbitals are the components of a double (or triple) bond. For states with closed shell RHF configurations, these excitations lead to two open σ shells. Configurations with the unpaired σ electrons singlet coupled are much more important than for triplet coupling.

(3) Two bond split-shell excitations. Classes (1) and (2) are identical to the molecular extra correlation energy (MECE) configurations, which are vital for an accurate description in diatomic molecules. However, unique to polyatomic molecules are configurations which correlate two orbitals which are not localized on the same pair of nuclear centers. The most important of these are

$$\text{a)}\ \sigma_{A-B}\sigma_{B-C} \rightarrow \sigma^{*}_{A-B}\sigma^{*}_{B-C}$$

and

$$\text{b)}\ \sigma_{A-B}\pi_{B-C} \rightarrow \sigma^{*}_{A-B}\pi^{*}_{B-C}$$

in which there is a nuclear center common to the two localized bonds being correlated. Again, as in class (2), overall singlet coupling of the σ open shells contributes much more than triplet coupling.

Other excitations such as $n^2 \rightarrow \sigma^{*2}_{A-B}$ or $n^2 \rightarrow \pi^{*2}_{A-B}$, where "n" is a lone-pair orbital localized on a single center, or single excitations are an order of magnitude less important for introduction of correlation than the configurations of classes (1), (2), and (3).

As illustrations, the ground electronic states of HO_2, HONO, and CH_3NO will be discussed.

I. HO_2.

The hydroperoxyl radical ground state has the electronic symmetry $^2A''$ and as a free radical does not quite conform to our definition of a molecule with a "good valence-bond" structure. However, the deviation is not large and some extensive CI calculations exist for the HO_2 ground state which provide some interesting comparisons.

The RHF configuration of HO_2 in its $^2A''$ ground state corresponds in a localized description to

$$(1s_{O1})^2(1s_{O2})^2(2s_{O1})^2(2s_{O2})^2(\sigma_{H-O})^2(\sigma_{O-O})^2(p_{z,O2})^2(\pi_{O-O})^2(\pi^{*}_{O-O})^1$$

where $p_{z,O2}$ is an in-plane lone-pair orbital perpendicular to the O–O bond.

Due to the influence of the unpaired electron, the bonding π orbital electron density is predominately on the central oxygen atom, while the π^* orbital is located more on atom O2. The $\tilde{X}^2A''$ bond angle in HO_2 is approximately 105° and the central oxygen atom is essentially unhybridized.

The basis set used in this study was the [4s3p] contraction of Dunning, augmented with single component d-functions on oxygen (exponent = 1.35) and p-functions on hydrogen (exponent = 1.00). For a nuclear geometry of R_{H-O1}=1.80 bohrs, R_{O1-O2}=2.55 bohrs, θ=100°, 8 configurations were included in the OVC orbital optimization. These configurations are included along with their mixing coefficients in Table XXXIII; the four core orbitals which are doubly occupied in all configurations have been omitted from the table.

The single configuration (SC) energy of the RHF configuration for the OVC orbitals is -150.20112 hartrees; this is probably less than 0.01 hartrees higher than the true SCF energy in this basis. For the 8 OVC configurations, the energy is -150.28847 hartrees. A CI calculation which includes all single and double excitations from the RHF configuration within the space of valence orbitals (those given in Table XXXIII) using the OVC orbitals gave an energy of -150.29064 hartrees. From the SCF estimate of -150.21 hartrees, we obtain an energy lowering of 0.078 hartrees for the 8 OVC configurations, with an additional improvement of only 0.002 hartrees for the extension to the valence-singles-and doubles (VSD-CI) level. Thus, a small

TABLE XXXIII

OVC CONFIGURATIONS AND MIXING COEFFICIENTS FOR HO_2

σ_{H-O1}	σ_{O1-O2}	$p_{z,O2}$	σ^*_{H-O1}	σ^*_{O1-O2}	π_{O1-O2}	π^*_{O1-O2}	Spin-coupling	Mixing Coefficients
2	2	2	0	0	2	1		0.97888
2	0	2	0	2	2	1		-0.12645
0	2	2	2	0	2	1		-0.08814
2	1	2	0	1	1	2	0 0.5	0.11811
2	1	2	0	1	1	2	1 0.5	0.02051
1	1	2	1	1	2	1	0 0.5 0 0.5	0.04344
1	1	2	1	1	2	1	1 0.5 0 0.5	0.03239
1	2	2	1	0	1	2	0 0.5	0.02708

subset of configurations selected in a priori fashion yields ~97% of the valence correlation energy of the $\tilde{X}^2A''$ ground state of HO_2.

Gole and Hayes [91] have performed a VSD-CI calculation in a smaller basis set and for a somewhat shorter O-O bond length (R_{H-O1}= 1.814 bohrs, R_{O1-O2}=2.324 bohrs, θ=100°, E_{SCF}=-150.0068 hartrees); however, the CI employed SCF orbitals as compared to our use of the multi-configurationally optimized OVC orbitals. Their energy lowering upon the introduction of correlation is 0.026 hartrees, or one-third that of our calculation. Clearly evident is the superiority of the OVC orbitals over the SCF orbitals for purposes of introduction of correlation into the wavefunction.

There is a study by Liskow, Schaeffer, and Bender [92] in a double-zeta basis set (E_{SCF}=-150.15621 hartrees for R_{H-O1}=1.80 bohrs, R_{O1-O2}=2.60 bohrs, θ=100°) which employed 500 configurations in an iterative natural orbital (INO) treatment. The final energy of -150.24138 hartrees gives a correlation energy lowering of 0.085 hartrees, an improvement of about 10% over our 8 configuration OVC wavefunction. For the low-lying doublet states of NO_2, though, the CI energy lowering decreased by about 10% when d-functions were added to the double-zeta basis. Thus, our 8 configuration OVC wavefunction produces the same amount of molecular correlation as the 500 configuration INO wavefunction of Liskow et al.

II. HONO.

No ab initio calculations of nitrous acid electronic structure have appeared to date in the published literature [93] and we have not examined all valence configurations; thus it is not possible to make detailed comparisons such as were done for HO_2.

The calculations were done in the Dunning [4s3p] basis at the experimental geometry of the trans isomer as determined by Cox et al. [94]

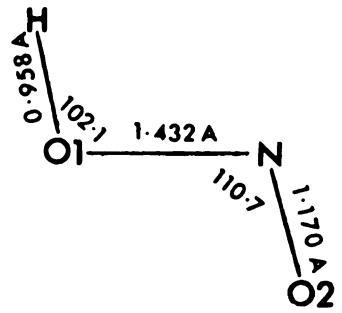

Exclusive of the six core orbitals, which correspond to the 1s and 2s atomic orbitals on the heavy atoms, the RHF configuration in the localized description is

$$(\sigma_{H-O1})^2(\sigma_{O1-N})^2(\sigma_{N-O2})^2(p_{\sigma,O2})^2(\pi_{N-O2})^2(p_{\pi,O1})^2$$

where $p_{\sigma,O2}$ is an in-plane lone-pair orbital perpendicular to the N-O2 σ bond and $p_{\pi,O1}$ is a lone-pair orbital perpendicular to the molecular plane. The OVC orbital optimization was performed for the configurations given in Table XXXIV.

The SC and OVC energies are respectively -204.5773 and -204.7301 hartrees and the energy improvement due to correlation for the 13 a priori selected configurations is 0.1528 hartrees; this compares favorable to the lowering of 0.1592 hartrees for 18 carefully selected configurations in the $\tilde{X}^2A_1$ ground state of NO_2 and in the same basis set.

We note that configurations 6 and 7 have very small mixing coefficients; this is as expected since there is no nuclear center common to the two bonds which are being correlated by these configurations.

TABLE XXXIV

OVC CONFIGURATIONS AND MIXING COEFFICIENTS FOR HONO

σ_{H-O1}	σ_{O1-N}	σ_{N-O2}	$p_{\sigma,O2}$	$p_{\pi,O1}$	σ^{*}_{H-O1}	σ^{*}_{O1-N}	σ^{*}_{N-O2}	π_{N-O2}	π^{*}_{N-O2}	Spin-coupling	Mixing Coefficient
2	2	2	2	2	0	0	0	2	0		0.96190
2	2	0	2	2	0	0	2	2	0		-0.06756
0	2	2	2	2	2	0	0	2	0		-0.08692
2	0	2	2	2	0	2	0	2	0		-0.12812
2	2	2	2	2	0	0	0	0	2		-0.17228
1	2	1	2	2	1	0	1	2	0	0 0.5 0	0.00219
1	2	1	2	2	1	0	1	2	0	1 0.5 0	0.00432
2	1	1	2	2	0	1	1	2	0	0 0.5 0	-0.02396
2	1	1	2	2	0	1	1	2	0	1 0.5 0	-0.01199
1	1	2	2	2	1	1	0	2	0	0 0.5 0	0.04752
1	1	2	2	2	1	1	0	2	0	1 0.5 0	0.03873
2	2	1	2	2	0	0	1	1	1	0 0.5 0	-0.10530
2	2	1	2	2	0	0	1	1	1	1 0.5 0	-0.03081

III. CH_3NO.

For nitrosomethane we have only considered the configurations of classes (1) and (2). In addition to five doubly occupied core orbitals, ls_O^2, ls_N^2, ls_C^2, $2s_O^2$, and $2s_N^2$, and an in-plane lone-pair orbital, $p_{\sigma,O}^2$, which is perpendicular to the N-O σ bond, the CH_3NO RHF configuration contains 6 bonding orbitals

$$(\sigma_{C-H1})^2(\sigma_{C-H2})^2(\sigma_{C-H3})^2(\sigma_{C-N})^2(\sigma_{N-O})^2(\pi_{N-O})^2$$

For this calculation the Dunning [4s2p] contraction was used and the geometry was identical to that chosen by Ha and Wild [95], who performed an SCF-CI computation in a basis set which is about 0.05 hartrees inferior to the Dunning basis at the SCF level.

The 9 class (1) and (2) OVC configurations, expressed in an excitation formalism notation, are included in Table XXXV along with the mixing coefficients.

The OVC energy of -168.9292 hartrees is an improvement of 0.1572 hartrees over the SC energy. In contrast, Ha and Wild obtained a lowering of only 0.1037 hartrees over their SCF result for a CI calculation of 169 configurations; this set was selected from a very much larger set by application of an energy criterion designed to identify those configurations most efficient for the introduction of correlation.

In none of the examples cited have we rigorously examined the effect of various classes of configurations in introducing correlation into the wavefunction; also, only ground electronic states were considered. Nevertheless, it is evident that at least for some molecules, the majority of the valence correlation energy

TABLE XXXV

OVC CONFIGURATIONS AND MIXING COEFFICIENTS FOR CH_3NO

Configuration	Mixing Coefficient
RHF	0.95863
$(\sigma_{C-H1})^2 \rightarrow (\sigma^*_{C-H1})^2$	-0.07908
$(\sigma_{C-H2})^2 \rightarrow (\sigma^*_{C-H2})^2$	-0.07908
$(\sigma_{C-H3})^2 \rightarrow (\sigma^*_{C-H3})^2$	-0.07906
$(\sigma_{N-O})^2 \rightarrow (\sigma^*_{N-O})^2$	-0.07386
$(\sigma_{C-N})^2 \rightarrow (\sigma^*_{C-N})^2$	-0.09811
$(\pi_{N-O})^2 \rightarrow (\pi^*_{N-O})^2$	-0.18264
$(\sigma_{N-O})(\pi_{N-O}) \rightarrow (\sigma^*_{N-O})(\pi^*_{N-O})$	0.08624[#]
"	0.07988[##]

[#]Spin-coupling 0 0.5 0.

[##]Spin-coupling 1 0.5 0.

can be accounted for within a small set of configurations chosen in a priori fashion. This is of great significance for the extension of ab initio techniques to larger polyatomic molecules, for which the huge total number of valence configurations precludes a "brute force" approach to introduction of molecular correlation.